

The role of cloud-radiative effects and diabatic processes for the dynamics of the North Atlantic Oscillation on synoptic time-scales

Zur Erlangung des akademischen Grades eines
DOKTORS DER NATURWISSENSCHAFTEN
von der KIT-Fakultät für Physik des
Karlsruher Instituts für Technologie (KIT)

genehmigte

DISSERTATION

von

M.Sc. Georgios Papavasileiou
aus Larisa, Griechenland

Tag der mündlichen Prüfung:	24.07.2020
Referent:	Prof. Dr. Peter Knippertz
Korreferent:	Prof. Dr. Corinna Hoose
Korreferent:	Dr. Aiko Voigt, KIT-Associate Fellow

This work is licensed under a Creative Commons “Attribution-ShareAlike 4.0 International” license.



Abstract

Clouds shape weather and climate by regulating the latent and radiative heating in the atmosphere. Recent work demonstrated the importance of cloud-radiative effects (CRE) for the mean circulation of the extratropical atmosphere and its response to global warming. In contrast, little research has been done regarding the impact of CRE on internal variability. During the northern hemisphere winter the dominant mode of atmospheric variability over the North Atlantic and the surrounding continental areas of North America and Europe is the North Atlantic Oscillation (NAO). Here, we study how clouds and the NAO couple on synoptic time-scales during northern hemisphere winter via CRE within the atmosphere (ACRE) in observations and model simulations.

A regression analysis based on 5-day-mean data from CloudSat/CALIPSO reveals a robust dipole of cloud-incidence anomalies during a positive NAO, with increased high-level clouds along the storm track (near 45°N) and the subpolar Atlantic, and decreased high-level clouds poleward and equatorward of it. Opposite changes occur for low-level cloud incidence. Satellite retrievals from CloudSat/CALIPSO, CERES and GERB as well as ERA-Interim short-term forecast data show that these cloud anomalies lead to an anomalous column-mean heating due to ACRE over the region of the Iceland low, and to a cooling over the region of the Azores high. To quantify the impact of the ACRE anomalies on the NAO, and to thereby test the hypothesis of a cloud-radiative feedback on the NAO persistence, we apply the surface pressure tendency equation (PTE) to ERA-Interim short-term forecast data. The NAO-related surface pressure tendency anomalies due to ACRE amplify the NAO-related surface pressure anomalies over the Azores high but have no area-averaged impact on the Iceland low. In contrast, surface pressure tendency anomalies due to total diabatic heating, including latent heating and clear-sky radiation, strongly amplify the NAO-related surface pressure anomalies over both the Azores high and the Iceland low, and their impact is much more spatially coherent. This suggests that while ACRE lead to an increase in NAO persistence on synoptic time-scales, their impact is relatively minor and much smaller compared to other diabatic processes.

To test the robustness of our PTE-based hypothesis, numerical simulations in ICON are carried out. The PTE analysis in ICON shows results that are qualitatively consistent with the observational analysis, in particular regarding the feedback mechanisms of ACRE and total diabatic heating, which is dominated by latent heating. These PTE-based results are further tested by means of sensitivity simulations in ICON, where a NAO-related diabatic heating

pattern is imposed either due to ACRE or total diabatic heating. These heating patterns are based on 5-day-mean NAO regressions of either ACRE or total diabatic heating. The sensitivity simulations confirm the observational hypothesis and show that ACRE feed back positively by up to 1–2% of 1σ NAO, while the total diabatic heating feeds back positively by up to 10% of 1σ NAO. Overall, the observational and modeling work both illustrate the substantial impact of the total diabatic heating for the NAO, while ACRE play a minor role. This highlights that diabatic processes are essential for understanding and accurately modeling the NAO short-term dynamics.

Preface

The PhD candidate confirms that the research presented in this thesis contains significant scientific contributions by himself. This thesis reuses material from the following publication (Papavasileiou et al., 2020):

Papavasileiou, G, Voigt, A, Knippertz, P. The role of observed cloud-radiative anomalies for the dynamics of the North Atlantic Oscillation on synoptic time-scales. *Q J R Meteorol Soc.* 2020; 146: 1822–1841. <https://doi.org/10.1002/qj.3768>

Chapters 1, 2, 3, 4, 5 and 7 reuses material from Papavasileiou et al. (2020) ©2020 The Authors. *Quarterly Journal of the Royal Meteorological Society* published by John Wiley and Sons Ltd on behalf of the Royal Meteorological Society. The research leading to these results has been accomplished within the project "High definition clouds and precipitation for advancing climate prediction" HD(CP)² funded by the German Ministry of Education and Research (BMBF) and Research for Sustainable Development (FONA) under grant number 01LK1509A, and the project "C5 Dynamical feature-based ensemble postprocessing of wind gusts within European winter storms" of the Transregional Collaborative Research Centre SFB/TRR 165 "Waves to Weather" funded by the German Research Foundation (DFG). The research proposals of these projects were written by Dr. Aiko Voigt and Prof. Dr. Peter Knippertz, respectively. The analysis in Papavasileiou et al. (2020) was solely carried out by the candidate, who also wrote the text with the advice and comments from Dr. Aiko Voigt and Prof. Dr. Peter Knippertz during the manuscript preparation.

The candidate confirms that appropriate credit has been given within the thesis where reference has been made to the work of others. This copy has been supplied on the understanding that this is copyright material and that no quotation from the thesis may be published without proper acknowledgment.

© 2020, Karlsruhe Institute of Technology and Georgios Papavasileiou

Contents

Abstract	III
Preface	V
1 Introduction	1
2 State of the art	5
2.1 North Atlantic Oscillation	5
2.2 Coupling between the extratropical circulation and cloud-radiative effects	12
2.3 Coupling between the NAO and diabatic processes	20
3 Research questions	23
4 Data and methods	25
4.1 Satellite observations	25
4.1.1 CloudSat/CALIPSO cloud incidence	25
4.1.2 CloudSat/CALIPSO cloud-radiative effects	27
4.1.3 CERES and GERB/SEVIRI cloud-radiative effects	27
4.2 ERA-Interim reanalysis data	28
4.3 ICON simulations	29
4.3.1 Control simulations	29
4.3.2 Sensitivity tests	30
4.4 North Atlantic Oscillation index	31
4.5 Surface pressure tendency equation (PTE)	32
4.6 Regression analysis and statistical significance	34
5 The role of observed cloud-radiative effects for the NAO short-term dynamics	37
5.1 NAO impact on clouds and ACRE in satellite observations	37
5.1.1 Zonal-mean perspective	37
5.1.2 Latitude-longitude perspective over the North Atlantic region	38
5.1.3 Vertical structure over Iceland and the Azores	41
5.2 Robustness in other observational datasets	44

5.3	Role of the ACRE for the dynamics of the NAO: ERA-Interim analysis . .	45
5.3.1	Latitude-longitude perspective of the PTE regression analysis . .	49
5.3.2	Vertical perspective on the PTE regression analysis over Iceland and the Azores	51
5.4	Comparison to Li et al. (2014a)	53
5.5	Conclusions	55
6	The role of cloud-radiative effects and diabatic processes for the NAO short-term dynamics in ICON	59
6.1	The North Atlantic Oscillation in ICON	59
6.2	NAO impact on clouds and cloud-radiative effects in ICON	61
6.2.1	Zonal-mean perspective	68
6.2.2	Latitude-longitude perspective	70
6.3	Role of ACRE and total diabatic heating for the dynamics of the NAO in ICON	73
6.3.1	PTE analysis	74
6.4	Short-term NAO response to imposed diabatic heating	77
6.4.1	Latitude-longitude perspective of the response to the NAO-related ACRE heating pattern	77
6.4.2	Latitude-longitude perspective of the response to the NAO-related total diabatic heating pattern	78
6.4.3	Time dependence of the response to the NAO-related ACRE heating pattern	80
6.4.4	Time dependence of the response to the NAO-related total dia- batic heating pattern	80
6.5	Conclusions	83
7	Summary and outlook	85
7.1	Summary	85
7.2	Outlook	89
A	Bibliography	91
B	List of abbreviations	111
C	Acknowledgements	113

1. Introduction

The North Atlantic region (90°W-40°E, 20°N-80°N) comprises the eastern parts of North America, Greenland, Europe and northern Africa and includes some of the most populated and economically developed areas of the world. A big portion of socioeconomic activities such as trade logistics, agriculture, renewable energy and construction industry is highly dependent on weather and climate conditions. The weather and climate in the North Atlantic region is characterized by large variability on a wide range of spatiotemporal scales and has major impact on these socioeconomic activities across the seasons. Thus, understanding and improving the medium- and long-range weather forecasting would create a great benefit to society as it would allow for planning and mitigating the impacts of severe weather. This includes cold outbreaks and winter wind storms (Renggli et al., 2011), which can lead to disruptions on transport infrastructure networks (Palin et al., 2013) and can substantially impact the energy demand (Clark et al., 2017).

Sir Gilbert Walker in 1924, using surface pressure measurements in Iceland and the Azores, identified a large-scale atmospheric pressure seesaw over the North Atlantic region that he named the so-called North Atlantic Oscillation (NAO; Walker, 1925; Walker and Bliss, 1932). This concept and its impact on the weather and climate in the neighbouring and remote areas gained a lot of research popularity in the following decades, during which the NAO was examined using newly developed technologies such as numerical weather prediction models and statistical techniques. The NAO can be simply described as a giant surface pressure seesaw between an area around Iceland, known as the subpolar or Iceland low, and another over west of the Iberian Peninsula around the Azores, known as the subtropical or Azores high. The relative changes in surface pressure between these two areas define the NAO phase. A positive phase of the NAO is defined when the surface pressure decreases over the Iceland low and increases over the Azores high, while opposite changes define a negative phase of the NAO (Hurrell, 1995; Visbeck et al., 2001; Hurrell et al., 2003). As illustrated in the schematic in Fig. 1.1, a positive phase of the NAO is associated with more low pressure systems moving from the eastern USA towards northern Europe bringing warmer and wetter conditions, while the Mediterranean region tends to be drier. On the other hand, a negative NAO is associated with more low pressure systems moving towards the Mediterranean and southern Europe bringing wetter conditions, while northern Europe and eastern USA tend to be colder and drier.

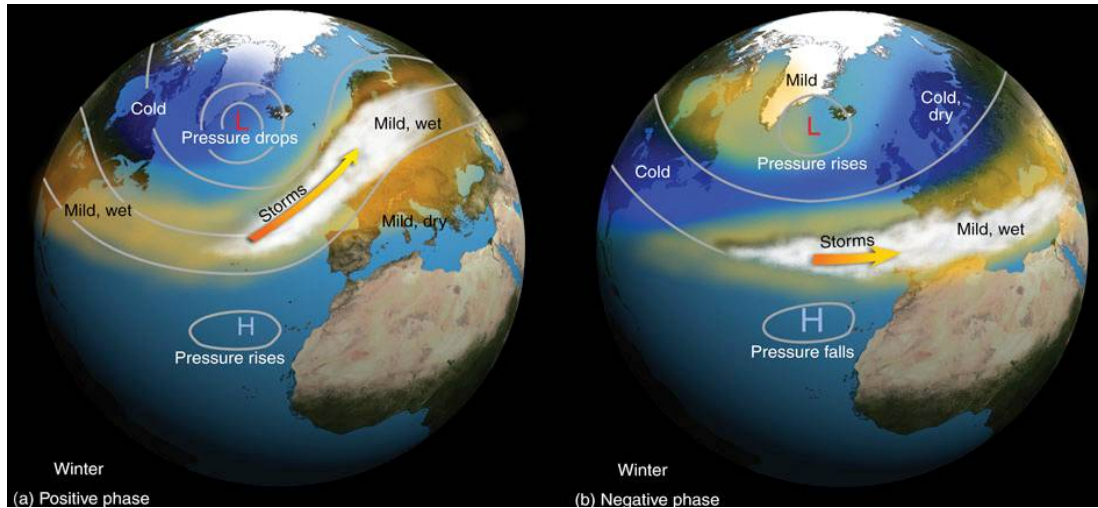


Figure 1.1.: Schematic diagram of the major effects of a (a) positive and (b) negative NAO phase in the European and North American continental areas. Copyright ©Thomson Higher Education, 2007 (can be accessed at <http://apollo.lsc.vsc.edu/classes/met130/notes/chapter10/graphics/nao.jpg>)

This large-scale atmospheric pressure seesaw is also linked to changes in the intensity and latitudinal position of the North Atlantic jet stream. The North Atlantic jet stream is a meandering ribbon of fast moving winds near the tropopause (the boundary between the troposphere and stratosphere) at roughly 10 km height and is found at the boundary between cold and warm airmasses. Because this boundary is stronger during the winter, the North Atlantic jet stream is also stronger during the winter (Blackmon, 1976; Athanasiadis et al., 2009). This air stream interacts and steers synoptic-scale weather systems in the midlatitudes, e.g., systems of high pressure or low pressure and their accompanied storms. The synoptic variability over the North Atlantic region and its impacts on weather and climate timescales is well examined and linked to the NAO (Hurrell, 1995; Visbeck et al., 2001; Wanner et al., 2001; Marshall et al., 2001; Hurrell et al., 2003; Cohen and Barlow, 2005). Extreme and persistent NAO phases are associated with high-impact weather events such as heavy precipitation, damaging winds, droughts and cold outbreaks (Leckebusch et al., 2006; Scaife et al., 2008; Pinto et al., 2009; Jung et al., 2011; Nobre et al., 2017; Ferranti et al., 2018; Papritz and Grams, 2018; Pasquier et al., 2019; Zanardo et al., 2019). In some winters a particular NAO state is more persistent, leading to substantial seasonal temperature and precipitation anomalies. Figure 1.2 illustrates the temperature and precipitation anomalies of three examples of such persistent NAO events. A very exceptional case is the winter from December to February (DJF) of 2009/10, when a very cold winter was associated with a record-breaking negative NAO that resulted in negative temperature anomalies and heavy snow for many areas of Eurasia and the eastern USA (Osborn, 2011; Jung et al., 2011). On the other side of the spectrum, very persistent positive NAO winters

during DJF of 1989/90 and a more recent one during 2019/20 were associated with mild and wetter winter periods for northern Europe (Fig. 1.2).

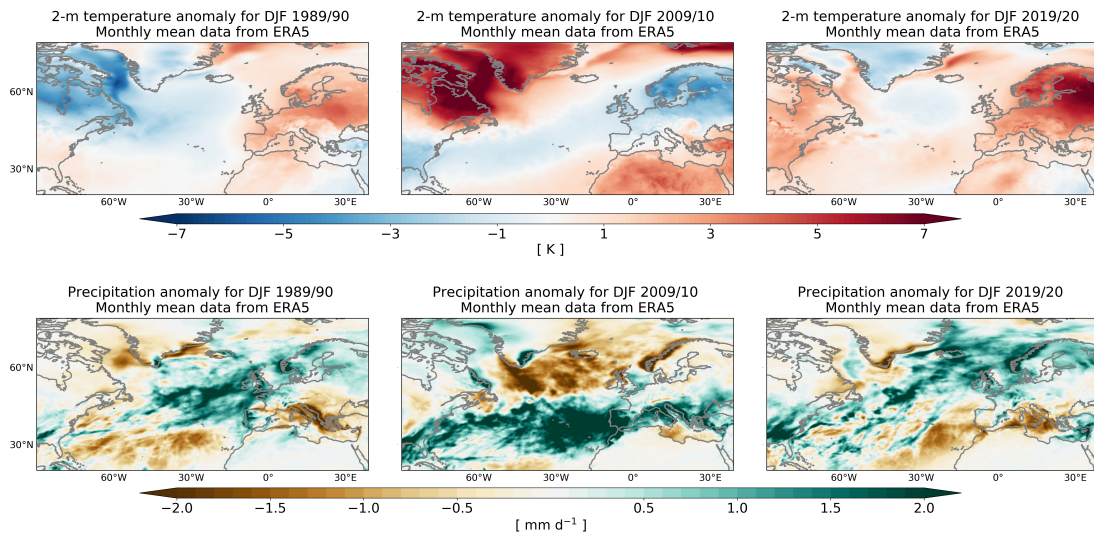


Figure 1.2.: Temperature at 2-m (top) and precipitation (bottom) anomalies during December-January-February of 1989/90 (left column), 2009/10 (middle column) and 2019/20 (right column) over the North Atlantic, Europe, Africa and North America. Results are based on ECMWF ERA5 data and the anomalies are calculated using the 1981–2010 as a reference period.

During the recent years a lot of research effort has been done mainly by European research centers and national weather services, regarding the predictability of NAO and its representation in operational numerical weather prediction (NWP) models for medium-range weather forecasts, seasonal and climate predictions. In general, predicting the weather in the midlatitudes tends to be particularly difficult beyond 5–10 days, therefore the strong relationship between the NAO variability and the weather around the North Atlantic illustrates the need for more skilful predictions of the NAO (Scaife et al., 2014). However, many different dynamical internal and external factors are driving the NAO variability, which leads to its chaotic behaviour. During the last couple of years, substantial progress has been made in connecting the NAO predictability on subseasonal-to-seasonal timescales with external forcing processes such as the stratosphere (Scaife et al., 2005, 2014; Stockdale et al., 2015; Hansen et al., 2017), the tropical forcing either in terms of sea surface temperature variability such as the El Niño–Southern Oscillation (ENSO) (Scaife et al., 2014; Domeisen et al., 2014; Butler et al., 2016) or in terms of convective rainfall such as the Madden–Julian Oscillation (MJO) (Cassou, 2008), and sea ice (Petoukhov and Semenov, 2010; Semenov and Latif, 2015). Yet, little research progress has been made on synoptic timescales. The NAO predictability is also partly limited due to our lack of knowledge of the interplay between the large-scale dynamics and diabatic processes (e.g., cloud-radiative effects and latent heating due to condensation).

Advancing our understanding of processes linked to the persistence of the NAO and other modes of atmospheric circulation variability can improve medium-range weather forecasts, subseasonal-to-seasonal predictions and climate projections, all of which are essential for the society. In the following chapter (Chapter 2) we extensively discuss the state of the art regarding this interplay between different processes and the NAO. The main goal of this PhD thesis is to systematically investigate the role of the cloud-radiative effects as well as the total diabatic heating for the NAO short-term dynamics in satellite observations, reanalysis data and numerical simulations.

2. State of the art

Here we introduce fundamental theories and an overview of the state of the art regarding NAO dynamics and its predictability, diabatic processes, the coupling between the circulation and diabatic processes, and the coupling between the NAO and diabatic processes. This chapter is inspired by previous work and different books such as "An Introduction to Dynamic Meteorology" by Holton (2004), "Atmospheric and Oceanic Fluid Dynamics: Fundamentals and Large-scale Circulation" by Vallis (2006) and "Nonlinear and Stochastic Climate Dynamics" by Franzke and O’Kane (2017). Parts of this chapter, with minor adjustments in the text, are based on the article "The role of observed cloud-radiative anomalies for the dynamics of the North Atlantic Oscillation on synoptic time-scales" by Georgios Papavasileiou, Aiko Voigt and Peter Knippertz, first published on 18 February 2020 by the Quarterly Journal of the Royal Meteorological Society (doi: 10.1002/qj.3768 ©2020 The Authors. Quarterly Journal of the Royal Meteorological Society published by John Wiley and Sons Ltd on behalf of the Royal Meteorological Society). This article is available under the terms of the Creative Commons Attribution License (CC BY).

2.1. North Atlantic Oscillation

The weather and climate of the North Atlantic region and the neighbouring North American and European continental areas exhibit considerable variability on a wide range of spatiotemporal scales. This variability is usually characterized in terms of anomalies, where an anomaly is defined as the difference between the instantaneous state of the system with respect to a specified reference period or climatology. The climatology is defined as the mean state of the system computed over many years in order to be representative. Over the North Atlantic but also the entire northern hemisphere, a large part of this variability is explained by the North Atlantic Oscillation (NAO) (Hurrell, 1995; Visbeck et al., 2001; Hurrell et al., 2003), which is a surface pressure seesaw with centers of action near Iceland and around the Azores. The NAO is the dominant mode of atmospheric variability over the North Atlantic and the surrounding continental areas of North America and Europe during winter (Wallace and Gutzler, 1981; Wanner et al., 2001; Visbeck et al., 2001; Hurrell and Deser, 2010). It is worth noting that there are also other modes of atmospheric variability relevant for the European weather and climate such as

the East Atlantic (EA) pattern and the Eurasian Pattern (Wallace and Gutzler, 1981; Barnston and Livezey, 1987; Luterbacher et al., 1999).

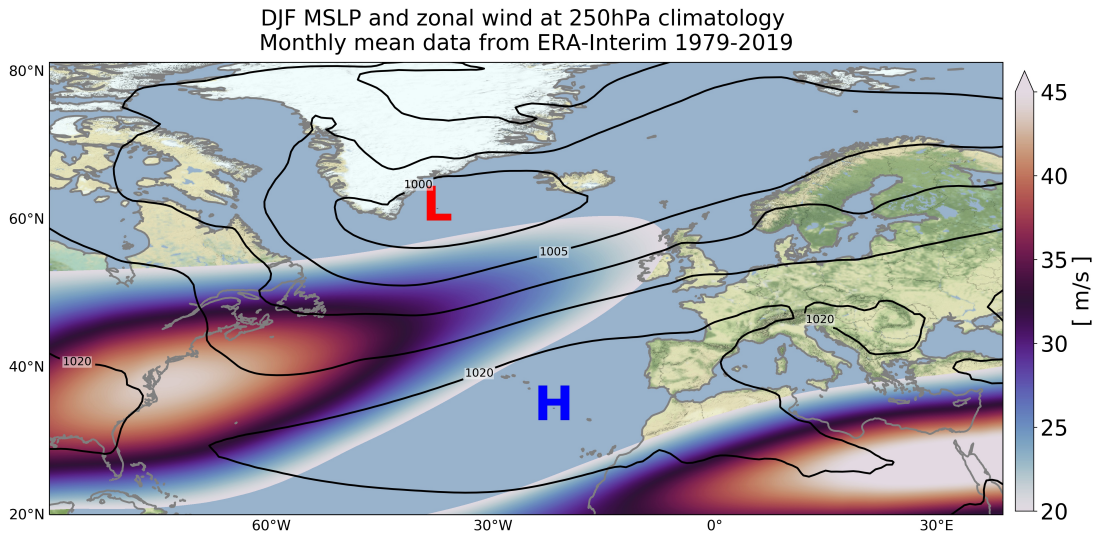


Figure 2.1.: December–February climatology of mean sea-level pressure (contours) and zonal wind at 250 hPa (shading). Results are based on ERA-Interim reanalysis data from 1979-2019.

From a climatology perspective, during the winter period over the North Atlantic the surface pressure is lower in higher latitudes where the minimum is located over the Irminger Sea west of Iceland, and higher in the lower latitudes where the maximum is located near the Azores (Fig. 2.1). Regarding the upper-tropospheric zonal winds at 250 hPa (roughly at 10 km altitude; shading in Fig. 2.1), a tilted band of very fast moving air occurs, which is called the "jet stream". During the winter, the North Atlantic jet stream is tilted from the southwest to the northeast. The reason for the tilt is the mean planetary scale flow, which is influenced by the longitudinal variation of orography over North America and the land-ocean heating contrast over the western North Atlantic (Gerber and Vallis, 2009; Woollings, 2010). During the winter, a low pressure trough is found over the eastern North America and a high pressure ridge just to the west of Europe (Fig. 2.2). These zonal asymmetries reveal a so-called stationary Rossby wave which is induced by the Rocky mountain range and the large land-ocean temperature gradient at the US and Canada east coast (Fig. 2.2; Blackmon, 1976; Holton, 2004; Hall et al., 2015). Synoptic-scale disturbances, which span over thousands of kilometres and have lifetimes of a few days to a week or more, tend to develop preferentially near the areas of maximum time-mean zonal winds. They mainly develop in the right entrance and left exit regions of the jet due to upper level divergence, e.g., over the western North Atlantic jet stream, interact and propagate further downstream along storm tracks that approximately follow the jet stream axis (Hoskins and Valdes, 1990; Chang et al., 2002).

The impact of the mean state of the dynamics can also be seen in cloud cover fields from reanalysis data as well as cloud incidence from satellite retrievals. Cloud cover illustrates the fraction of the sky covered by clouds, while cloud incidence shows the likelihood of a cloud to be observed. On average during the winter more high-level clouds occur over the ocean areas along the axis of the North Atlantic jet stream (Fig. 2.3a,b). These high-level clouds are associated with midlatitude cyclones and their warm conveyor belts (WCB), which are areas of strong large-scale ascending motions (Browning, 1986; Eckhardt et al., 2004). In mid-levels more clouds are found everywhere in the higher latitudes compared to the lower latitudes (Fig. 2.3c,d), while low-level clouds are mostly evident over the ocean and the cold continental areas of eastern Canada and eastern Europe and are linked to increased downward vertical velocity anomalies and low level static stability (Li et al., 2014b; Grise and Medeiros, 2016). On a day to day basis the North Atlantic jet stream varies substantially due to its interaction with transient synoptic-scale baroclinic waves, and, thus, changes the temperature advection, vertical motions and in turn clouds and precipitation. It therefore becomes apparent that changes in the North Atlantic jet stream across different spatiotemporal scales have a profound impact on the weather and climate variability over the North Atlantic area (Hall et al., 2015).

DJF geopotential height at 500hPa, 2m-temperature and zonal wind at 250hPa climatology
Monthly mean data from ERA5 1979-2019

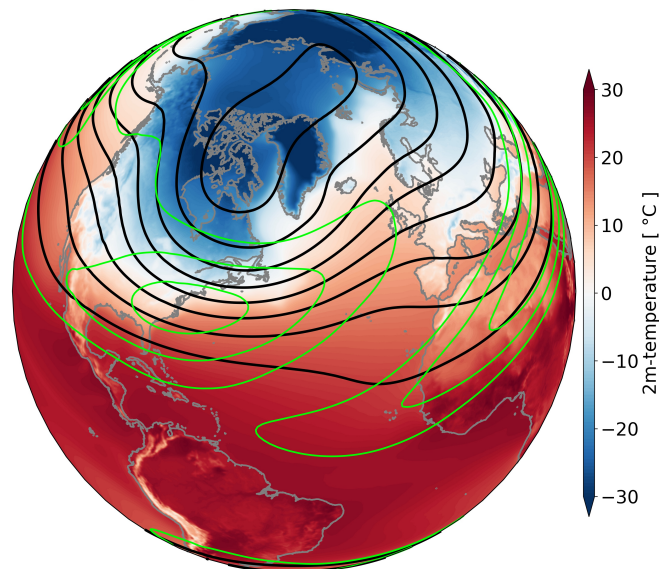


Figure 2.2.: December–February climatology of geopotential height at 500 hPa (black contours; values between 500 and 580 dam are shown with 10 dam intervals), temperature at 2m (shading) and zonal wind at 250 hPa (green contours; only values larger than 20 m/s are shown with 10 m intervals). Results are based on monthly mean ERA5 reanalysis data from 1979-2019.

There is no unique way to define the North Atlantic Oscillation index and its spatial structure. Early studies define the NAO index based on the difference between the normalized

2. State of the art

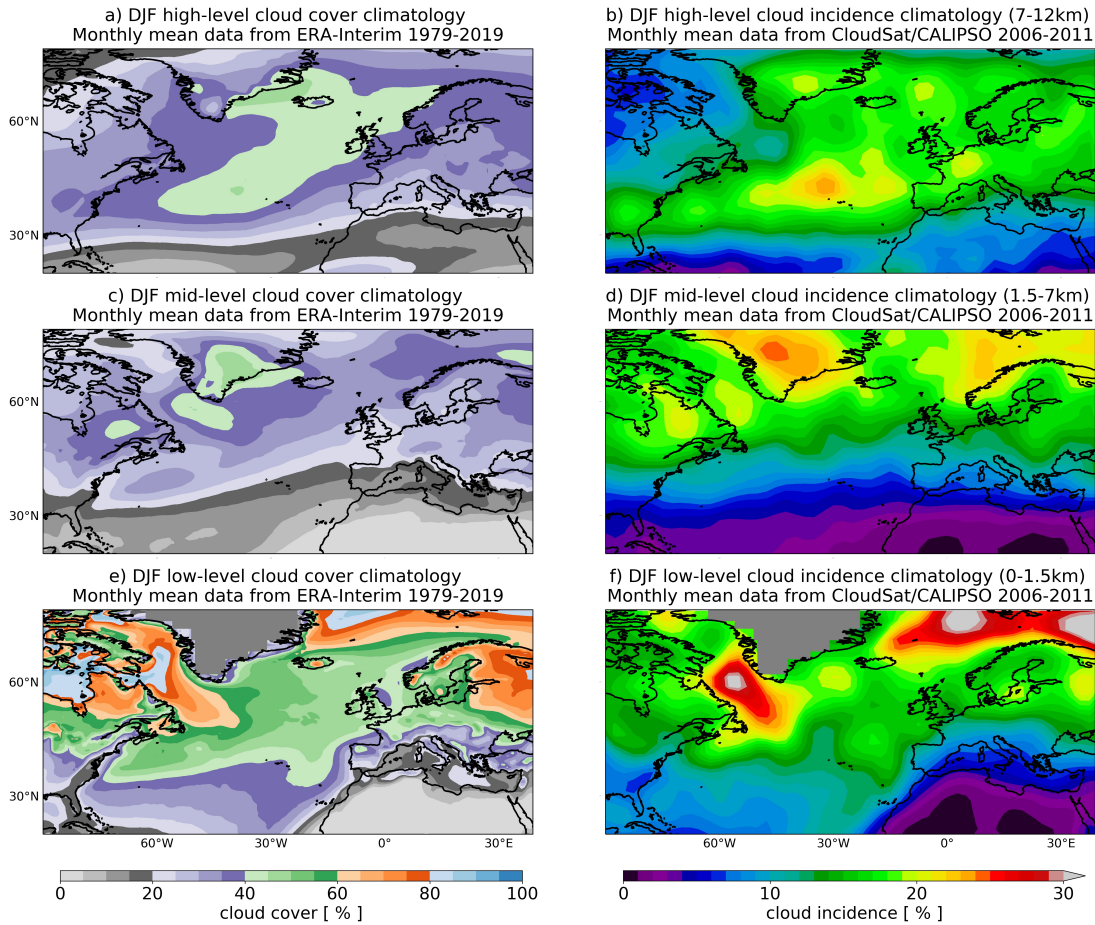


Figure 2.3.: December–February climatology of (a, b) high-, (c, d) mid-, and (e, f) low-level (a, c, e) cloud fraction from ERA-Interim during 1979-2019 and (b, d, f) cloud incidence from CloudSat/CALIPSO during 2006-2011. The cloud incidence illustrates the likelihood of a cloud sensed by the satellite within a given atmospheric volume (for details see chapter 4).

station-based surface pressure measurements from Reykjavik in Iceland and Ponta Delgada in the Azores, Lisbon in Portugal or Gibraltar (Hurrell, 1995; Jones et al., 1997; Osborn, 2006). The major advantage of this definition is that it allows one to reconstruct the NAO index back to the 19th century using the available measurements from stations near the two centers of action. Monthly mean NAO records based on Gibraltar, Lisbon, and the Azores extend back to 1821, 1864, and 1865, respectively (Hurrell, 1995; Jones et al., 1997; Osborn, 2006, 2011; Cropper et al., 2015). An example of this NAO timeseries extending back to 1821 based on surface pressure records from Iceland and Gibraltar during the winter from December-February is shown in Fig. 2.4. Here we can easily notice the large interannual variability and the chaotic behaviour of the winter NAO. Several studies have attempted to extend the temporal length of the NAO timeseries further back in time by making use of proxy-based reconstructions, however the quality of the reconstructions depends on the data availability (Luterbacher et al., 1999; Glueck and Stockton, 2001; Cook et al., 2002; Schöne et al., 2003; Lehner et al., 2012). More modern pa-

leoclimate studies, in which climate models and proxy-data have been jointly used, reconstruct the NAO timeseries for the past millennium in order to investigate the low frequency climate variability in the North Atlantic ocean basin (Trouet et al., 2009; Ortega et al., 2015). Cornes et al. (2013) attempted to reconstruct the monthly NAO index back to 1692 by analysing digitized historical data from London and Paris, illustrating also the value of such datasets for similar studies. The major advantage of the station-based definition previously discussed is that it can reconstruct the NAO index records back in time by using available measurements or proxy data from stations near the two centers of action (Jones et al., 1997; Luterbacher et al., 1999; Cook et al., 2002; Cornes et al., 2013). The shortcomings of the station-based NAO timeseries is that it can be significantly affected by transient and small-scale weather phenomena that do not reflect the NAO state. Another major disadvantage of the station-based timeseries is that they are fixed in space, and, thus, are not able to capture the seasonal cycle as the two centers of action shift throughout the year (Hurrell et al., 2003).

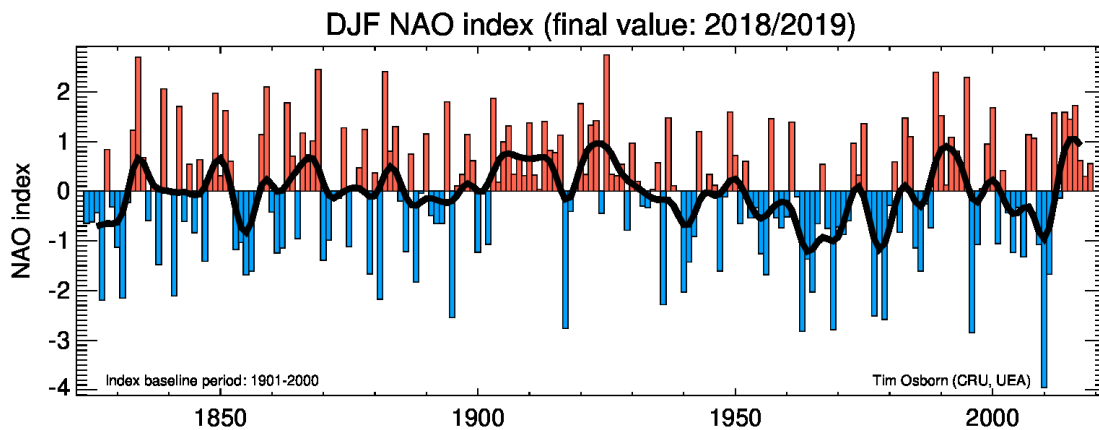


Figure 2.4.: Observed NAO index timeseries during the winter period December–February (DJF) from 1821–2019. The NAO index is based on the normalized surface pressure difference between Gibraltar and Reykjavik in Iceland. The timeseries has zero mean and unit variance over the 1901–2000 period. The thick black line shows smoothed values from a 10-year Gaussian-weighted filter. Figure as in Osborn (2011). Copyright ©Osborn, 2019 and Climatic Research Unit, University of East Anglia (can be accessed at <https://crudata.uea.ac.uk/cru/data/nao/viz.htm>)

In more modern studies with the development of gridded reanalysis data, the NAO is defined as the leading Empirical Orthogonal Function (EOF) of area-weighted sea-level pressure over the North Atlantic domain (90°W – 40°E , 20°N – 80°N). The weighting accounts for the decrease in area towards the pole. The EOF analysis, also known as Principal component analysis (PCA), introduced by Obukhov (1947) and following the work of Lorenz (1956) is one of the most widely used statistical techniques in atmospheric sciences. The aim of the EOF analysis is to reduce the large number of variables contained in a dataset to a dataset that contains fewer new variables. The new variables are linear combinations of the original ones and these combinations are selected in such a way to represent the maximum possible fraction of variability

of the original dataset. The linear combination can be achieved more effectively when the variables of the original dataset are highly correlated, as is the case with atmospheric pressure here. In this way the EOF analysis excludes unnecessary information within the initial dataset. For a more detailed description and applications of the EOF analysis the reader is referred to Wilks (2011). The NAO index is then derived by projecting the spatiotemporal sea-level pressure data onto this EOF-based NAO pattern (Hurrell et al., 2003; Hurrell and Deser, 2010). The EOF-based NAO provides a better overview of the full NAO spatial pattern and can also capture the annual cycle variation (Hurrell et al., 2003; Hurrell and Deser, 2010). A disadvantage of the EOF-based NAO is that it can be used only on gridded data and therefore its observational timeseries length is limited to the available reanalysis data (e.g., ERA5, ERA-Interim, NCEP/NCAR Reanalysis, JRA-55).

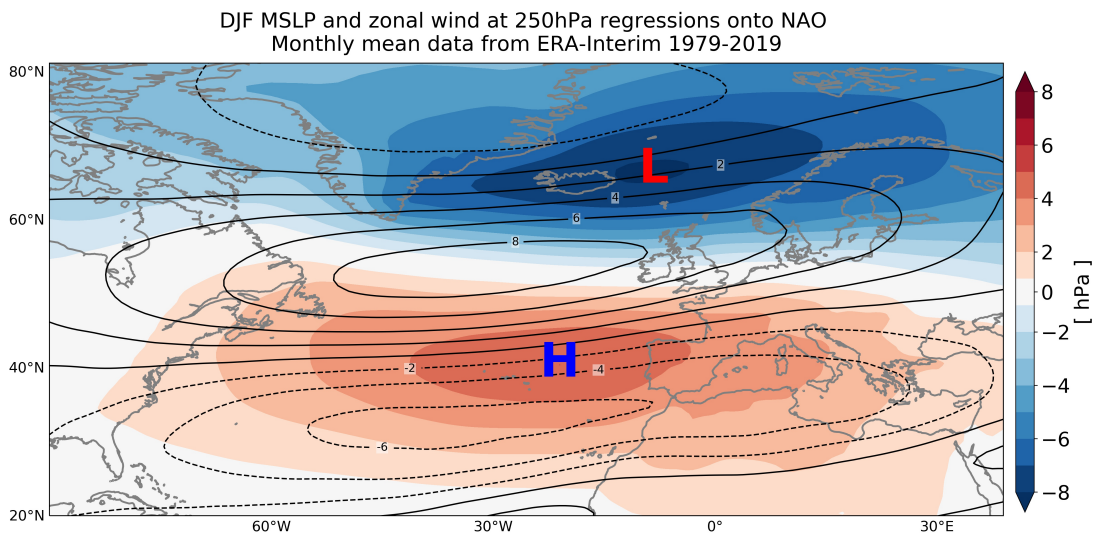


Figure 2.5.: December–February regressions of mean sea-level pressure (shading) and zonal wind at 250 hPa (contours) onto monthly mean North Atlantic Oscillation (NAO). Results are based on ERA-Interim reanalysis data from 1979-2019.

The map in Fig. 2.5 shows the spatial pattern of the EOF-based NAO expressed as mean sea-level pressure (MSLP) anomalies during the winter from December to February based on monthly mean data from ERA-Interim during 1979–2019. A positive phase of NAO is associated with negative anomalies of MSLP around the Iceland low and positive anomalies of MSLP over the Azores high (shading in Fig. 2.5), as well as a poleward shift of the jet stream (contours in Fig. 2.5). A negative phase of the NAO is associated with an opposite sign of MSLP anomalies and an equatorward shift of the jet stream. Note that the negative NAO does not necessarily imply a reversed pressure distribution but opposite sign of surface pressure anomalies. As previously illustrated in three examples (Fig. 1.2), these NAO-related MSLP anomalies are accompanied by substantial changes in temperature, precipitation and wind via modulating the latitudinal position of the eddy-driven jet and the storm track (Hurrell

and Deser, 2010; Woollings et al., 2010; Athanasiadis et al., 2010). The eddy-driven jet is found in areas of enhanced baroclinicity and arises due to eddy momentum flux convergence by transient midlatitude eddies (Hartmann, 2007; Li and Wettstein, 2012).

Another important aspect of the NAO influence on the weather and climate of the North Atlantic and northern hemisphere is the distinction between the NAO and the Northern Annular Mode. Early studies inspired by previous influential work of Rossby and Willett (1948) and Namias (1950) tried to connect the interannual variability of the northern hemisphere surface pressure and temperature with changes in the upper tropospheric and stratospheric mean circulation during the winter from a "zonal index" perspective using observations and gridded data (Lorenz, 1951; Kutzbach, 1970; Wallace and Gutzler, 1981; Trenberth and Paolino, 1981). This zonal index configuration that was later extensively examined by Baldwin et al. (1994), Perlwitz and Graf (1995) and Thompson and Wallace (1998, 2000) corresponds to the leading EOF of northern hemisphere wintertime monthly mean sea level pressure, to which they referred as the Arctic Oscillation (AO) or the Northern Annular Mode (NAM). They found that the winter AO/NAM exhibits a strong coupling between fluctuations of the lower-stratospheric polar vortex and the geopotential height anomalies in the mid-troposphere that strongly resemble the NAO pattern. However, the northern center of action is located over the Arctic and there is another dipole over the North Pacific. These findings led to a fast growing body of literature regarding the impact of the AO/NAM and how it differs from the NAO. Many following studies showed that the correlation between NAM and NAO is high and they are almost indistinguishable (Deser, 2000; Ambaum et al., 2001; Feldstein and Franzke, 2006). However, other studies showed that despite the high correlation between the AO/NAM and NAO impacts over the North Atlantic, there is weak temporal coherence between the North Atlantic and North Pacific (Deser, 2000), which is suggested to be explained by the differences in the jet dynamics between the two ocean basins (Ambaum et al., 2001).

On synoptic time-scales the NAO arises as an internal mode of the tropospheric circulation from eddy-mean flow interactions (Thompson et al., 2003; Hurrell et al., 2003; Barnes and Hartmann, 2010). Thompson et al. (2003) showed that the NAO owes its existence mainly to dynamics intrinsic to the extratropical troposphere, and Hurrell et al. (2003) in numerical experiments demonstrated that the atmospheric processes alone are able to produce NAO-like pattern of variability over the North Atlantic. In another influential paper on NAO dynamics, Feldstein (2003) found that the NAO undergoes a full life cycle within a time period of about 2 weeks and studied the mechanisms that drive its growth and decay. Feldstein (2003) showed that both high-frequency (less than 10 days) and low-frequency (more than 10 days) transient eddy momentum fluxes contribute to the NAO growth. In an idealized modeling study for the NAO-related anomalies life cycle Franzke et al. (2001) found the same time scale. Other studies illustrate the link between cyclonic and anticyclonic Rossby wave breaking events (McIntyre

and Palmer, 1985) and the NAO. In a modeling study Franzke et al. (2004), motivated by previous observational hypothesis of Benedict et al. (2004), showed that each NAO phase arises from a wave breaking event over the North Pacific and North Atlantic, while in another observational work Strong and Magnusdottir (2008) highlighted the sensitivity of these processes to the latitudinal position of the wave breaking. In a follow-up observational work Woollings et al. (2008) presented a different perspective of the NAO via illustrating the linkages between high-latitude atmospheric blocking induced by Rossby wave-breaking events and the NAO (Tyrllis and Hoskins, 2008; Yao and Luo, 2018).

External forcings such as the stratosphere (Baldwin and Dunkerton, 1999; Ambaum and Hoskins, 2002; Kidston et al., 2015; Hansen et al., 2017), the ocean (Visbeck, 2002; Knight et al., 2005) and sea-ice (Krahmann and Visbeck, 2003; Semenov and Latif, 2015) can also play a role in shaping the NAO state and lifecycle across different temporal scales. Recent studies illustrated that these external forcings can contribute to skilful dynamical (Müller et al., 2005; Scaife et al., 2014; Butler et al., 2016; O'Reilly et al., 2017; Weisheimer et al., 2017) and statistical (Wang et al., 2004; Hall et al., 2017; Dobrynin et al., 2018) seasonal predictions of the winter NAO. Others have studied the impact of the tropics on the NAO by investigating the teleconnections between the El Niño–Southern Oscillation (ENSO) or the Madden–Julian Oscillation (MJO) and the NAO (Wallace and Gutzler, 1981; Yadav and Straus, 2017; Barnes et al., 2019). These studies found that El Niño winters tend to be associated with a stronger and equatorwards shifted Pacific subtropical jet stream, enhanced cyclonic activity in the southeastern USA and a negative NAO (Li and Lau, 2012a,b; Zhang et al., 2019). More recent studies highlighted the importance of the tropical atmospheric heating due to convection associated with the Madden–Julian Oscillation (MJO) for the NAO predictability in both medium-range and seasonal predictions (Cassou, 2008; Yadav and Straus, 2017; Barnes et al., 2019; Madonna et al., 2019). Some of these forcings involve the interplay between the large-scale dynamics and diabatic processes such as cloud-radiative effects. In the following section we present some basic concepts regarding cloud-radiative effects and we discuss their coupling with the large-scale extratropical circulation.

2.2. Coupling between the extratropical circulation and cloud-radiative effects

The primary driver of the earth's general circulation is the uneven distribution of incoming and outgoing radiation on earth. More incoming shortwave radiation reaches the tropics compared to the higher latitudes, while the polar regions emit more longwave radiation back to space than they gain via incoming solar radiation. This induces differential radiative heating between the tropics and polar regions. One of the main implications of that energy imbalance is the formation of a temperature gradient between the tropics and the polar regions, with higher

temperatures in the tropics and lower temperatures in the polar regions. In combination with the earth's rotation this induces three large-scale atmospheric circulation cells in each hemisphere: the Hadley cell at low latitudes, the Ferrel cell at mid-latitudes and the Polar cell at high latitudes (Fig. 2.6). This large-scale atmospheric circulation and its seasonal variations set the environment for climate and weather variability (e.g., NAO, NAM). During the northern hemisphere winter the temperature gradient between the tropics and the polar regions is larger compared to summer, and the jet streams are stronger and more variable. The jet streams are important components of the large-scale circulation as they dominate the momentum, heat and moisture transport from the tropics to higher latitudes via troughs and synoptic-scale eddies (Hoskins and Valdes, 1990; Chang et al., 2002).

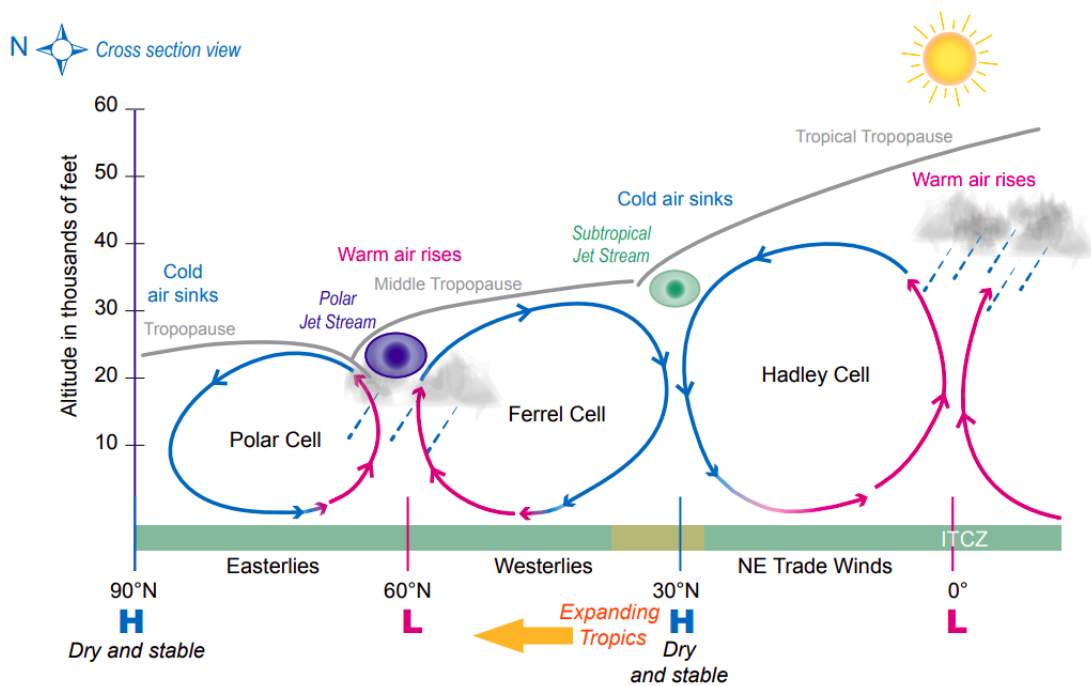


Figure 2.6.: Schematic illustrating the large-scale circulation of the atmosphere. The three main circulations are the: 1) Hadley cell over the low latitudes where air rises vertically and moves poleward at higher levels, while near the surface air moves towards the equator, 2) Ferrel cell over the midlatitudes where near the surface the air moves poleward and eastward, while at upper levels the air moves equatorward and westward, and 3) Polar cell over the high latitudes where the air near the surface moves equatorward while in the upper levels it moves poleward. This air movement introduces zonal bands of sinking and rising air. At about 30°N/S the descending motions introduce a high pressure (subtropical high) which leads to dry and hot weather. In the midlatitudes at about 50–60°N/S the rising motions introduce a low pressure that leads to rainy and stormy weather associated with the polar jet stream in the upper levels. Figure and caption adapted from Perlwitz et al. (2017) Copyright ©U.S. Global Change Research Program and U.S. National Weather Service

The influence of the large-scale atmospheric circulation on clouds has long been well recognized and examined in both satellite observations and modeling studies. Changes in the large-scale dynamics impact clouds by shaping the environment for vertical motions. In the

extratropics, large-scale cloud systems are found in the vicinity of upper-tropospheric baroclinic waves associated with cyclogenesis and their storm tracks (Ceppi and Hartmann, 2015). In particular, deep cloud structures occur within the extratropical cyclone's warm sector and the embedded warm conveyor belt, where strong large-scale ascent occurs (e.g., the comma shaped cloud bands in Fig. 2.7; Browning, 1986; Eckhardt et al., 2004). In an overview study based on satellite observations of clouds from CloudSat/CALIPSO (Mace et al., 2009), Li et al. (2014b) thoroughly examined relationships between the large-scale dynamics and clouds over all ocean basins and illustrated how cloud incidence varies with changes in atmospheric temperature, static stability, sea surface temperatures and vertical motions. Li et al. (2014b) showed that in the extratropics upper-level cloud fraction (6–12 km) increases for stronger ascending motion, a weaker upper-tropospheric stability and a lower tropopause temperature. Moreover, Li et al. (2014b) illustrated that in the lower troposphere of the extratropics cloud fraction (below 3 km) increases as the low-level static stability and descending motions increase (Grise and Medeiros, 2016).

Other studies using a compositing method illustrated the cloud structures related to midlatitude cyclones and their accompanied warm and cold sectors in both satellite observations (Lau and Crane, 1995; Field and Wood, 2007; Naud et al., 2010; Govekar et al., 2014) and models (Field et al., 2008, 2011; Bodas-Salcedo et al., 2012; Govekar et al., 2014; Hawcroft et al., 2017; Naud et al., 2019). Wall et al. (2017) in a joint observational and modeling study illustrated the sensitivity of cloud properties to meteorology using cloud observations from CERES-CloudSat/CALIPSO-MODIS (CCCM) dataset (Kato et al., 2010) and highlighted the cloud biases in General Circulation Models (GCMs) using numerical simulations with the Community Atmosphere Model, version 5 (CAM5; Neale et al., 2011). Hawcroft et al. (2017) using composites of cloud fields around midlatitude cyclones from satellite observations, reanalysis and model data showed large biases which can influence the evolution and track of cyclones (Willison et al., 2013). In another recent observational study using cloud products from MODIS, Madenach et al. (2019) investigated the interannual variability of the cloud vertical distribution over the tropical Atlantic and showed how teleconnections between ENSO (Bjerknes, 1969; Timmermann et al., 2018) and tropical Atlantic atmospheric and sea surface temperatures influence clouds distribution and variability. Tropical clouds play a key role not only for the tropical but also for the extratropical circulation on various temporal scales (Mo and Livezey, 1986; Tyrrell et al., 1996; F. Panagiotopoulos et al., 2002; Liu and Alexander, 2007; Stan et al., 2017).

Nevertheless, clouds are not simply a result of the circulation. There is increased evidence that clouds impact the circulations in which they are embedded and shape the weather and climate by regulating the latent and radiative heating in the atmosphere (Slingo and Slingo, 1988; Ramanatha et al., 1989; Hartmann et al., 1992; Fasullo and Trenberth, 2008). Clouds

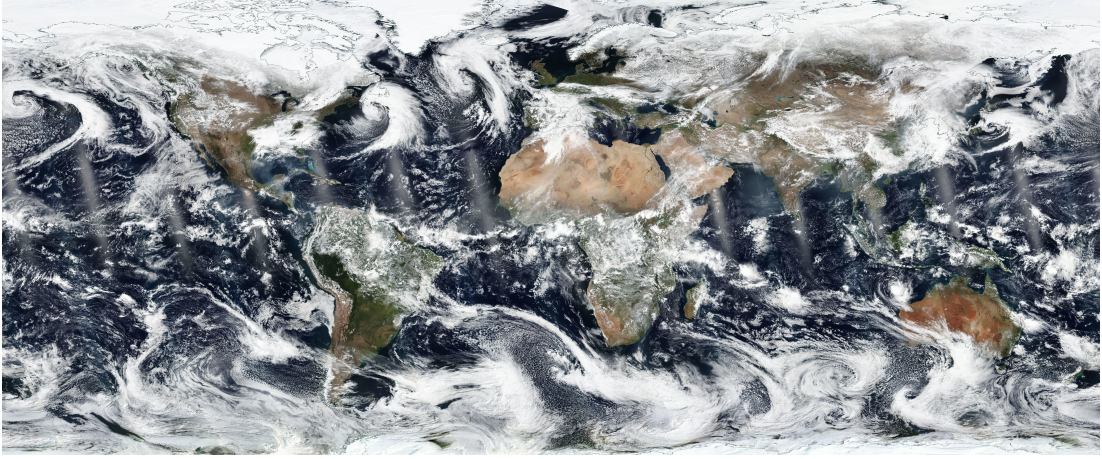


Figure 2.7.: Composite of satellite images from the Visible Infrared Imaging Radiometer Suite (VIIRS) Corrected Reflectance Imagery instrument on board NASA/NOAA Suomi National Polar orbiting Partnership (Suomi NPP) satellite on April 19, 2020. The image is accessible via <https://worldview.earthdata.nasa.gov/>

and their radiative effects are one of the major sources of uncertainty in climate projection of the earth's radiative balance (IPCC, 2013; Stocker et al., 2013; Bony et al., 2006; Sanderson et al., 2008; Ceppi et al., 2012; Vial et al., 2013; Bony et al., 2015; Zelinka et al., 2020). Recent work demonstrated the importance of clouds and their radiative effects for the mean atmospheric circulation and its response to global warming. The last two decades there has been substantial advancement in remote sensing of the earth's energy budget, clouds and their radiative effects (Stephens and Kummerow, 2007; L'Ecuyer et al., 2008; Loeb et al., 2009; Oreopoulos and Rossow, 2011; Haynes et al., 2013; Rutan et al., 2015; Oreopoulos et al., 2017; Loeb et al., 2018) as well as in climate modeling (Simpkins, 2017). These advancements led to a fast growing body of literature on the impact of cloud radiative effects (CRE) on the current and future large-scale atmospheric circulation.

Atmospheric CRE (ACRE) at a given atmospheric pressure level are defined as the all-sky minus the clear-sky radiative heating rates (in units of K/d). The all-sky and clear-sky radiative heating rates are computed from the longwave and shortwave radiative fluxes (in units of W/m^2). ACRE measure the impact of cloud-radiative heating/cooling on atmospheric temperatures and are calculated as (Haynes et al., 2013)

$$\left. \frac{dT}{dt} \right|_{\text{CRE}} = \left. \frac{dT}{dt} \right|_{\text{all-sky}} - \left. \frac{dT}{dt} \right|_{\text{clear-sky}}, \quad (2.1)$$

where the all-sky and clear-sky heating rates are calculated as

$$\left. \frac{dT}{dt} \right|_{\text{all-sky/clear-sky}} = - \frac{1}{\rho c_p} \frac{dF_{\text{all-sky/clear-sky}}}{dz}. \quad (2.2)$$

T is the air temperature and ρ is the air density, c_p is the specific heat of dry air at constant pressure, F is the net (longwave + shortwave) radiative flux, z is altitude, and t is time. Vertically-integrated ACRE is calculated from the difference of top-of-atmosphere (TOA) and bottom-of-atmosphere (BOA) fluxes and is expressed in units of W/m^2 .

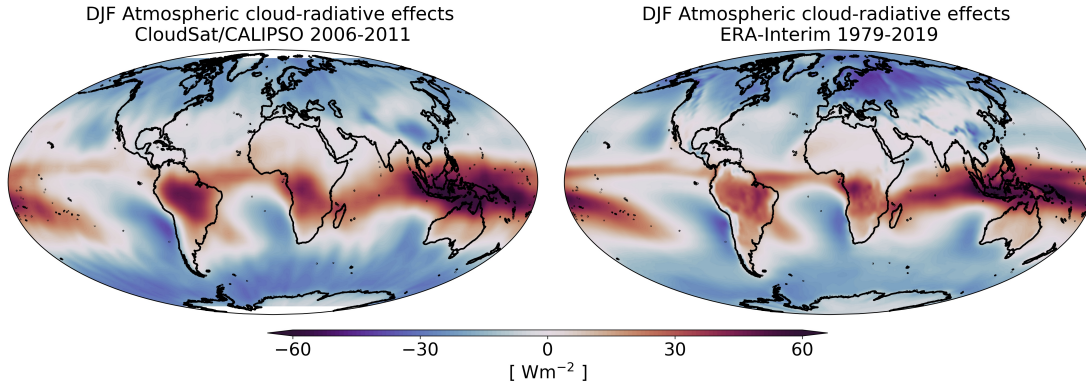


Figure 2.8.: DJF climatology of atmospheric cloud-radiative effects (ACRE) from CloudSat/CALIPSO during 2006–2011 (left) and from ERA-Interim during 1979–2019 (right).

From a climatology perspective during the northern hemisphere winter from December–February, ACRE satellite observations from CloudSat/CALIPSO and reanalysis data from ERA-Interim illustrate that clouds heat the atmosphere over the tropics as well as over the storm tracks, while clouds cool the atmosphere over the higher latitudes (Fig. 2.8). A comparison of ACRE between reanalysis data and satellite retrievals in Figure 2.8 shows qualitatively consistent patterns for most areas, however substantial differences are evident in some regions. The ACRE pattern is driven by the vertical distribution of clouds within the atmosphere. Oreopoulos et al. (2017) in a comprehensive analysis of cloud vertical structure (CVS; Rossow and Zhang, 2010; Tselioudis et al., 2013) classes at global scales combining observations from active space-based sensors illustrated the linkages between the CVS classes and CRE at the top-of-atmosphere (TOA) and bottom-of-atmosphere (BOA), as well as within the atmosphere in terms of ACRE. Figure 2.9 shows that areas where high-level clouds occur are associated with column-mean ACRE heating, while areas where only mid- and low-level clouds occur are linked to column-mean ACRE cooling. However, the magnitude of ACRE varies substantially depending on the vertical distribution and overlap of different cloud types. For example, when clouds extend between different levels the ACRE magnitude tends to be larger compared to when an overlap of clouds occurs. This characteristic of ACRE could also partly explain the discrepancies between observations and reanalysis data (Fig. 2.8). In an earlier study Su et al. (2010) using model simulations and satellite observations attempted to link ACRE with different dynamical regimes based on vertical motions at 500 hPa, and highlighted the model deficiencies in properly simulating clouds and their ACRE.

2.2. Coupling between the extratropical circulation and cloud-radiative effects

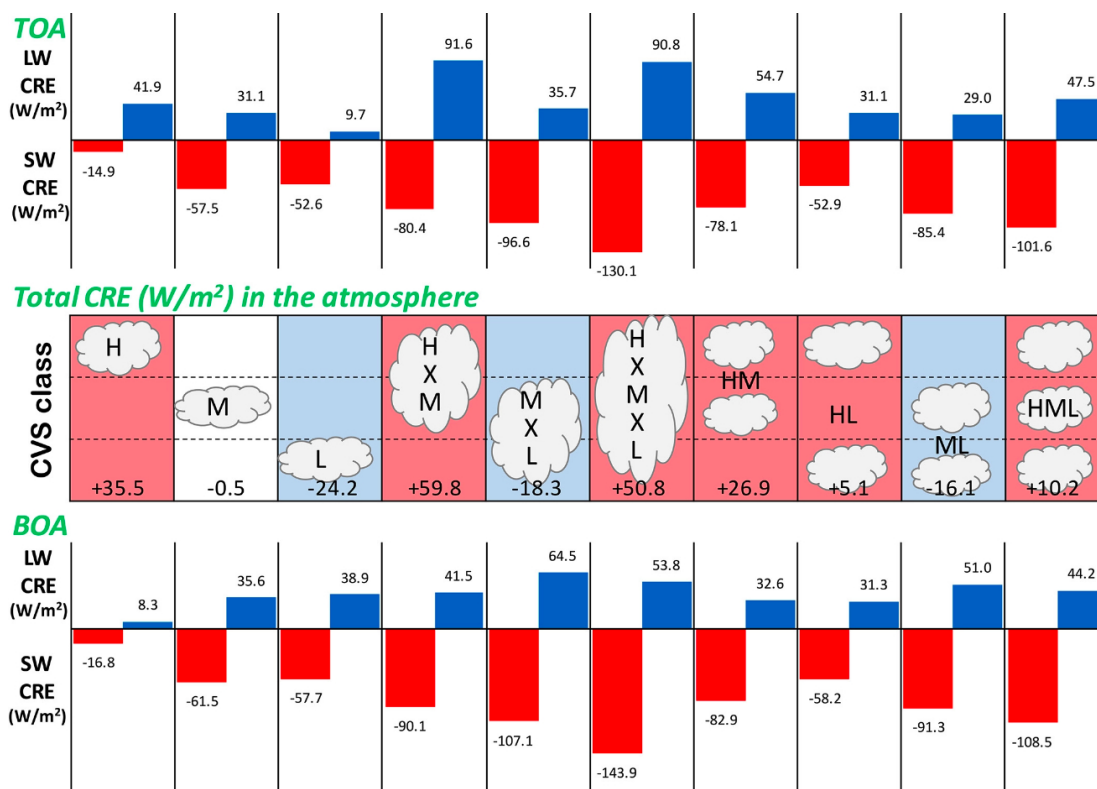


Figure 2.9.: Schematic diagram summarizing the longwave and shortwave CRE for various CVS classes (top panel) at the top-of-atmosphere (TOA), (bottom panel) at the bottom-of-atmosphere (BOA) as well as (middle panel) the net ACRE within the atmosphere. The middle panel illustrates the CVS classes. Figure from Oreopoulos et al. (2017). Copyright ©2017. American Geophysical Union.

Clouds live on a range of spatiotemporal scales, and the spatiotemporal variations of ACRE can impact the mean circulation. Observational studies have attempted to quantify the response of clouds and TOA CRE to dynamical changes in satellite retrievals but show diverse results. Tselioudis et al. (2016) using satellite observations illustrated the linkages between high-level cloud changes and meridional shifts of the Hadley cell and the jet streams. Over the North Atlantic they showed that poleward shifts of high-level clouds either due to the Hadley cell or due to the jet stream are linked to longwave TOA CRE heating in the higher latitudes and longwave TOA CRE cooling in the lower latitudes, while the opposite occurs for shortwave TOA CRE. In other similar studies Grise and Medeiros (2016) and Zelinka et al. (2018) using satellite observations and model simulations studied the relationships between TOA CRE and jet shifts and illustrated that cloud changes follow the changes in vertical motions. However, they showed that TOA CRE in the lower latitudes of the extratropical ocean basins during a poleward shift of the jet stream are poorly represented in models primarily due to biases in vertical motions over these areas.

Previous present-day model climate studies, where clouds are made transparent to radiation (Stevens et al., 2012) showed that the inclusion of ACRE leads to a consistent strengthening of

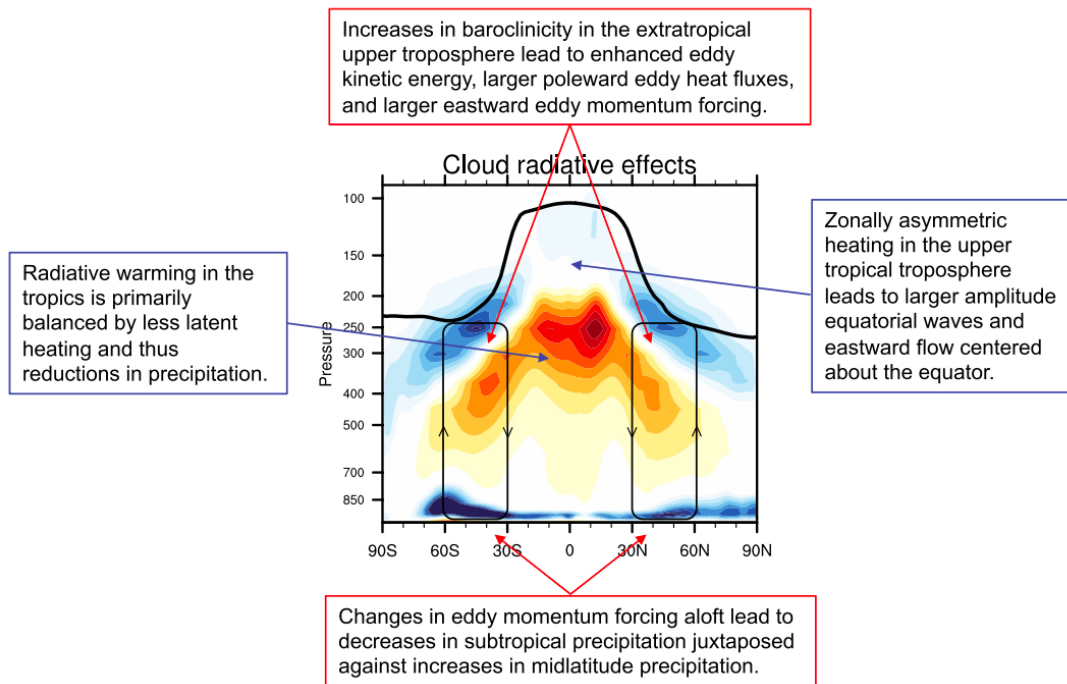


Figure 2.10.: Schematic diagram summarizing the basic impacts of atmospheric cloud-radiative effects (ACRE) on the zonal-mean circulation, as revealed in Fig. 4c of Li et al. (2015). The shading indicates the ACRE impact in the clouds-on experiment; the solid line indicates the long-term mean tropopause height from the clouds-on experiment. Figure from Li et al. (2015). Copyright ©2015 American Meteorological Society

the Hadley cell (Harrop and Hartmann, 2016; Albern et al., 2018) and meridional shifts of the extratropical jets (Li et al., 2015; Watt-Meyer and Frierson, 2017). In a modeling study Li et al. (2015) illustrated that the inclusion of ACRE increases the upper-tropospheric baroclinicity in the extratropics, which in turn leads to increased eddy kinetic activity, poleward eddy heat fluxes and eastward eddy momentum forcing. These changes induce a dipole of zonal winds which in turn strengthens the dipole of vertical motions and subsequently the dipole of precipitation between the higher and lower midlatitudes (Fig. 2.10). In another multi-model study Watt-Meyer and Frierson (2017) using an idealized aquaplanet setup showed that the eddy-driven response to the inclusion of ACRE exhibits large discrepancies among the models, with some models showing an equatorward shift and other models showing a poleward shift. In an attempt to understand these discrepancies Watt-Meyer and Frierson (2017) illustrated that the overall response of the circulation depends on the opposing impacts of the inclusion of ACRE in the tropics and the extratropics. Their modeling work showed that tropical ACRE shift the eddy-driven jet equatorwards while extratropical ACRE shift the eddy-driven jet polewards (Fig. 2.11). All these observational and modeling studies together highlight the importance of ACRE for the present-day mean circulation of the extratropics.

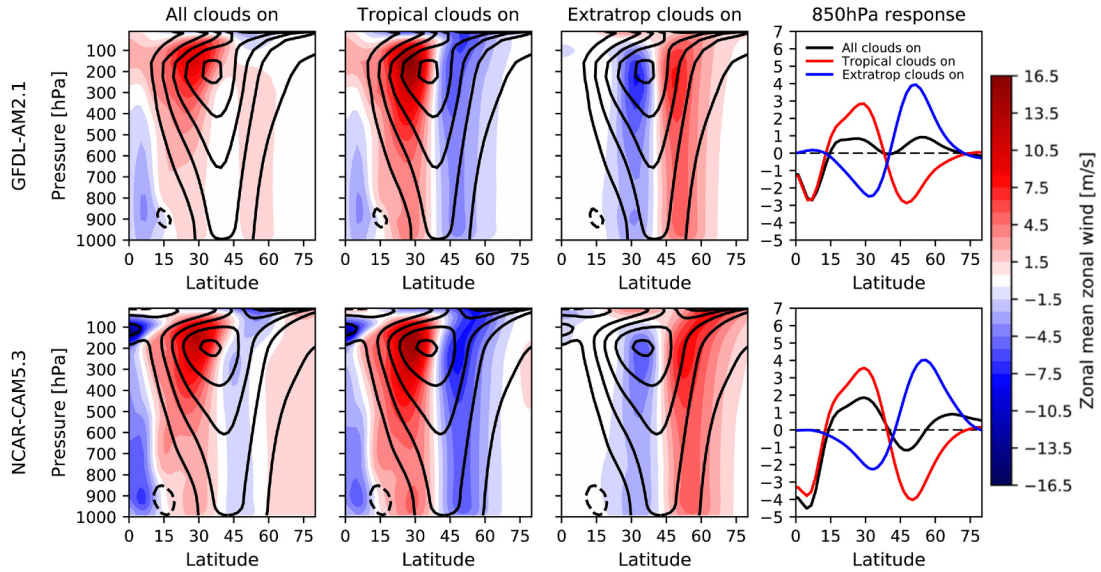


Figure 2.11.: The zonal-mean zonal wind without the inclusion of ACRE (black contours) and the wind response to the inclusion of ACRE (shading) for the GFDL-AM2.1 (top) and NCAR-CAM5.3 aquaplanet models (bottom). The rightmost column illustrates the difference in zonal wind at 850 hPa between the simulations with and without ACRE. Figure from Watt-Meyer and Frierson (2017) ©2017. American Geophysical Union.

Recent modeling work showed that cloud-radiative interactions are not only substantial in contributing to model uncertainties in future global warming and climate sensitivity (Bony et al., 2015; Ceppi and Hartmann, 2015, 2016; Zelinka et al., 2020), but also constitute a key driver of the mean circulation response (Voigt and Shaw, 2015, 2016; Ceppi and Shepherd, 2017; Voigt et al., 2019). Previous studies illustrated that both changes in surface cloud-radiative heating from low-level clouds (Ceppi and Shepherd, 2017) and changes in atmospheric cloud-radiative heating from high-level clouds (Voigt et al., 2019; Li et al., 2019) are shaping the mean circulation response to global warming. This impact is mostly evident in the extratropical circulation response, where recent findings demonstrated that changes in cloud-radiative heating most likely force a poleward shift of the jet streams and storm tracks (Chang et al., 2012; Barnes and Polvani, 2013; Ceppi et al., 2014; Shepherd, 2014; Simpson et al., 2014; Voigt and Shaw, 2015; Vallis et al., 2015; Shaw et al., 2016; Ceppi and Hartmann, 2016; Albern et al., 2019). In a recent study Voigt et al. (2019) using three global models found that both the surface and atmospheric pathways are equally contributing to the poleward circulation expansion, and in fact half of the total circulation response was attributed to the changes of cloud-radiative heating from high-level clouds. However, their work also illustrated the model shortcomings in properly representing high-level clouds and their associated ACRE, where the models exhibit large differences among them as well as with observations. These model issues also highlight the need for reducing cloud-radiative heating deficiencies in order to improve future climate projections. As a whole, these studies illustrate the need for understanding and

constraining the radiative impact of clouds on the circulation (Bony et al., 2015). This need is exacerbated by the difficulties of current global climate models to adequately represent clouds and their radiative effects.

Although the coupling of the extratropical circulation with clouds and their radiative effects is well examined in previous literature for both the present-day and future climates, little research has been done regarding the impact of clouds on internal synoptic circulation variability. In the following section we provide an overview of the state of the art in NAO persistence and its coupling to diabatic processes.

2.3. Coupling between the NAO and diabatic processes

The persistence of the NAO, or more generally the annular modes and the extratropical jet streams, was mostly examined in past studies from the perspective of the adiabatic circulation and dynamical feedbacks involving eddies and Rossby wave breaking (Lorenz and Hartmann, 2001; Feldstein, 2003; Franzke et al., 2004; Barnes and Hartmann, 2010).

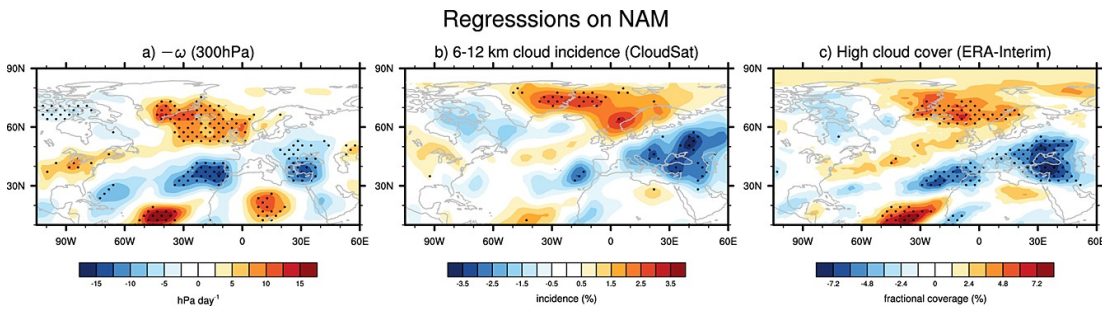


Figure 2.12.: Monthly mean NAM/NAO regressions of (a) pressure velocity at 300 hPa (positive values denote upward motions), (b) 6–12 km cloud incidence, and (c) high-level cloud fraction. Pressure velocity in (a) and high-level cloud fraction in (c) are based on ERA-Interim reanalysis data and cloud incidence in (b) is based on CloudSat/CALIPSO data. The NAM/NAO index is standardized. Stippling denotes statistical significant results. Figure from Li et al. (2014a) ©2014. American Geophysical Union.

However, there is evidence that diabatic processes can also modulate the NAO variability. Previous studies illustrated that diabatic processes, such as latent heating, can modify the NAO persistence (Hoskins and Valdes, 1990; Greatbatch and Jung, 2007; Xia and Chang, 2014; Woollings et al., 2016). Hoskins and Valdes (1990) concluded that latent heating within the storm tracks was feeding back to maintain baroclinicity and in that way they described the storm tracks as being self-sustaining (Robinson, 2006). Investigating the zonal index variability over the southern hemisphere Xia and Chang (2014) in model experiments showed that diabatic heating associated with precipitation anomalies acts to reduce the temperature gradient across the jet anomaly and leads to a decrease in eddy generation, constituting a negative feedback to the zonal index. In a later climatological study, Greatbatch and Jung (2007), using model

simulations where the model was forced with a NAO-related diabatic heating, showed a weak negative feedback to the NAO and the storm tracks. However, the response was not spatially coherent with the NAO centers of action. In a more recent study Woollings et al. (2016) using observationally constrained analysis data investigated the very exceptional negative NAO winter of 2010 and found a positive feedback of latent heating to the NAO variability and the storm track.

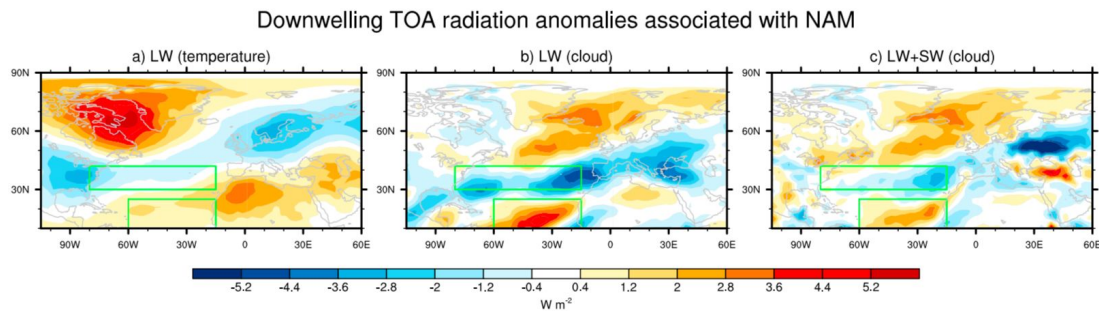


Figure 2.13.: TOA downwelling radiation anomalies associated with the NAM/NAO due to (a) temperature (longwave), (b) clouds (longwave), and (c) clouds (longwave + shortwave). Green boxes denote regions where the TOA radiation anomalies due to clouds coincide with the TOA radiation changes due to changes in temperature. Figure from Li et al. (2014a) ©2014. American Geophysical Union.

While the importance of CRE for the present-day mean circulation of the extratropics and its long-term climate change response is well established, at least from a modeling perspective, little research has been done regarding a possible impact of CRE on the extratropical circulation on synoptic time-scales. There is reason to believe that besides latent heating, radiative heating from clouds can affect the NAO persistence. This idea is motivated by observational and modeling studies that highlighted the close coupling between CRE and the extratropical circulation across a range of time-scales. This includes observational studies that have shown the impact of the extratropical circulation, i.e. the position of the extratropical jet, static stability and large-scale vertical motion, on the patterns of cloud and CRE based on internal circulation variability on time-scales of days to weeks (Grise et al., 2013; Grise and Polvani, 2014; Grise and Medeiros, 2016; Li et al., 2014b; Tselioudis et al., 2016; Hawcroft et al., 2017; Zelinka et al., 2018). Schäfer and Voigt (2018) proposed that CRE weaken idealised extratropical cyclones, which would seem to suggest a possible impact on storm tracks, the jet stream, and hence the NAO. In another modeling study Grise et al. (2019) found that CRE lead to a small but statistically significant weakening of extratropical storm tracks and cyclones. Moreover, their work showed that this negative feedback of CRE arises due to changes in low-level static stability induced by CRE (Grise et al., 2019). In an observational study Li et al. (2014a) investigated the linkages between clouds and the Arctic Oscillation (to which they refer to as the Northern Annular Mode/North Atlantic Oscillation; NAM/NAO) on monthly time-scales using satellite observations from CloudSat/CALIPSO and ECMWF ERA-Interim reanalysis data. Li

et al. (2014a) found that the NAM/NAO is associated with robust changes in high-level clouds which are in line with large-scale vertical motions (Fig. 2.12). Their analysis showed that a positive phase of the NAO is associated with increased high-level clouds along the storm track region and over the subpolar Atlantic, and decreased high-level clouds over the lower midlatitudes of the Atlantic. These changes are in line with enhanced upward motions over the higher latitudes and enhanced downward motions over the lower latitudes. Moreover, they showed that these high-level cloud changes lead to robust changes in TOA CRE with anomalous heating over the higher latitudes and anomalous cooling over the lower latitudes. Furthermore, Li et al. (2014a) argued that this meridional anomalous TOA CRE dipole in the zonal mean works against the temperature anomalies accompanying the NAM/NAO (Fig. 2.13), and they interpreted this as a negative cloud-radiative feedback that shortens the NAM/NAO time-scale. Over the North Atlantic region, however, evidence for a negative cloud-radiative feedback only emerged in the lower mid-latitude region near the Azores. This, and the fact that the North Atlantic storm track and jet stream are tilted meridionally, suggests that a regional latitude-longitude perspective is warranted, and a more thorough investigation of these interactions is necessary.

3. Research questions

The NAO is the dominant mode of synoptic-scale variability over the North Atlantic region and plays a key role for the weather and climate of the neighbouring continental areas. In the previous chapter we introduced the pathways of different drivers that give rise to the NAO growth, and processes that are linked to its persistence via complex interactions. These play a key role for the NAO predictability and constitute a considerable challenge for both operational weather forecasters and numerical weather prediction systems on a wide range of temporal scales from a few days to seasons. Advancing our understanding of processes linked to the persistence of the NAO and its predictability can improve medium-range weather forecasts, subseasonal-to-seasonal predictions and climate projections which are essential to society for both civil protection and economic growth. The aim of this thesis is to advance understanding on how the NAO couples to diabatic processes by assessing the relative role of the latter for the NAO dynamics on synoptic time-scales. In this chapter we summarize the research questions that we address in this thesis.

Motivated by the hypothesis of Li et al. (2014a) that top-of-atmosphere cloud-radiative effects (CRE) act as a negative feedback on the NAO and damp the NAO variability, we study the coupling between the NAO and atmospheric CRE (ACRE) on synoptic time-scales and quantify the importance of ACRE relative to the large-scale dynamics and the total diabatic heating (chapters 5 and 6). This work addresses the following research questions (RQ):

RQ 1) How does the NAO impact clouds and their radiative effects?

RQ 2) To what extent are the NAO-related changes in ACRE robust in observations, reanalysis and model simulations?

RQ 3) What is the role of the NAO-related ACRE anomalies for the dynamics of the NAO on synoptic time-scales, and how does the ACRE impact compare to the impact of total diabatic heating?

To address the first research question we study the linkages between the NAO and clouds as well as their associated radiative effects in satellite observations from CloudSat/CALIPSO, CERES-SYN1deg, CERES-EBAF and GERB/SEVIRI, ECWMF ERA-Interim reanalysis data and numerical simulations in ICON. We investigate the spatial and vertical distribution of cloud changes linked to the NAO and the impact of these cloud changes on ACRE. A description of the data and methods that we use for this analysis is given in chapter 4. Chapter 5 addresses

the research questions from the perspective of observations and reanalysis data, while chapter 6 studies them based on ICON simulations.

Regarding the second research question, based on our analysis of the ACRE changes linked to the NAO in observations and numerical simulations we discuss the robustness of these findings. In this part, we focus on a thorough investigation of NAO-related ACRE anomalies over the two centers of action of the NAO, namely the Iceland low and the Azores high.

After having investigated the observed and modeled linkages between the NAO and ACRE, we quantify the role of the NAO-related ACRE changes for the short-term dynamics of the NAO. Here, based on a diagnostic approach using the surface pressure tendency equation in ERA-Interim data (chapter 5) and ICON simulation (chapter 6), we quantify the relative role of ACRE compared to the large-scale dynamics as well as other diabatic processes for the NAO dynamics. We address to what extent the reanalysis-based results from the surface pressure tendency equation are reproduced in the ICON simulations. Finally, we perform ICON sensitivity simulations to explicitly test the NAO impact of ACRE and total diabatic heating diagnosed from the surface pressure tendency equation.

The methods and data used in chapters 5 and 6 are described in detail in chapter 4. The thesis closes with overall conclusions and an outlook in chapter 7.

4. Data and methods

In this chapter, we provide a description of the data and methods that are used in this thesis in order to address the research questions introduced in chapter 3. In the first part of this chapter, we describe the satellite observations from CloudSat/CALIPSO, CERES and GERB/SEVIRI (4.1) and the ECMWF ERA-Interim reanalysis data (4.2) that we discuss in chapter 5. Then we introduce the numerical simulations in ICON (4.3) that we discuss in chapter 6. For each dataset a brief overview of the postprocessing is also provided. In 4.4 we describe the NAO index that we use in the observational and modeling work. Furthermore, the diagnostic framework of the surface pressure tendency equation (PTE) that we use to assess the relative role of adiabatic and diabatic processes for the NAO dynamics is illustrated (4.5). Finally, we illustrate the regression analysis that we use to assess the linkages between the NAO and various fields such as clouds, ACRE and temperature, as well as the method that we use to address the statistical significance of the regressions (4.6).

4.1. Satellite observations

4.1.1. CloudSat/CALIPSO cloud incidence

We use cloud observations for the years 2006 to 2011 from the 2B-GEOPROF-LIDAR product (version P2R04; Mace et al., 2009), which combines retrievals from the National Aeronautics and Space Administration (NASA) CloudSat Cloud Profiling Radar (CPR; Stephens et al., 2008) and the NASA–Centre National d’Études Spatiales (CNES) Cloud–Aerosol Lidar and Infrared Pathfinder Satellite Observations (CALIPSO; Winker et al., 2010). CloudSat’s CPR is a non-scanning nadir-pointing space-borne W-band radar operating at 94GHz frequency and provides reflectivity profiles with along and cross-track horizontal resolutions of about 1.7 and 1.4 km, respectively, and a vertical resolution of 240m. CALIPSO’s lidar collects footprints with a horizontal resolution of 70m and a vertical resolution of 30 m. The vertical profiles from the 2B-GEOPROF-LIDAR product are provided at the CloudSat’s CPR resolution within 82°N/S (Tanelli et al., 2008; Mace et al., 2009; Verlinden et al., 2011). The main advantage of this synergy is that it combines the capacity of CloudSat’s CPR to probe optically thick hydrometeor layers with CALIPSO’s lidar to detect optically thin hydrometeor layer whose weak reflectivity is not detectable by CloudSat’s CPR. This allows us to characterize the vertical

distribution of hydrometeors along the satellite's orbit. However, there are many limitations in these retrievals due to the instruments, such as the inability to detect hydrometeors from the surface up to 1 km as a result of clutter in the radar measurements, the low spatial resolution that leads to missing small-scale clouds, CPR's limitation to detect weak reflectivities, and the high sensitivity of CALIPSO's lidar during daylight (Marchand et al., 2008; Mace et al., 2009). Another major limitation of this product is the spatiotemporal sampling compared to other satellite observations, such as those from geostationary satellites. Nevertheless here we focus on large-scale changes and assume that our profiles are representative of the large-scale cloud fields. An example of vertical profiles of cloud fraction for one orbit is given in Fig. 4.1a, and the path of CloudSat/CALIPSO orbit is shown in Fig. 4.1c.

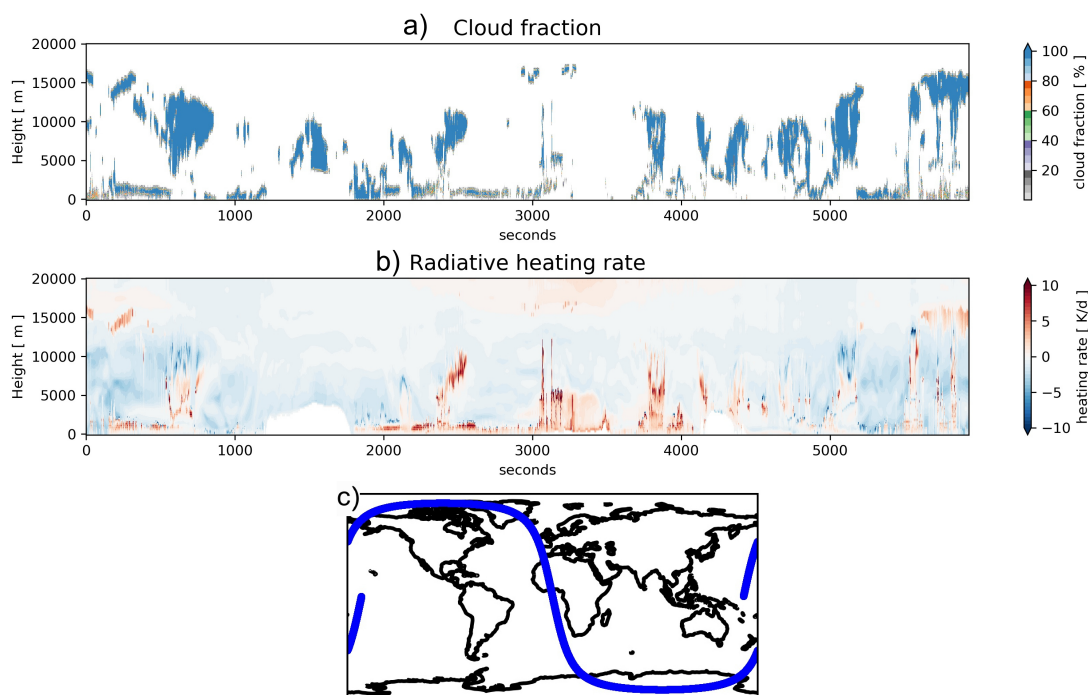


Figure 4.1.: Cloud fraction (a) and all-sky radiative heating (b) on June 29, 2007 from CloudSat/CALIPSO. (c) The orbit of the satellites. The masked areas near the surface in (b) are due to elevated surface over Antarctica and Greenland. Results are based on 2B-GEOPROF-LIDAR product (version P2R04 Mace et al., 2009) and 2B-FLXHR-LIDAR product (version P2R04; L'Ecuyer et al., 2008; Henderson et al., 2013)

Here we analyse cloud incidence. Cloud incidence is the likelihood that within a given atmospheric volume the satellite senses a cloud. Following Verlinden et al. (2011) and Li et al. (2014a) we use cloud incidence in a binary framework. If within a given atmospheric volume, the cloud fraction is larger than 50%, then we assign a "1", otherwise if the cloud fraction is less than 50% we assign a "0". Then, the resulting values are averaged over a given time period and depending on the analysis over a given volume. For example, the mean cloud incidence between 7 and 12 km height is calculated by averaging the cloud incidence over all volumes

within this layer. A mean cloud incidence value of 30% indicates that at least half of the volume was cloudy 30% of the time. Due to the spatiotemporal limitations of CloudSat/CALIPSO on daily time-scales (Mace et al., 2009; Li et al., 2014a), we bin the vertical profiles into a $2.5^\circ(\text{longitude}) \times 2.5^\circ(\text{latitude}) \times 240 \text{ m}$ (vertical) grid, and average the binned data over time periods of 5 days.

4.1.2. CloudSat/CALIPSO cloud-radiative effects

In addition to cloud incidence we are also interested in the radiative heating associated with these clouds (Fig. 4.1b). For that purpose we use the CloudSat/CALIPSO 2B-FLXHR-LIDAR product over the time period 2006-2011 (version P2R04; L'Ecuyer et al., 2008; Henderson et al., 2013). The 2B-FLXHR-LIDAR product is based on radiative transfer calculations that make use of the CloudSat/CALIPSO cloud retrievals and allows for a detailed look at the vertical structure of atmospheric cloud-radiative effects (ACRE). ACRE at a given atmospheric pressure level are defined as the all-sky minus the clear-sky radiative heating rates (in units of K/d). We compute the all-sky and clear-sky radiative heating rates from the longwave and shortwave radiative fluxes (in units of W/m^2) at every 240m height level provided by 2B-FLXHR-LIDAR, and by using auxiliary data from the ECMWF-AUX product. The ECMWF-AUX product provides atmospheric state variable data interpolated onto the same spatiotemporal resolution of a CloudSat/CALIPSO track. ACRE is calculated as per equation (2.1) and the all-sky and clear-sky heating rates are calculated as per equation (2.2) where the air temperature and the air density are derived from the ECMWF-AUX product (CIRA, 2007), while the altitude, and time are derived from 2B-FLXHR-LIDAR product. ACRE is binned in the same way as cloud incidence and averaged over time-periods of 5 days. Vertically-integrated ACRE is calculated from the difference of top-of-atmosphere (TOA) and bottom-of-atmosphere (BOA) fluxes provided by the 2B-FLXHR-LIDAR product and is expressed in units of W/m^2 .

4.1.3. CERES and GERB/SEVIRI cloud-radiative effects

To test the robustness of the CloudSat/CALIPSO results we also analyse CERES (Clouds and Earth's Radiant Energy System) and GERB/SEVIRI (Geostationary Earth Radiation Budget/Spinning Enhanced Visible and InfraRed Imager) observations of TOA and BOA cloud-radiative effects. The CERES project aims to monitor the earth's radiation budget through the CERES instruments that are on board of polar-orbiting satellites (TRMM, Terra, Aqua, S-NPP, NOAA-20). A CERES instrument is a narrow field-of-view scanning radiometer with nadir footprint size of 10–24 km depending on the platform and different scanning options. CERES provides measurements of the reflected solar radiation and emitted thermal radiation from the earth to space, across all wavelengths between the ultraviolet and far-infrared. CERES ob-

Table 4.1.: Summary of the satellite data used in chapter 5. The middle column shows the data availability and the right column shows the temporal resolution of each dataset.

Satellite data	Data availability	Temporal resolution
CloudSat/CALIPSO	2006–2011	5-day
CERES-SYN1deg	2000–2017	5-day
GERB/SEVIRI	2006–2011	monthly
CERES-EBAF	2002-2017	monthly

servations, together with higher spatiotemporal resolution data from other polar-orbiting and geostationary satellites are used to derive the earth’s radiation budget. Among these products is GERB/SEVIRI which provides estimates of TOA and BOA broadband radiative fluxes derived from GERB broadband and SEVIRI narrowband radiometer sensors onboard the Meteosat second generation (MSG) satellites.

Here we use the CERES-SYN1deg product edition 4A (Rutan et al., 2015) for daily-mean CRE at the TOA and BOA. Apart from CERES observations, CERES-SYN1deg makes use of cloud observations from MODIS and geostationary satellites, and CRE at the BOA are derived from radiative transfer calculations. Again, we calculate the vertically-integrated ACRE from the CRE difference at the TOA and BOA. We use CERES-SYN1deg for the same 2006 to 2011 period for which CloudSat/CALIPSO is available, as well as for a longer period from 2000 to 2017.

We further use monthly-mean fields from CERES-EBAF edition 4.0 (Loeb et al., 2018) for 2002 to 2017 and from GERB/SEVIRI (Harries et al., 2005) for years 2006-2011. For CERES-EBAF we analyse longwave and shortwave CRE at the TOA and BOA, from which we derive vertically-integrated ACRE. For GERB/SEVIRI, we use TOA and BOA all-sky and clear-sky longwave radiative fluxes. TOA fluxes are available at 0.1° spatial resolution, while BOA fluxes are available at 0.05° . We remap the the fluxes onto a common 0.1° grid and derive TOA and BOA longwave CRE as well as vertically-integrated longwave ACRE.

A summary of the satellite observations that we use in chapter 5 is given in table 4.1.

4.2. ERA-Interim reanalysis data

We use short-term forecasts from the ERA-Interim reanalysis dataset in full spatial resolution T255 (0.75° grid spacing). ERA-Interim was generated by the European Centre for Medium-Range Weather Forecasts covering the time period from 1979 to 2019 (Dee et al., 2011). We use short-term forecasts because some of the input data for our surface pressure tendency analysis equation, e.g., the radiative heating rates, are only available in the forecast. The 4D-variational data assimilation scheme of ERA-Interim makes use of a time window of 12 hours. This means that the short-term forecasts are strongly tied to the analysis and hence observations,

implying that there is substantial knowledge of the synoptic-scale features. Given that the diabatic processes are not directly observed, we have no alternative to using model-generated fields (see Maranan et al., 2019).

We study two periods, 2006–2011 and 1979–2017. Our use of ERA-Interim serves two purposes: First, it supplements the satellite observations by means of cloud fraction and ACRE derived from accumulated TOA and BOA radiative fluxes in all-sky and clear-sky conditions in the 6-h and 12-h forecasts initialised from the analyses at 00 UTC and 12 UTC. 6-hourly-means of radiative fluxes are derived from the accumulated fluxes by a) dividing the 6-h accumulated flux by the time period of 6 hours, and b) by differencing the 12-h and 6-h accumulated fluxes and then also dividing by 6 hours. Given the different treatment of clouds in models and satellite data, we do not aim to validate ERA-Interim but rather look for broad consistency between the complementary sources of information. We remind the reader that cloud cover from ERA-Interim and cloud incidence from CloudSat/CALIPSO should not be compared quantitatively because of different treatments of cloud overlap and the way we treat the cloud likelihood. Second, we use ERA-Interim for the surface pressure tendency analysis. 6-hourly snapshot values of wind, temperature, geopotential height, humidity and surface pressure are taken from the 6-h and 12-h forecasts initialised from the analyses at 00 UTC and 12 UTC. For evaporation, precipitation and the temperature tendencies from ACRE, clear-sky radiative heating, and the sum of all diabatic processes, we use accumulated fields from the 6-h and 12-h forecasts and convert these to 6-hourly-means in the same manner as described above for radiative fluxes.

4.3. ICON simulations

4.3.1. Control simulations

We perform numerical simulations with the atmospheric component of the ICOSahedral Non-hydrostatic model (ICON; Zängl et al., 2015) and using the physics package that is used for numerical weather prediction (version 2.1.00). The ICON model is jointly developed by the German national weather service (Deutscher Wetterdienst; DWD) and the Max Planck Institute for Meteorology (MPI-M), aiming for a unified global NWP and climate modeling system. The ICON model was introduced as the new global NWP operational forecast system of DWD in January 2015 as a successor of the global NWP model Global Model Europe (GME). One of the main goals in developing the ICON model was the need to develop a nonhydrostatic dynamical core that can be applied on a wide range of spatial scales from 1 km to hundreds of kilometers. The model equations are based upon the prognostic variables recommended by Gassmann and Herzog (2008), where the mass conservation is achieved by using density as a prognostic variable and a barycentric velocity is chosen as reference velocity (Zängl et al., 2015). The spatial discretization of the model equations is implemented on an icosahedral-triangular Arakawa C

grid (Wan et al., 2013). The triangular grid of ICON is based on successive refinement of a spherical icosahedron, which consists of 20 equilateral triangles of the same size. Then, in the root division step, the edges of the basic triangles are divided into n equal arcs per edge, termed R_n . Afterwards, connecting the new edge points by great circle arcs yields n^2 spherical triangles within each of the original triangles of the icosahedron. This step is followed by k bisection steps, termed B_k , where each triangle is repeatedly subdivided into 4 smaller triangles. The resulting grid is then termed $R_n B_k$ grid. For a specific grid resolution, the total number of cells n_c , edges n_e and vertices n_v are given by:

$$n_c = 20n^2 4^k; \quad n_e = 30n^2 4^k; \quad n_v = 10n^2 4^k + 2 \quad (4.1)$$

Then the average grid resolution $\overline{\Delta x}$ can be calculated by:

$$\overline{\Delta x} = \sqrt{\frac{\pi}{5}} \frac{r_e}{n 2^k}, \quad (4.2)$$

where r_e is the earth's radius. For more details about the ICON model we refer the reader to Zängl et al. (2015).

Here, the simulations are conducted in R2B04 horizontal resolution (approximately 160 km) with 47 vertical levels extending up to 75 km and a time step of 720 s. We run ICON for 25 extended winter seasons from November to March with prescribed SST and sea-ice fields. The SST and sea-ice fields are derived by calculating the multiyear monthly means over the Atmospheric Model Intercomparison Project (AMIP) period from 1979 to 2008 (Gates, 1992). To derive the 25 initial conditions on November 1 we first integrate ICON forward in time for 5 years, initialised from a random initial state based on data from the ECMWF Integrated Forecast System (IFS) and we derive 5 November 1 states. Then by adding random noise in the temperature field of these 5 November 1 states, we derive 5 additional initialisations for each one of them, ending up with 25 November 1 initialisations. Based on these 25 initialisations we run ICON from November 1 to March 31. Because here we focus on the synoptic time-scales during the extended winter season from December to March (DJFM) we exclude November from our analysis and so end up with 25 independent DJFM winter seasons. These are referred to as the control (CTRL) simulations. A schematic illustration of the CTRL simulations is given in Fig. 4.2.

4.3.2. Sensitivity tests

To assess the impact of the anomalous NAO-related diabatic heating pattern either due to ACRE or total diabatic heating onto the NAO short-term dynamics we perform sensitivity tests in ICON. In a hindcast perspective we rerun ICON initialised every 5 days from the CTRL simulations with an imposed additional NAO-related anomalous diabatic heating pattern either due

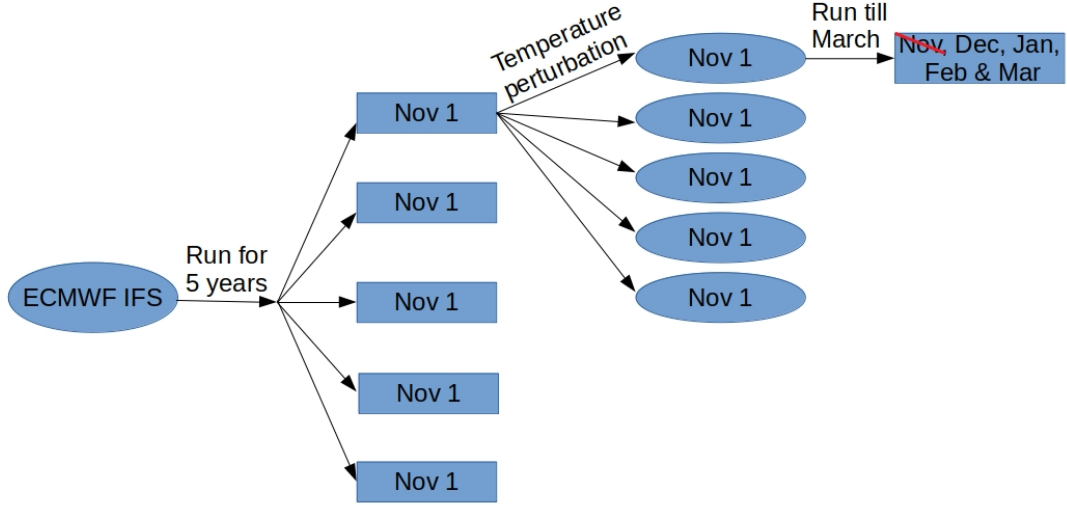


Figure 4.2.: Schematic illustration of the control (CTRL) simulations in ICON. We run ICON for 5 years initialised from a random ECMWF Integrated Forecast System (IFS) initial state. Then we perturb the temperature field in each one of the 5 November 1 states and we derive 25 initialisation. Based on these 25 initial states we run ICON till March 31. For our analysis we exclude November and we end up with 25 December–March (DJFM) extended winter seasons.

to ACRE or total diabatic heating. The time length of these hindcast simulations, which we refer to as the forced (FORC) simulations, is 15 days and we impose the additional NAO-related diabatic heating pattern constant in time. The imposed three-dimensional NAO-related diabatic heating pattern is based on regressions of 5-day mean ACRE or total diabatic heating temperature tendency onto standardised 5-day mean NAO index from the CTRL simulations. In these FORC simulations we perturb the temperature tendency field via adding the NAO-related temperature tendency either due to ACRE or total diabatic heating at each timestep of the model integration.

$$\left. \frac{dT}{dt} \right|_{\text{FORC}} = \left. \frac{dT}{dt} \right|_{\text{NAO-ACRE/TOTAL DIAB}}, \quad (4.3)$$

where $\left. \frac{dT}{dt} \right|_{\text{NAO-ACRE/TOTAL DIAB}}$ denotes the additional NAO-related temperature tendency either due to ACRE or total diabatic heating. Given that for each one of the 25 DJFM seasons we have 24 initialisations, for this assessment we end up with a comparison of 600 pairs of 15-day simulations between the CTRL and the FORC simulations.

4.4. North Atlantic Oscillation index

For the observational analysis (chapter 5) we use daily values of the NAO index provided by the National Oceanic and Atmospheric Administration Climate Prediction Centre (NOAA-CPC) to

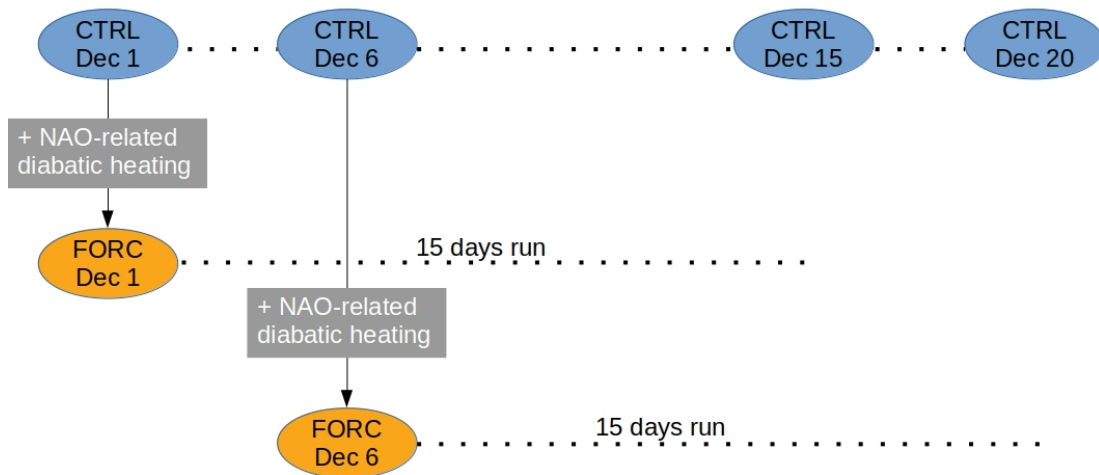


Figure 4.3.: Schematic illustration of the forced (FORC) simulations in ICON for two initialisation on December 1 and 6. For example, the FORC Dec 1 simulation is initialised from the state of the CTRL simulation on December 1 with an additional NAO-related diabatic heating which is imposed constant in time for 15 days.

construct 5-day means. The index is based on the anomalous geopotential height at 500hPa. Normalised daily values are available from year 1950 onwards and can be downloaded from <ftp://ftp.cpc.ncep.noaa.gov/cwlinks/>.

In the modeling analysis using ICON simulations, we define the NAO based on the first Empirical Orthogonal Function (EOF) of 5-day mean sea-level pressure data over the North Atlantic sector (20° - 80° N, 90° W- 40° E), which captures the full spatial NAO pattern (Hurrell et al., 2003). The NAO in ICON is based on sea-level pressure data from the control simulations of 25 extended winter seasons.

For the regression analyses presented in chapters 5 and 6 the NAO timeseries is standardised to a standard deviation of 1.

4.5. Surface pressure tendency equation (PTE)

The PTE allows us to quantify the impact of heating and moisture anomalies on the surface pressure evolution. We use the PTE to assess the relative importance of NAO-generated ACRE changes with respect to changes in other diabatic processes, such as latent heating and clear-sky radiation, and changes in temperature advection by the circulation. The PTE is given by

$$\underbrace{\frac{\partial p_{\text{sfc}}}{\partial t}}_{\text{Dp}} = \underbrace{\rho_{\text{sfc}} \frac{\partial \phi_{p_2}}{\partial t}}_{\text{D}\phi} + \underbrace{\rho_{\text{sfc}} R_d \int_{\text{sfc}}^{p_2} \frac{\partial T_v}{\partial t} d \ln p}_{\text{ITT}} + \underbrace{g(E - P)}_{\text{E-P}} + RES_{\text{PTE}}, \quad (4.4)$$

where p_{sfc} is the surface pressure, p is air pressure, ρ_{sfc} is the surface air density, R_d is the gas constant of dry air, ϕ_{p_2} is the geopotential at pressure p_2 , T_v is the virtual temperature, g is the gravitational acceleration, E is evaporation, P is precipitation, and RES_{PTE} represents the analysis residual due to, e.g., spatiotemporal discretization. Equation (4.4) measures the surface pressure tendency (Dp) from changes in the upper boundary of the vertical integral, here chosen as the geopotential at 100 hPa level in ERA-Interim and at 90 hPa in ICON (D ϕ), changes in virtual temperature between this boundary and the surface (ITT), and changes in column mass due to evaporation and precipitation (E-P).

Because we are interested in clouds, we focus on the ITT term, which we decompose further into

$$ITT = \rho_{\text{sfc}} R_d \int_{\text{sfc}}^{p_2} -\vec{v} \cdot \vec{\nabla}_p T_v d \ln p \quad \text{TADV} \quad (4.5a)$$

$$+ \rho_{\text{sfc}} R_d \int_{\text{sfc}}^{p_2} \left(\frac{R_d T_v}{c_p p} - \frac{\partial T_v}{\partial p} \right) \omega d \ln p \quad \text{VMT} \quad (4.5b)$$

$$+ \rho_{\text{sfc}} R_d \int_{\text{sfc}}^{p_2} \frac{T_v Q}{c_p T} d \ln p \quad \text{PHY} \quad (4.5c)$$

$$+ \rho_{\text{sfc}} R_d \int_{\text{sfc}}^{p_2} 0.608 T \frac{dq}{dt} d \ln p \quad \text{HUM} \quad (4.5d)$$

$$+ RES_{\text{ITT}} \quad (4.5e)$$

where \vec{v} is the horizontal wind, ω is the pressure velocity, c_p is the specific heat capacity at constant pressure, T is the air temperature, Q is the total temperature tendency from subgrid-scale diabatic processes, q is the specific humidity, and RES_{ITT} is the analysis residual. Thus, the ITT term is decomposed into contributions from horizontal temperature advection (TADV), vertical motions (VMT) and diabatic processes (PHY+HUM). PHY measures the impact of diabatic processes on temperature, e.g. latent heat release due to phase changes of water, radiative heating, sensible heat fluxes and boundary-layer turbulence, whereas HUM measures the impact of diabatic processes on the amount of specific humidity (e.g. a specific humidity decrease due to condensation of water vapor). In the observational analysis using ERA-Interim data in chapter 5, the sum of PHY and HUM is referred to as the total diabatics term (DIAB), DIAB=PHY+HUM. The DIAB term contains the all-sky radiative heating, which we further separate into contributions from ACRE and clear-sky radiative heating. In the modeling analysis using ICON (chapter 6), the HUM is term is neglected.

The PTE is a budget equation of the surface pressure tendency. Given a constant upper boundary in geopotential height ($D\phi = 0$), a process that warms the atmosphere between the surface and the upper boundary leads to decreased air density, mass loss and surface pressure fall. Analogously, a process that cools the atmosphere works in favour of a surface pressure rise. A detailed description of the PTE analysis is given in Fink et al. (2012). In ERA-Interim data (chapter 5) we chose the upper boundary at 100 hPa, following Fink et al. (2012), while in ICON we chose the upper boundary at 90 hPa. The choice of the upper boundary can affect the relative contributions of ITT and $D\phi$ (Knippertz et al., 2009). Because clouds are limited to the troposphere, the 90 or 100 hPa boundary ensures that the cloud-radiative impact is captured as part of the ITT term. We note that the vertical integrals are performed over $dlnp$ (and not dp), so that a heating in the upper troposphere has a stronger impact on the surface pressure tendency than a heating in the lower troposphere. This is done because the volume in the upper troposphere is larger compared to the lower troposphere and thus the changes in the upper troposphere have a larger impact on the surface. As we will show later for the ACRE impact over Iceland in ERA-Interim data (chapter 5), this can lead to a zero surface pressure tendency impact despite a vertically-integrated anomalous ACRE heating.

4.6. Regression analysis and statistical significance

In chapters 5 and 6 we analyse the linkages between the NAO and other variables such as clouds, ACRE, temperature, wind and PTE terms by means of linear least-squares regressions for the two timeseries. For n data pairs of (x_i, y_i) , $i = 1, \dots, n$ the relationship between the variables x_i and y_i can be described by:

$$y_i = ax_i + b, \quad (4.6)$$

where a denotes the slope and b the intercept of a line. We aim to find a line which best fits all these pairs of data (x_i, y_i) . We can achieve that by aiming to minimise the squared error:

$$e = \sum_{i=1}^n (y_i - ax_i - b)^2. \quad (4.7)$$

Then the slope a of a linear least-squares regression can be calculated as:

$$a = \frac{\sum_{i=1}^n (x_i - \bar{x})(y_i - \bar{y})}{\sum_{i=1}^n (x_i - \bar{x})^2} = \frac{S_{x,y}}{S_x^2} = r_{x,y} \frac{S_y}{S_x}, \quad (4.8)$$

where \bar{x} and \bar{y} denote the mean of x_i and y_i respectively, $S_{x,y}$ is the sample covariance of x and y , S_x and S_y is the sample variance of x and y respectively and $r_{x,y}$ is the sample correlation coefficient of x and y . The intercept b can be calculated as:

$$b = \bar{y} - a\bar{x} \quad (4.9)$$

The statistical significance of the slope (a) of the linear regression is assessed by a two-sided Wald test. The two-sided significance level of 5% is used to assess whether the slope is significantly different from zero in each grid point or atmospheric volume. The null hypothesis (a_0) is that the slope of the linear regression is zero. Then under the Wald test the estimated slope is compared to zero weighted by the standard error of the estimated slope coefficient, and the Wald-statistic (W) which is used to compute the p-values is given by

$$W = \frac{a - a_0}{se_a}. \quad (4.10)$$

se_a is the standard error of the estimated slope and is given by

$$se_a = \frac{\sqrt{\frac{1}{n-2}e}}{\sqrt{\sum_{i=1}^n (x_i - \bar{x})^2}}. \quad (4.11)$$

The sampling distribution of the Wald-statistic is a t-distribution with $n-2$ degrees of freedom and the Wald-statistic in equation (4.10) based on which we calculate the p-value can be written as

$$W = r\sqrt{\frac{n-2}{1-r^2}}, \quad (4.12)$$

where r is the correlation coefficient. Then based on the p-value we either reject or accept the null hypothesis.

5. The role of observed cloud-radiative effects for the NAO short-term dynamics

In this chapter we illustrate an observational analysis of the linkages between the NAO and clouds as well as their ACRE in various satellite datasets (5.1, 5.2). To assess the relative role of ACRE for the NAO short-term dynamics we present a diagnostic approach based on an application of the surface pressure tendency equation to ERA-Interim short-term forecast data (5.3).

This chapter, with minor adjustments in the text, is based on the article "The role of observed cloud-radiative anomalies for the dynamics of the North Atlantic Oscillation on synoptic time-scales" by Georgios Papavasileiou, Aiko Voigt and Peter Knippertz, first published on 18 February 2020 by the Quarterly Journal of the Royal Meteorological Society (doi: 10.1002/qj.3768 ©2020 The Authors. Quarterly Journal of the Royal Meteorological Society published by John Wiley and Sons Ltd on behalf of the Royal Meteorological Society). This article is available under the terms of the Creative Commons Attribution License (CC BY).

5.1. NAO impact on clouds and ACRE in satellite observations

In this section we study the NAO impact on clouds and ACRE in satellite observations by means of linear regressions of 5-day-means (for CloudSat/CALIPSO and CERES-SYN1deg) or monthly-means (for CERES-EBAF and GERB/SEVIRI), respectively. We start with an analysis of the zonal mean and then proceed with a latitude-longitude view over the North Atlantic region. We further analyse vertical profiles over the two domains around the Iceland low and Azores high, which are the centers of action of the NAO sea-level pressure seesaw.

5.1.1. Zonal-mean perspective

Motivated by the zonal-mean analysis of Li et al. (2014a), we start with studying the NAO impact on zonal-mean cloud incidence and ACRE in the northern hemisphere (20° – 80° N) for 5-day means. Figure 1a shows regressions of zonal-mean cloud incidence from CloudSat/CALIPSO onto the NAO. During its positive phase, the higher midlatitudes (55° – 70° N) experience a statistically significant decrease in high-level cloud incidence around 10 km and an increase in mid-level cloud incidence around 5 km. Further equatorward, low-level cloud

incidence is increased in the subtropics and lower midlatitudes (20° – 40° N), and around 25° N cloud incidence is increased around 8 km and decreased around 12 km. These findings are very similar to those of Li and Thompson (2016), who calculated year-round regressions (their Fig. 2d). However, the NAO impact on zonal-mean cloud incidence is small and not statistically significant in most regions. This indicates that the zonal-mean perspective is of limited use to understand the NAO impact on the cloud pattern.

The NAO impact on zonal-mean vertically-integrated ACRE from CloudSat/ CALIPSO (2006-2011) and CERES-SYN1deg (2006-2011 and 2000-2017) exhibits a much clearer and statistically-significant meridional pattern (Fig. 5.1b). During a positive phase of the NAO, ACRE decreases in the subtropics and lower mid-latitudes (equatorward of 45° N), and increases in the higher mid-latitudes between 50° and 65° N. The anomalies in ACRE are dominated by the longwave component. The heating dipole of subtropical and lower-midlatitude cooling and higher mid-latitude warming is robust in both CloudSat/CALIPSO and CERES-SYN1deg, which agree well for the time period between 2006 and 2011. Despite some decadal-scale variability in the magnitude of the NAO impact on higher mid-latitude ACRE (compare the 2006-2011 and 2000-2017 periods in CERES-SYN1deg), the heating dipole is robust with respect to the observational time period and consistent with previous findings of Li et al. (2014a) (compare our Fig. 5.1b with Fig. 2e of Li et al., 2014a).

There is no clear relationship between the changes in zonal-mean cloud incidence, which are small and have a complex vertical structure, and the robust dipole in ACRE changes. In the following we therefore change to a regional latitude-longitude perspective and investigate the NAO impact on clouds and ACRE specifically over the North Atlantic region.

5.1.2. Latitude-longitude perspective over the North Atlantic region

The North Atlantic jet stream is tilted from southwest to northeast, different from the more zonally-oriented jet streams in the North Pacific and the Southern Hemisphere. The tilt of the North Atlantic jet stream suggests that the NAO leads to zonally-asymmetric cloud anomalies over the North Atlantic. This indicates that instead of a zonal mean, a latitude-longitude perspective is necessary.

The regression analysis reveals a rich pattern of the NAO impact on cloud incidence at different levels over the North Atlantic (Fig. 5.2). At higher levels (7–12 km; Fig. 5.2a), a positive phase of the NAO leads to increased cloud incidence along the storm track region (around 45° N; see also Athanasiadis et al., 2010) from eastern Canada/USA to Scandinavia and over the subpolar Atlantic. Decreased cloud incidence is evident in near-zonal bands from southwest of the Azores to the eastern Mediterranean and from the Labrador Sea to Iceland.

At mid-levels (1.5–7 km; Fig. 5.2b), cloud incidence is increased poleward of the storm track over the eastern part of Greenland and over the subpolar North Atlantic. At the same

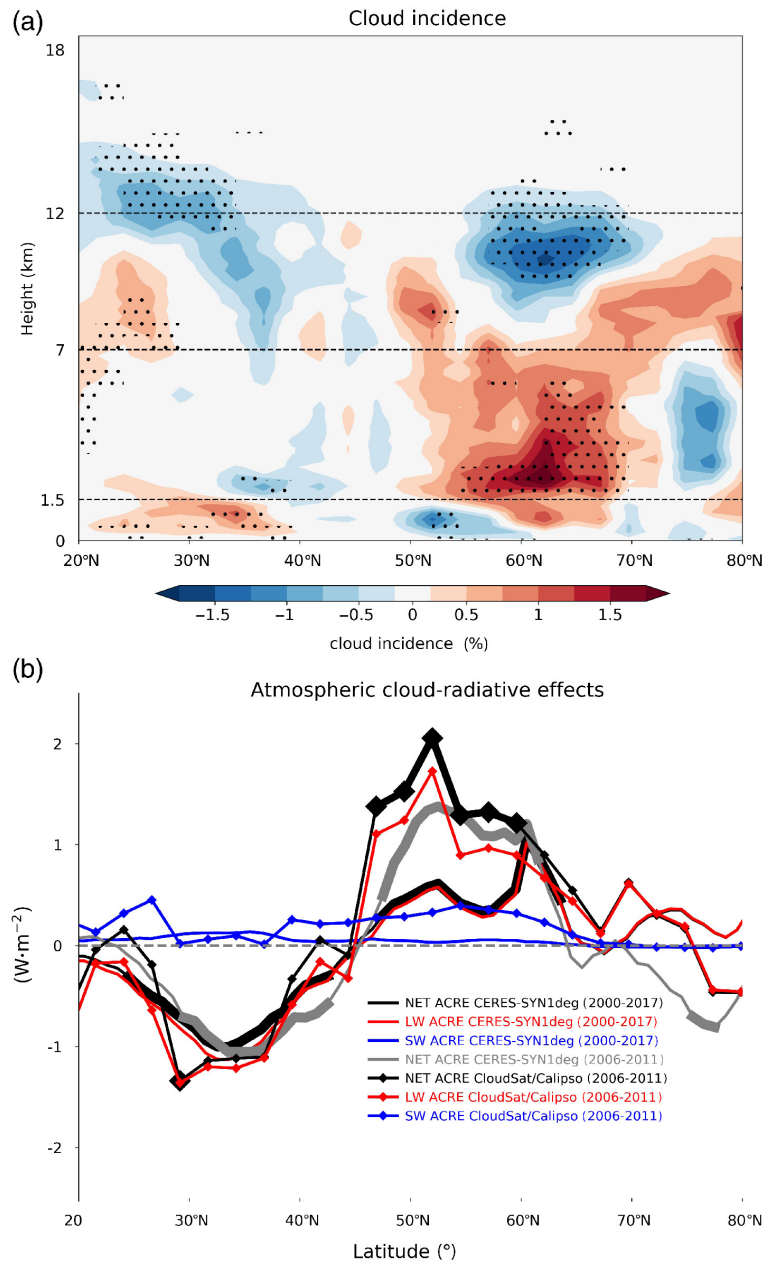


Figure 5.1.: NAO regression of DJF 5-day mean zonal-mean (a) cloud incidence from CloudSat/CALIPSO from 2006–2011 and (b) vertically integrated ACRE from CloudSat/CALIPSO during 2006–2011 (black with diamond marker) as well as from CERES-SYN1deg during 2006–2011 (grey) and 2000–2017 (black). The long-wave (LW) and short-wave (SW) components are also shown. Stippling in (a) and a thick line in (b) indicate statistical significance at the 5% level according to a two-sided Wald test. Figure from Papavasileiou et al. (2020), ©2020 The Authors. Quarterly Journal of the Royal Meteorological Society published by John Wiley and Sons Ltd on behalf of the Royal Meteorological Society.

time, the lower midlatitudes experience reduced mid-level cloud incidence during a positive NAO.

5. The role of observed cloud-radiative effects for the NAO short-term dynamics

At lower levels (0–1.5km; Fig. 5.2c) the NAO impact on cloud incidence is opposite to that at high levels for many regions. Specifically, a positive NAO leads to increased low-level cloud incidence around the Azores and around the Labrador Sea, and decreased low-level cloud incidence in an area south of Iceland that extends from the Irminger Sea to Scandinavia.

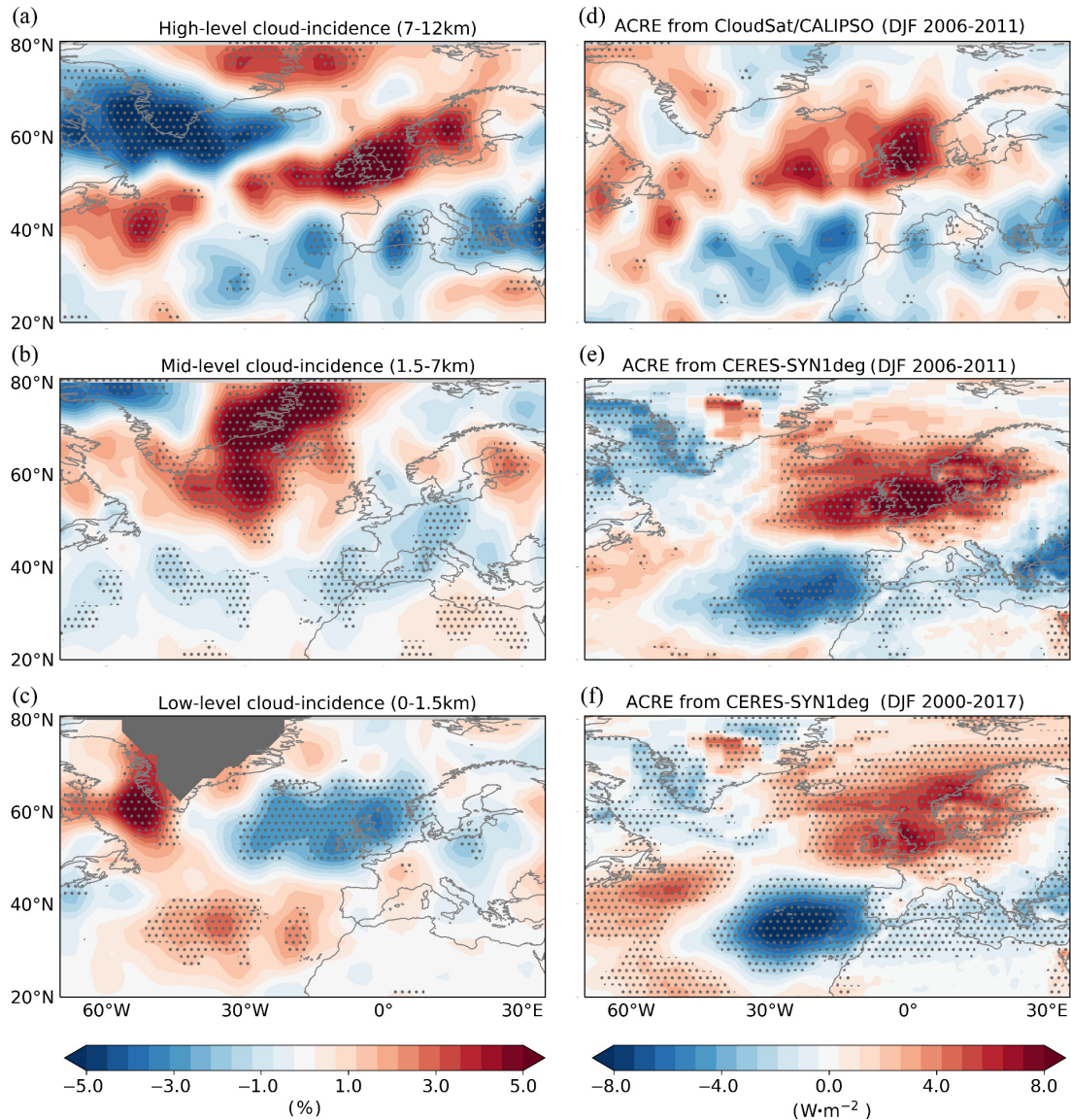


Figure 5.2.: (a–c) NAO regression of DJF 5-day mean cloud incidence from CloudSat/CALIPSO from 2006–2011 for (a) high-, (b) mid- and (c) low-level clouds over the North Atlantic region. (d–f) NAO regressions of DJF 5-day mean vertically integrated ACRE for (d) CloudSat/CALIPSO during 2006–011, and for CERES-SYN1deg during (e) 2006–2011 and (f) 2000–2017. Stippling indicates statistical significance at the 5% level according to a two-sided Wald test. For low-level clouds, Greenland is masked out. The CloudSat/CALIPSO data are smoothed using the 9-point smoothing function from the Climate Data Operator. Figure from Papavasileiou et al. (2020), ©2020 The Authors. Quarterly Journal of the Royal Meteorological Society published by John Wiley and Sons Ltd on behalf of the Royal Meteorological Society.

The NAO impact on cloud incidence is in line with changes in large-scale static stability and vertical motion accompanying the NAO (Li et al., 2014a; Li and Thompson, 2016; Grise and Medeiros, 2016). For example, the increase in high-level cloud incidence along the storm track region is consistent with large-scale ascent and the formation and eastward propagation of extratropical cyclones. The decrease in high-level and increase in low-level cloud-incidence around the Azores is consistent with a strengthening of the high-pressure system and large-scale descent.

The NAO also impacts vertically-integrated ACRE. For a positive NAO, changes in ACRE as derived from CloudSat/CALIPSO (Fig. 5.2d) show a tilted meridional heating dipole along the SW-NE axis, with warming in a broad area around the British Isles and cooling in a broad area around the Azores. ACRE from CERES-SYN1deg shows a consistent impact of the NAO with higher statistical significance, thanks to the better spatio-temporal coverage of CERES-SYN1deg (Fig. 5.2e for years 2006-2011; Fig. 5.2f for years 2000-2017). The ACRE changes are characterised by a quadrupole that consists of heating east off the coast of Nova Scotia as well as over the eastern North Atlantic, the British Isles and Scandinavia, and cooling over the Azores and the Mediterranean as well as the Labrador Sea.

The quadrupole of the ACRE anomalies is consistent with the NAO impact on high- and low-level cloud incidence (Oreopoulos et al., 2017). In many areas anomalous heating is associated with an increase in high-level cloud-incidence and a decrease in low-level cloud incidence. Likewise, anomalous cooling is associated with a decrease in high-level cloud incidence and an increase in low-level cloud incidence.

5.1.3. Vertical structure over Iceland and the Azores

We now analyse the vertical structure of cloud-incidence and ACRE from CloudSat/CALIPSO over the two centers of actions of the NAO sea-level pressure seesaw, namely Iceland and the Azores. The Iceland and Azores domains are shown in Fig. 5.3 and are selected based on NAO regressions of 5-day-mean surface pressure from ERA-Interim. The Iceland domain contains areas with a surface pressure anomaly of at least -9.3 hPa. Because the absolute magnitude of the regression over Iceland is 1.9 times larger than over the Azores, a lower threshold of surface pressure anomalies of 4.9 hPa is chosen for the Azores domain. Moreover, to avoid spurious effects due to orography land areas in the Iceland domain are neglected.

Figure 5.4a and b show cloud-incidence and ACRE averaged over the Iceland domain. The climatological cloud incidence exhibits two maxima; an upper-level maximum at 7 km and a low-level maximum at 1.5 km (Fig. 5.4a, black). This leads to climatological cooling from ACRE around the high-level and low-level cloud tops, and heating at the bottom of low-level clouds (Fig. 5.4b, black).

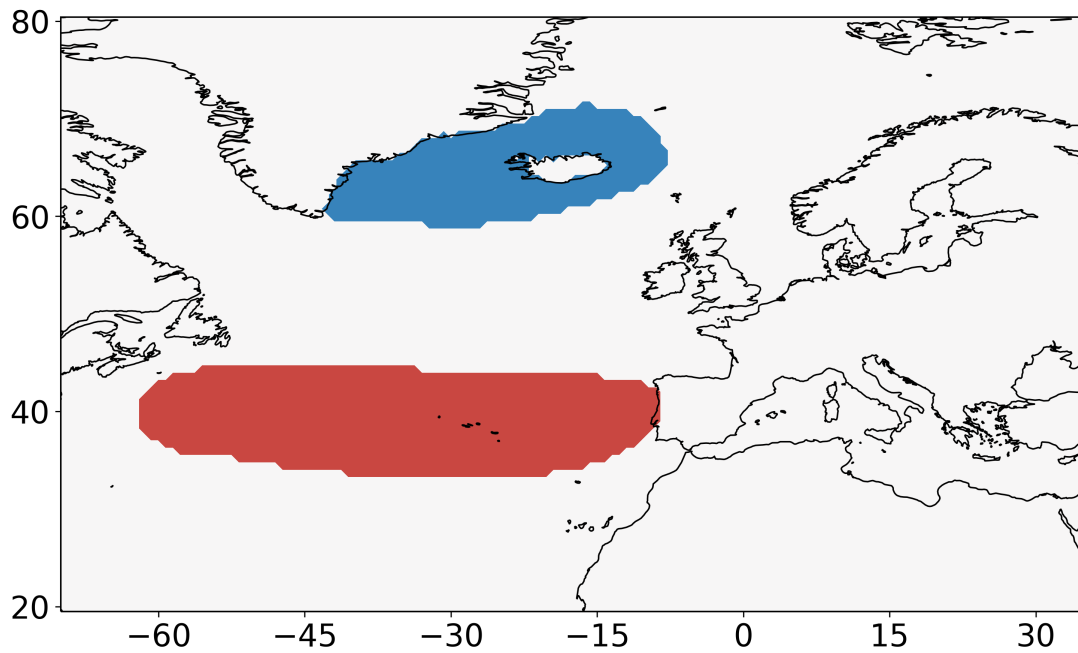


Figure 5.3.: Illustration of the Iceland (blue) and Azores (red) domains used for the area averages and vertical profiles. See text for details on how these domains are defined. Figure from Papavasileiou et al. (2020), ©2020 The Authors. Quarterly Journal of the Royal Meteorological Society published by John Wiley and Sons Ltd on behalf of the Royal Meteorological Society.

The impact of the NAO is on the order of 20% of the climatological value for cloud incidence (Fig. 5.4a, blue), and up to 80% for ACRE (Fig. 5.4b, red). During a positive phase of the NAO, high-level cloud incidence is decreased, and mid-level cloud incidence is increased. There is also an indication of decreased low-level cloud incidence. These changes indicate a downward shift of the climatological upper-level maximum in cloud incidence, probably a consequence of a lowered tropopause, and an upward shift of the climatological low-level maximum of cloud incidence. In the upper-troposphere, the downward shift of high-level cloud tops and the increased mid-level cloud incidence lead to anomalous ACRE cooling. In the lower-troposphere, the decrease in low-level cloud incidence leads to anomalous ACRE heating.

Over the Azores domain, the vertical profile of climatological cloud-incidence exhibits two maxima: an upper-level maximum at 10 km and a low-level maximum at 1.5 km (Fig. 5.4c; black). This leads to climatological ACRE cooling near the high-level and low-level cloud tops, and ACRE heating in between in the mid-troposphere and near the surface underneath the low-level clouds (Fig. 5.4d; black).

As for the Iceland domain, the impact of the NAO is on the order of 20% of the climatological value for cloud incidence (Fig. 5.4c, blue) and up to 50% for ACRE (Fig. 5.4d, red). The NAO impact is opposite to that over the Iceland domain. During a positive phase of the NAO, cloud incidence increases around 12 km and around 1.5 km, and decreases in between.

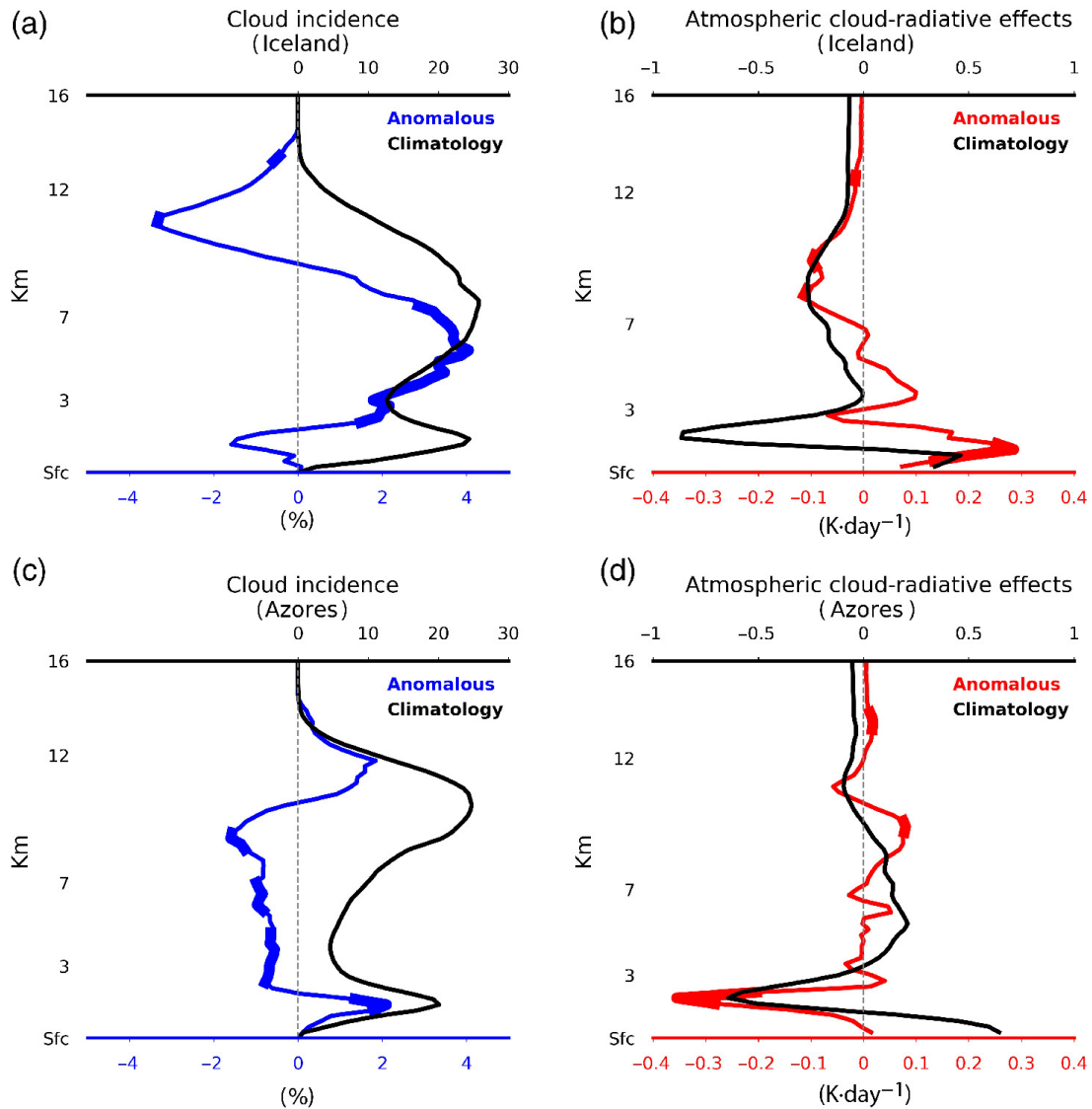


Figure 5.4.: Vertical profiles of NAO regressions of DJF 5-day mean (a, c) cloud incidence (blue) and (b, d) ACRE (red) averaged over the (a, b) Iceland and (c, d) Azores domains. The black lines indicate the DJF climatology during 2006–2011. Thick lines denote statistical significance at the 5% level according to a two-sided Wald test. Figure from Papavasileiou et al. (2020), ©2020 The Authors. Quarterly Journal of the Royal Meteorological Society published by John Wiley and Sons Ltd on behalf of the Royal Meteorological Society.

This indicates an upward shift of high-level clouds, consistent with a rising tropopause, and an increase in low-level clouds, consistent with enhanced large-scale descent and enhanced low level-stability. As a result, a positive phase of the NAO is associated with anomalous ACRE heating in the upper troposphere and increased ACRE cooling in the lower troposphere. These ACRE changes are opposite to those over the Iceland domain.

5.2. Robustness in other observational datasets

We now verify that the NAO impact on vertically-integrated ACRE averaged over the Iceland and Azores domains is robust in sign with respect to the choice of the observational dataset. To this end we compare the CloudSat/CALIPSO results to CERES-SYN1deg, CERES-EBAF and GERB/SEVIRI (Table 5.1).

Because GERB/SEVIRI is only available for the longwave component, the comparison is restricted to that for all datasets. This is unproblematic, since ACRE is dominated by this component anyway (Fig. 5.1b). CERES-EBAF and GERB/SEVIRI are only available on the monthly timescale. The comparison between the 5-day-means from CloudSat/CALIPSO and CERES-SYN1deg and the monthly-means from CERES-EBAF and GERB/SEVIRI indicates to what extent the NAO impact is sensitive to the averaging period.

Table 5.1.: NAO impact on longwave vertically-integrated ACRE as well as TOA and BOA CRE during DJF over the Iceland (top) and Azores (bottom) domain in satellite datasets and ERA-Interim. For CloudSat/CALIPSO, CERES-SYN1deg and ERA-Interim 5-day-means are used. For CERES-EBAF and GERB/SEVIRI monthly-means are used. The analyzed time periods are given in parentheses. Bold numbers indicate statistical significance at the 5% level according to a two-sided Wald test, with the confidence interval given in parentheses. Table from Papavasileiou et al. (2020), ©2020 The Authors. Quarterly Journal of the Royal Meteorological Society published by John Wiley and Sons Ltd on behalf of the Royal Meteorological Society.

Iceland

	CERES-SYN1deg (2000-2017)	CloudSat/ CALIPSO (2006-2011)	CERES-EBAF (2002-2017)	GERB/ SEVIRI (2006-2011)	ERA-Interim (1979-2017)
TOA	+2.7(±0.7)	+3.2(±1.0)	+2.1(±0.9)	+1.9(±1.0)	+2.1(±0.9)
ACRE	+1.9(±0.9)	+1.0(±0.7)	+2.1(±1.2)	+1.7(±1.1)	+4.0(±0.5)
BOA	+0.8(±0.5)	+2.2(±0.9)	0.0(±0.8)	+0.2(±0.7)	-1.9(±0.8)

Azores

	CERES-SYN1deg (2000-2017)	CloudSat/ CALIPSO (2006-2011)	CERES-EBAF (2002-2017)	GERB/ SEVIRI (2006-2011)	ERA-Interim (1979-2017)
TOA	-2.2(±0.7)	-0.1(±1.5)	-2.3(±1.2)	-1.5(±0.9)	-2.1(±0.7)
ACRE	-2.5(±0.8)	-1.5(±0.8)	-2.4(±1.1)	-0.7(±0.5)	-2.5(±0.5)
BOA	+0.3(±0.4)	+1.4(±1.5)	+0.1(±0.6)	-0.8(±0.5)	+0.4(±0.8)

The CRE anomalies at the TOA and BOA differ between the datasets by several $W m^{-2}$ and are not always statistically significant. Nevertheless, the vertically-integrated ACRE anomalies, which are computed from the difference of TOA and BOA anomalies, are more robust and agree on the sign. All datasets show vertically-integrated ACRE cooling over the Azores

domain during a positive NAO phase and heating over the Iceland domain. This robustness in sign supports the results of the CloudSat/CALIPSO analysis, although the comparison also illustrates the uncertainty in the magnitude of the NAO impact on ACREs. The comparison between ACRE changes derived from the 5-day-means from CloudSat/CALIPSO and CERES-SYN1deg and the monthly means from CERES-EBAF and GERB/SEVIRI shows that the uncertainty in the magnitude of the NAO impact does not primarily arise from the averaging period. We will study the importance of these heating/cooling anomalies for the dynamics of the NAO in the next section.

5.3. Role of the ACRE for the dynamics of the NAO: ERA-Interim analysis

In the previous section we found that a positive NAO leads to anomalous ACRE cooling over the Azores high and ACRE heating over the Iceland low. This heating pattern could alter atmospheric temperatures, air density, surface pressure and hence the NAO. More specifically, the heating pattern suggests the possibility of a positive cloud-radiative feedback that amplifies the sea-level pressure contrast between the Azores and Iceland and increases the NAO persistence. This is opposite to the negative cloud-radiative feedback suggested by Li et al. (2014a).

To study the role of ACRE for the NAO dynamics we apply the surface pressure tendency equation (PTE) of Knippertz and Fink (2008) and Fink et al. (2012) using ERA-Interim data. Before detailing the PTE analysis, we first confirm that ERA-Interim captures the observed NAO impact on clouds and ACRE.

Figure 5.5 shows the impact of the NAO on high-level, mid-level and low-level cloud cover in ERA-Interim for DJF from 1979 to 2017 by means of 5-day-mean regressions. In ERA-Interim, sigma levels are used to distinguish high-level, mid-level and low-level cloud cover (ECMWF, 2010), with boundaries at roughly 800 hPa and 450 hPa. The top panel (Fig. 5.5a) illustrates that a positive NAO is associated with increased high-level cloud cover along the storm track (near 45°N), the subpolar North Atlantic, and Scandinavia. Mid-level cloud anomalies (Fig. 5.5b) exhibit a meridional dipole structure with positive anomalies poleward of the storm track and east of Greenland, and negative anomalies equatorward of the storm track. The anomalies in low-level cloud cover are largely opposite to those of high-level cloud cover (Fig. 5.5c). These results are qualitatively consistent with CloudSat/CALIPSO (Fig. 5.2), apart from near Iceland and over the Norwegian Sea. These discrepancies might partly result from the fact that ERA-Interim measures cloud cover and CloudSat/CALIPSO cloud incidence, which leads to different treatments of cloud overlap and cloud likelihood in the two datasets (chapter 4).

More importantly, and more relevant to the NAO dynamics, the regression analysis of 5-day-mean vertically-integrated ACRE during DJF from 1979–2017 and 2006–2011 in the top

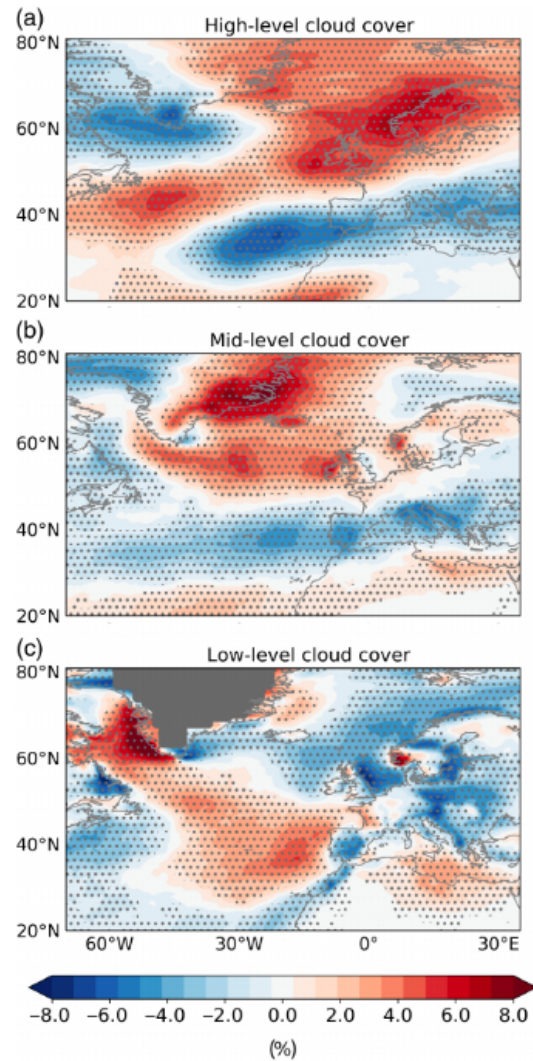


Figure 5.5.: NAO regressions of DJF 5-day mean ERA-Interim (a) high-level, (b) mid-level and (c) low-level cloud cover during 1979–2017. The boundary between the mid- and high-level clouds is at 450 hPa, and the boundary between mid- and low-level clouds is at 800 hPa. Stippling indicates statistical significance at the 5% level according to a two-sided Wald test. For (c), Greenland is masked out. Figure from Papavasileiou et al. (2020), ©2020 The Authors. Quarterly Journal of the Royal Meteorological Society published by John Wiley and Sons Ltd on behalf of the Royal Meteorological Society.

panels of Fig. 5.6 shows an ACRE dipole that is broadly consistent with the satellite observations (Fig. 5.2d-f), albeit weaker. An exception is the Labrador sea. The vertical profiles of the climatological ACRE and the NAO-generated ACRE anomalies over the Iceland and Azores domains (Figs. 5.6c and 5.6d) show a similar structure as in CloudSat/CALIPSO (Figs. 5.4b and 5.4d). In ERA-Interim the heating anomalies are statistically significant at almost all levels and smoother, while the maxima of the regressions are slightly weaker over the Azores and slightly stronger over Iceland compared to CloudSat/CALIPSO. For vertically-averaged ACRE, ERA-Interim is qualitatively consistent with the observations (Table 5.1). Thus, we

conclude that ERA-Interim overall captures the observed impact of the NAO on clouds and ACRE.

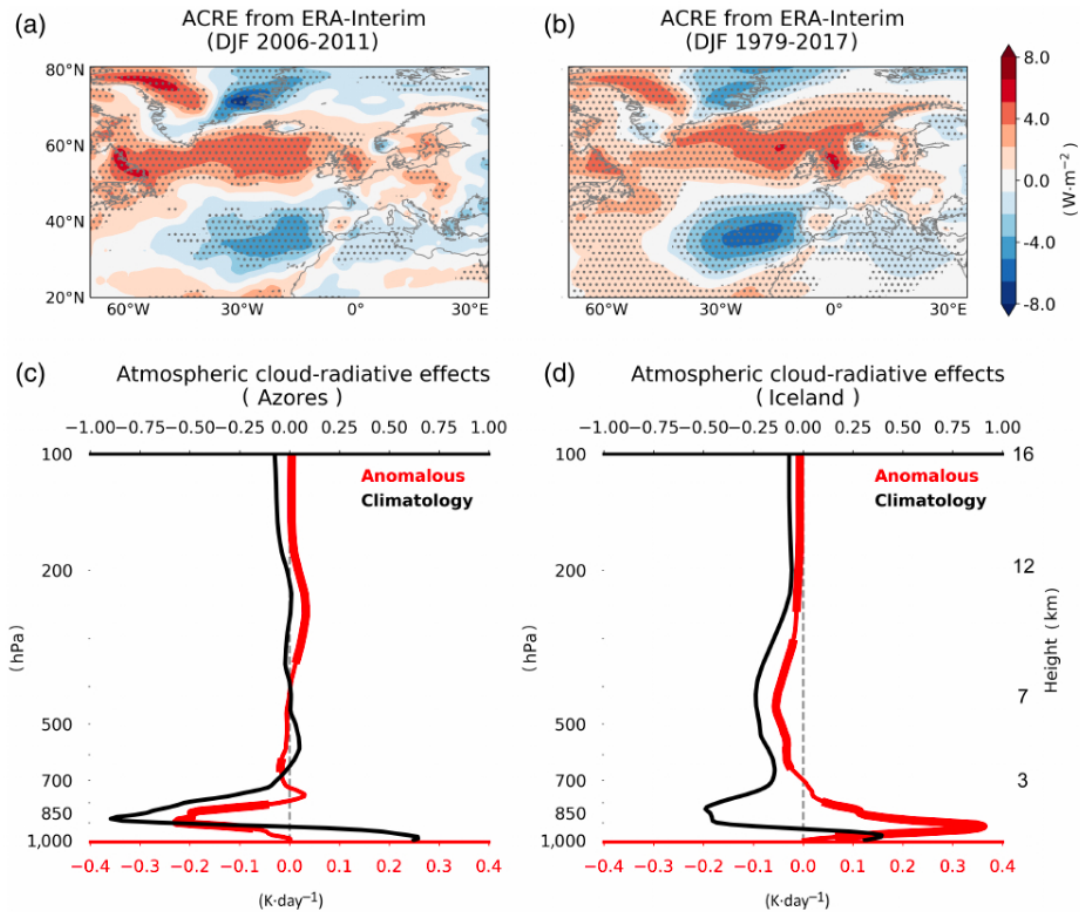


Figure 5.6.: NAO regression of DJF 5-day-mean ACRE in ERA-Interim. (a, b) Vertically-integrated ACRE during 2006-2011 and 1979-2017. (c, d) Vertical profiles of ACRE regression during 2006-2011 averaged over the Azores and Iceland domains. The black lines indicate the DJF climatology during 2006-2011. Stippling in (a) and (b) and thick lines in (c) and (d) indicate statistical significance at the 5% level according to a two-sided Wald test. Figure from Papavasileiou et al. (2020), ©2020 The Authors. Quarterly Journal of the Royal Meteorological Society published by John Wiley and Sons Ltd on behalf of the Royal Meteorological Society.

To assess the relative role of ACRE compared to large scale dynamics and other diabatic processes we use the PTE analysis (for details see chapter 4). We calculate the PTE and its decomposition every 6 hours over the entire North Atlantic region, and then construct 5-day-means. Fig. 5.7a illustrates the 5-day-mean PTE terms for the Iceland domain during DJF 2006/2007. Generally speaking both the ITT and $D\phi$ terms are substantial and often compensate each other. Note that the instantaneous correlation between the Dp term and the NAO index is not statistically significant. However when Dp leads the NAO by a 5-day mean period, there is a weak but statistically significant negative correlation. The decomposition of the ITT term (Fig. 5.7b) shows large and opposite contribution from horizontal temperature advection

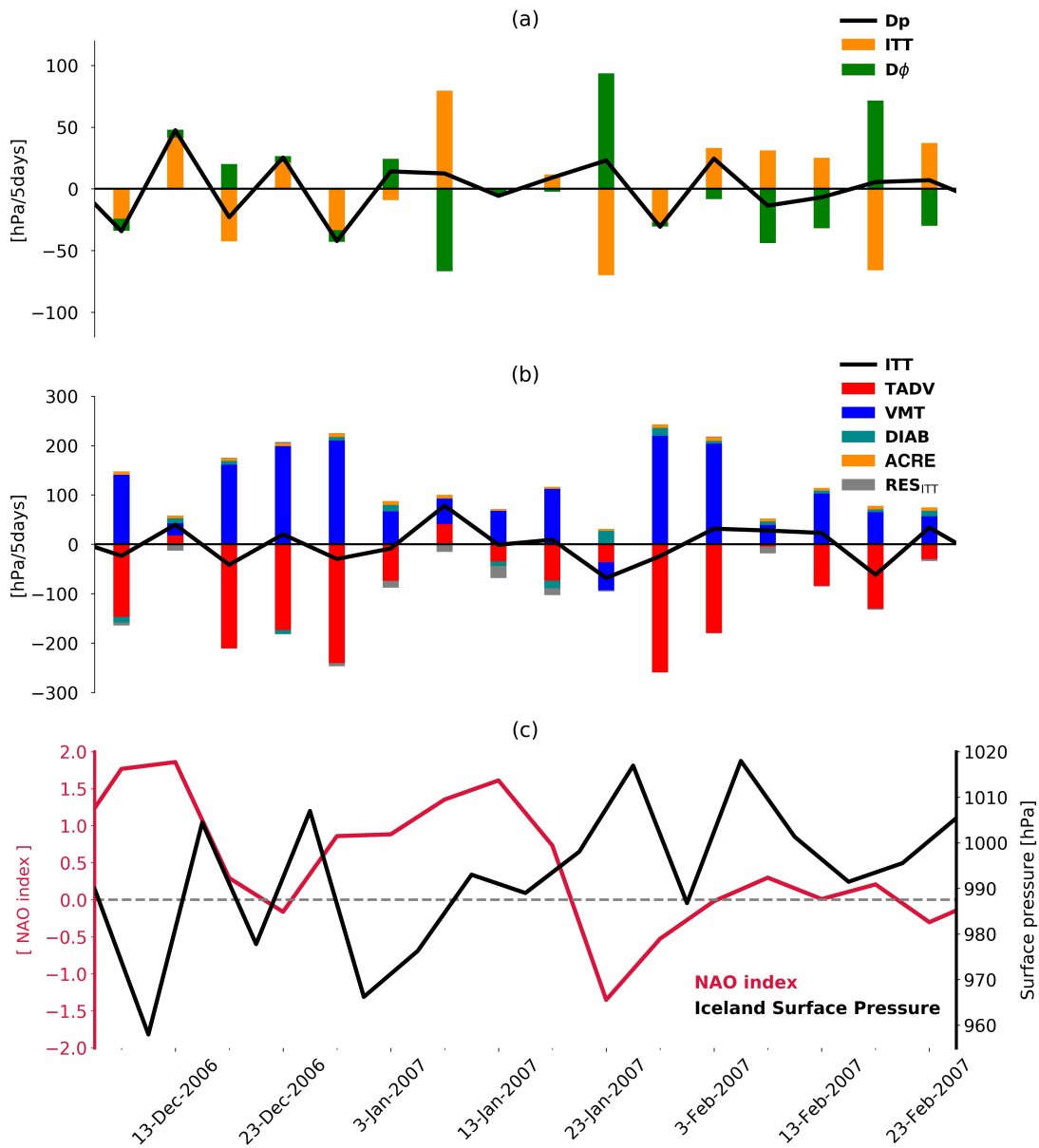


Figure 5.7.: Illustration of the PTE analysis using ERA-Interim data over the Iceland domain during DJF 2006/2007. (a) Surface pressure tendency and decomposition. (b) Decomposition of the ITT term. (c) NAO index and area-average surface pressure. Note that the instantaneous surface pressure is shown for the beginning of each 5-day period. The E-P and RES_{PTE} are near zero and not included here. See section 4 for a detailed explanation of the PTE terms. Figure from Papavasileiou et al. (2020), ©2020 The Authors. Quarterly Journal of the Royal Meteorological Society published by John Wiley and Sons Ltd on behalf of the Royal Meteorological Society.

(TADV) and vertical motions (VMT). TADV and VMT tend to be negatively correlated because a column-mean warming from horizontal temperature advection ($TADV > 0$) is associated with upward motions and adiabatic cooling ($VMT < 0$), and vice-versa. In the following, we will therefore consider the sum $DYN = TADV + VMT$ to measure the surface pressure impact of the circulation. The contributions from the sum of all diabatic processes (DIAB) and ACRE are

smaller than TADV and VMT, but they can still considerably affect the ITT term because of the compensation between TADV and VMT.

As for the analysis of the NAO impact on clouds in section 5.1, we regress the 5-day-means of the PTE terms onto the NAO index. In particular the diabatic heating terms in the PTE are not directly constrained by observations and therefore depend to some extent on the model parametrizations of ERA-Interim. Yet, the NAO-generated anomalies in vertically-integrated ACRE over the Azores and Iceland domains derived from ERA-Interim are qualitatively consistent with the observations (Table 5.1). Moreover, Ling and Zhang (2013) showed that ERA-Interim's diabatic heating profiles in the extratropics compare well with other reanalysis datasets and observations. This indicates that our PTE results should not be overly sensitive to the choice of the reanalysis dataset.

5.3.1. Latitude-longitude perspective of the PTE regression analysis

We start with the latitude-longitude perspective of the NAO regression of the PTE terms (Fig. 5.8). A positive NAO is associated with a positive surface pressure tendency in a region that extends from Iceland over the North Sea to the Iberian Peninsula, as well as over western parts of the North Atlantic west of the Azores. A negative surface pressure tendency is found over the Labrador Sea and the Irminger Sea. The surface pressure tendency pattern results from large and opposite tendencies of the $D\phi$ and ITT terms. The $D\phi$ term dominates over western Europe and over the Labrador Sea and the Irminger Sea (Fig. 5.8b).

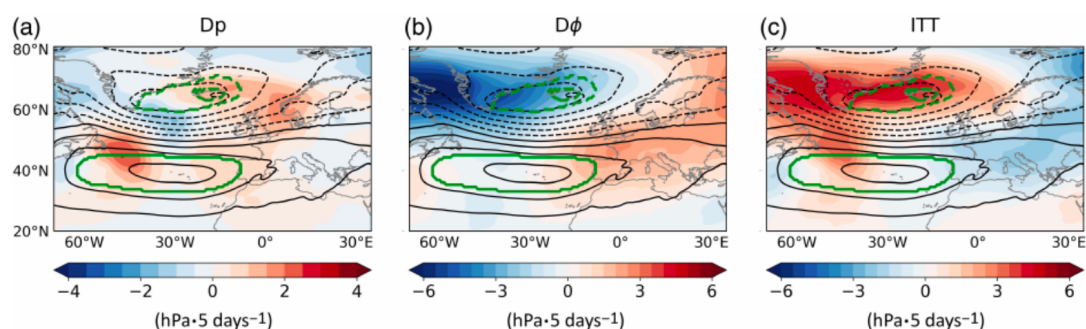


Figure 5.8.: NAO regressions of 5-day-mean (a) surface pressure tendency and contributions from tendencies of (b) the 100 hPa geopotential height and (c) the virtual temperature. Black lines show the NAO-related surface pressure anomaly (contour interval 2 hPa; dash lines indicate negative anomalies). The green lines indicate the Azores and Iceland regions as per Fig. S1. For the Iceland domain land is excluded, as indicated by the inner green dashed line. Results are based on DJF ERA-Interim data from 2006-2011. Note the different color scales. Figure from Papavasileiou et al. (2020), ©2020 The Authors. Quarterly Journal of the Royal Meteorological Society published by John Wiley and Sons Ltd on behalf of the Royal Meteorological Society.

The ITT term dominates over the northeastern and the western parts of the North Atlantic (Fig. 5.8c). A positive NAO is associated with a weakening of the Iceland low due to changes in virtual temperature changes between 100 hPa and the surface (i.e., the ITT term), and a

strengthening of the western and eastern edges of the Azores high. This is consistent with a beginning decay of the positive phase of the NAO.

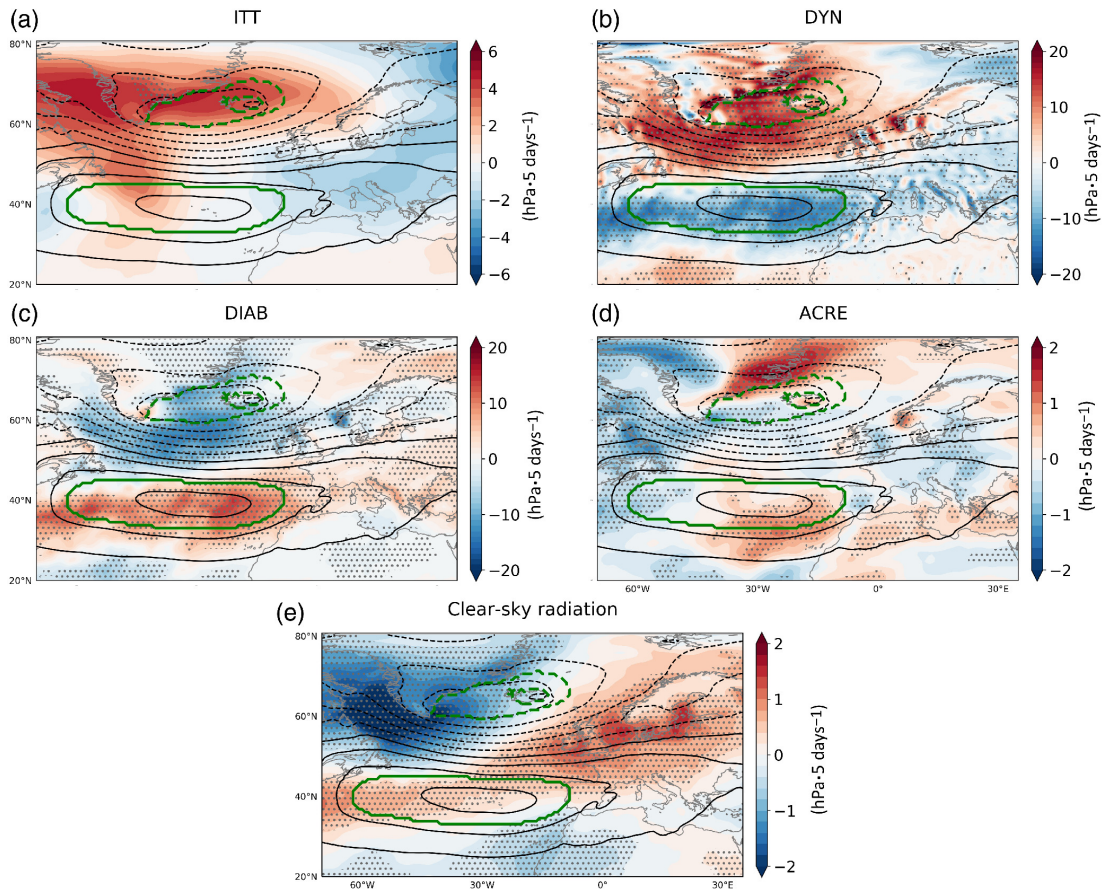


Figure 5.9.: NAO regressions of 5-day-mean surface pressure tendencies from (a) changes in virtual temperature (ITT), (b) large-scale dynamics (DYN), (c) diabatic processes (DIAB), (d) atmospheric cloud-radiative effects (ACRE) and (f) clear-sky radiation. Results are based on ERA-Interim data during DJF from 2006 to 2011. Black lines show the NAO-related surface pressure anomaly (contour interval 2 hPa; dash lines indicate negative anomalies). Stippling indicates statistical significance at the 5% level according to a two-sided Wald test. Note the different color scales. The green lines indicate the Azores and Iceland regions as per Fig. S1. For the Iceland domain land is excluded, as indicated by the inner green dashed line. Figure from Papavasileiou et al. (2020), ©2020 The Authors. Quarterly Journal of the Royal Meteorological Society published by John Wiley and Sons Ltd on behalf of the Royal Meteorological Society.

We now decompose the ITT anomalies into the contributions of Eq. (4.5) so as to assess their relative importance for the NAO dynamics, with the horizontal advection term TADV and the vertical motions term VMT shown as the sum $DYN=TADV+VMT$ (Fig. 5.9; note the different magnitudes of each term). The ITT anomalies result from meridional dipoles in DYN and DIAB, which largely oppose each other. The large-scale dynamics (DYN) work in favour of dampening the NAO surface pressure anomalies (shown in black, Fig. 5.9b), while diabatic processes as a whole (DIAB) work in favour of reinforcing them (Fig. 5.9c). The magnitude of the DIAB anomalies is almost as large as the DYN anomalies, and in fact larger west of the Azores.

This is not surprising since the DIAB and DYN terms are not physically independent. For example an area of strong diabatic heating is associated with stronger upward vertical motions and adiabatic cooling. This compensation leads to changes in the ITT term which in turn may also affect the geopotential at the upper boundary since the $D\phi$ and ITT terms in most cases compensate each other (Fig. 5.8). The meridional dipole of the DIAB anomalies suggests that diabatic processes as a whole positively feed back on the NAO by reinforcing both the Iceland low and the Azores high during a positive NAO phase. ERA-Interim does not allow us to quantify the individual contribution of latent heating, however by analysing precipitation anomalies associated with the NAO we can approximate its spatial distribution. Figure 5.10 illustrates that a positive phase of the NAO is associated with strong positive anomalies of 5-day-mean precipitation in the higher midlatitudes and strong negative anomalies in lower midlatitudes. The spatial correspondence of the diabatic anomalies with the NAO-generated precipitation anomalies indicates that latent heating is the dominant process, in line with Greatbatch and Jung (2007) and Woollings et al. (2016).

The DIAB anomalies contain the sum of all diabatic processes. To assess the role of ACRE and clear-sky radiative heating, we also regress surface pressure tendencies due to ACRE (Fig. 5.9d) and clear-sky radiative heating (Fig. 5.9e) onto the NAO. A positive NAO is associated with positive surface pressure tendency anomalies due to ACRE around the Azores, consistent with anomalous vertically-integrated ACRE cooling (Fig. 5.6). Around Iceland, the pattern is less consistent, with negative surface pressure tendency anomalies south of Iceland and positive anomalies north of Iceland. Averaged over the Azores and Iceland domains, during a positive NAO phase the ACRE anomalies slightly reinforce the Azores high but have no impact on the strength of the Iceland low (Table 5.2). The PTE regressions thus indicate that the ACRE anomalies, via strengthening the Azores high, are a small positive feedback on the NAO and its persistence. Similarly, the anomalies from clear-sky radiative heating act as a positive feedback by reinforcing both the Iceland low and Azores high. The clear-sky radiative heating impact over the Azores is associated with anomalous column-mean heating (Fig. 5.13) which leads to anomalous column-mean clear-sky radiative cooling, while the opposite occurs over Iceland. Yet, the contribution of ACRE and clear-sky radiative heating to the diabatic processes as a whole is relatively minor, suggesting that radiative feedbacks on the NAO are small (Table 5.2).

5.3.2. Vertical perspective on the PTE regression analysis over Iceland and the Azores

To better understand the impact of the ITT term and its decomposition, we study the vertical profiles of the regressions averaged over the Iceland and Azores domains. This is shown in Fig. 5.11.

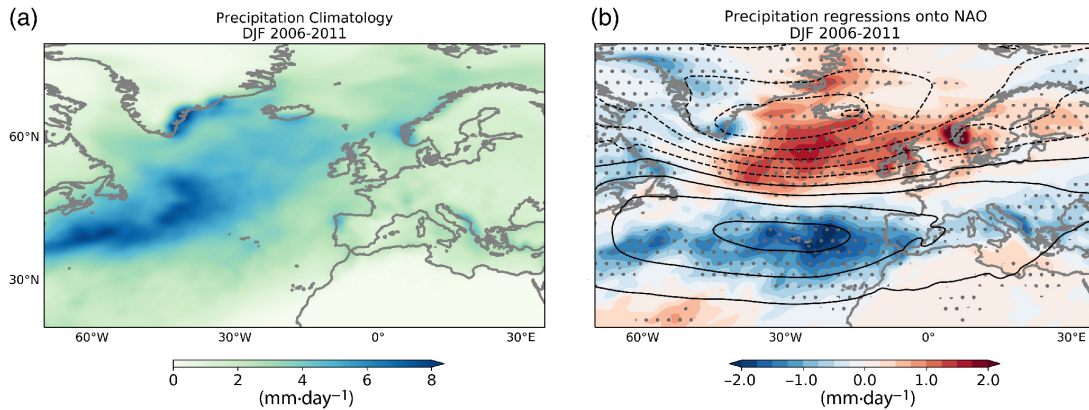


Figure 5.10.: ERA-Interim DJF precipitation from 2006-2011. (a) climatology. (b) NAO regressions of 5-day-means. In (b) stippling indicates statistical significance at the 5% level according to a two-sided Wald test and black lines show the NAO-related surface pressure anomaly (contour interval 2 hPa; dashed lines indicate negative anomalies). Figure from Papavasileiou et al. (2020), ©2020 The Authors. Quarterly Journal of the Royal Meteorological Society published by John Wiley and Sons Ltd on behalf of the Royal Meteorological Society.

Over the Azores domain (Fig. 5.11a), a positive NAO is associated with large negative tropospheric DYN anomalies between the surface and 300 hPa, which are opposed by large positive DIAB anomalies. In the upper troposphere, the DIAB contribution is slightly positive due to a positive anomaly from clear-sky radiation, with a small negative ACRE anomaly. Near the surface, i.e. from 950hPa to 800hPa, roughly 20–30% of the DIAB anomalies are caused by ACRE, but otherwise the ACRE anomalies are near zero. Overall, the surface pressure tendency anomaly over the Azores domain is positive during a positive NAO phase due to diabatic processes unrelated to radiation.

A very similar but opposite picture of anomalies occurs over the Iceland domain (Fig. 5.11b).

Table 5.2.: NAO regressions of 5-day mean surface pressure tendencies from different contributions to the ITT term. Values are vertically-integrated and averaged over the Azores and Iceland domains. The analysis is based on ERA-Interim during DJF from 2006 to 2011. Bold numbers indicate statistical significance at the 5% level according to a two-sided Wald test, with the confidence interval given in parentheses. Table from Papavasileiou et al. (2020), ©2020 The Authors. Quarterly Journal of the Royal Meteorological Society published by John Wiley and Sons Ltd on behalf of the Royal Meteorological Society.

	Azores	Iceland
DYN	-9.6(± 2.9)	+11.5(± 5.8)
DIAB	+8.5(± 2.2)	-7.0(± 2.2)
ACRE	+0.2(± 0.2)	0.0(± 0.3)
Clear-sky radiation	+0.4(± 0.2)	-0.8(± 0.5)

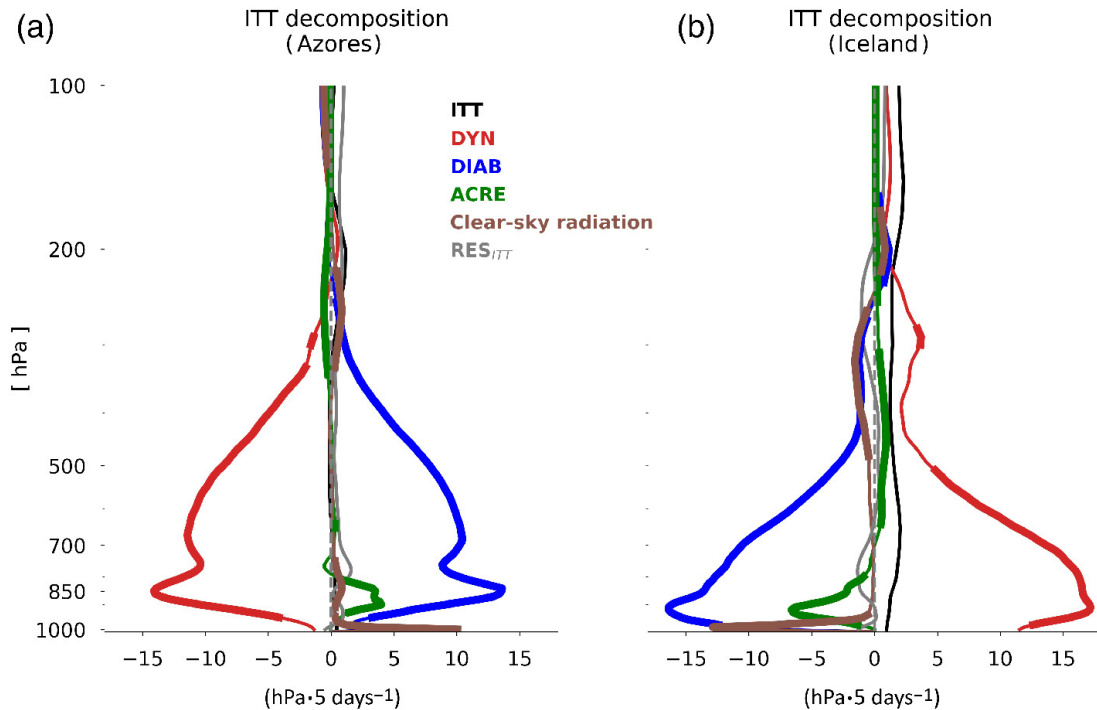


Figure 5.11.: NAO regressions of 5-day-mean vertical profiles of the ITT term and its decomposition over the Azores domain (a) and the Iceland domain (b). Results are based on ERA-Interim data during DJF from 2006 to 2011. Thick lines indicate statistical significance at the 5% level according to a two-sided Wald test. Figure from Papavasileiou et al. (2020), ©2020 The Authors. Quarterly Journal of the Royal Meteorological Society published by John Wiley and Sons Ltd on behalf of the Royal Meteorological Society.

5.4. Comparison to Li et al. (2014a)

Our work is motivated by Li et al. (2014a). In contrast to our conclusion of a weak positive cloud-radiative feedback on the NAO, Li et al. (2014a) argued for a negative feedback (note that they do not quantify the magnitude of the feedback). To understand this difference, this section contrasts our analysis method and interpretative framework with that of Li et al. (2014a).

The main differences are the analysis of CRE within the atmosphere (ACRE) instead of top-of-atmosphere CRE, the use of 5-day-means instead of monthly-means, the use of the NAO instead of the AO index, and the study of the winter months of December-January-February instead of the extended winter from October to March.

These differences lead to substantial deviations in the zonal-mean anomalies of Cloud-Sat/CALIPSO cloud incidence (Fig. 5.12), consistent with Li and Thompson (2016). However, apart from the zonal-mean cloud incidence, our regression results are very similar to those of Li et al. (2014a). This includes the zonal-mean CRE regression (compare our Fig. 5.1b with Fig. 2e of Li et al., 2014a) as well as the North Atlantic regressions for clouds and CRE (compare our Figs. 5.2a, 5.5a and 5.6a to Figs. 3b, 3c and 4c from Li et al., 2014a). Moreover, Table 5.2 indicates that the ACRE and top-of-atmosphere CRE anomalies closely resemble

each other, at least when averaged over the Azores and Iceland domains. Thus, the difference in the concluded direction of the cloud-radiative feedback on the NAO does not result from differences in the analysis method but from different interpretative frameworks.

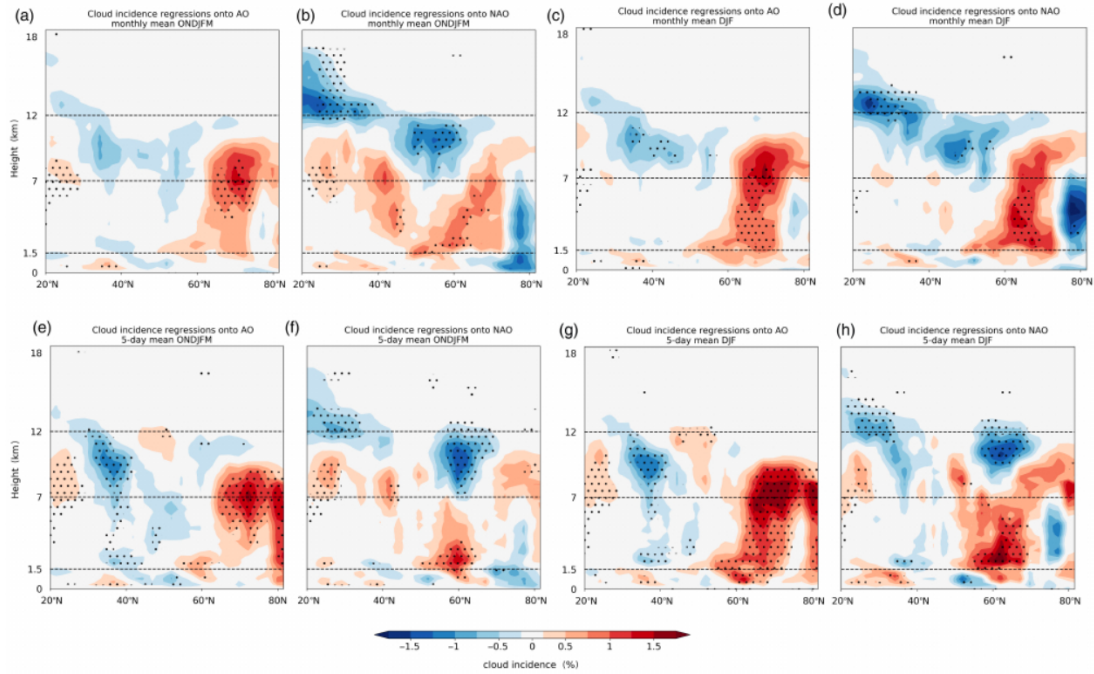


Figure 5.12.: Regression of zonal-mean cloud incidence from CloudSat/CALIPSO onto the AO (left) and NAO (right) for 5-day-means and monthly-means, and for DJF and ONDJFM. Panel (a) in the upper-left corner corresponds to Li et al. (2014a), panel (h) in the lower-right corner to our study. The other panels indicate the impact of changing the circulation index, the averaging period, and the number of months considered. Stippling indicates statistical significance at the 5% level according to a two-sided Wald test. Figure from Papavasileiou et al. (2020), ©2020 The Authors. Quarterly Journal of the Royal Meteorological Society published by John Wiley and Sons Ltd on behalf of the Royal Meteorological Society.

Li et al. (2014a) apply a temperature anomaly framework. Looking down from the top-of-atmosphere, they found negative CRE anomalies (i.e. cooling) around the Azores during a positive NAO, while tropospheric temperatures are anomalously warm (as inferred from TOA clear-sky longwave radiation). Li et al. (2014a) interpreted this as a cloud-radiative dampening of NAO-generated temperature anomalies and hence a negative cloud-radiative feedback. Yet, their framework ignores the vertical pattern of temperature and CRE anomalies. A comparison between Fig. 5.6c and d with Fig. 5.13 shows that the CRE anomalies do not follow the vertical profile of the temperature anomalies and are strongest in the lower troposphere where the temperature anomalies are weakest. In our view, the mismatch in vertical location questions the picture of a cloud-radiative dampening of temperature anomalies and hence Li et al.'s (2014a) conclusion of a negative cloud-radiative feedback.

We instead apply a surface pressure tendency framework, where the vertically-integrated effect of CRE matters but not the vertical location of CRE with respect to temperature anoma-

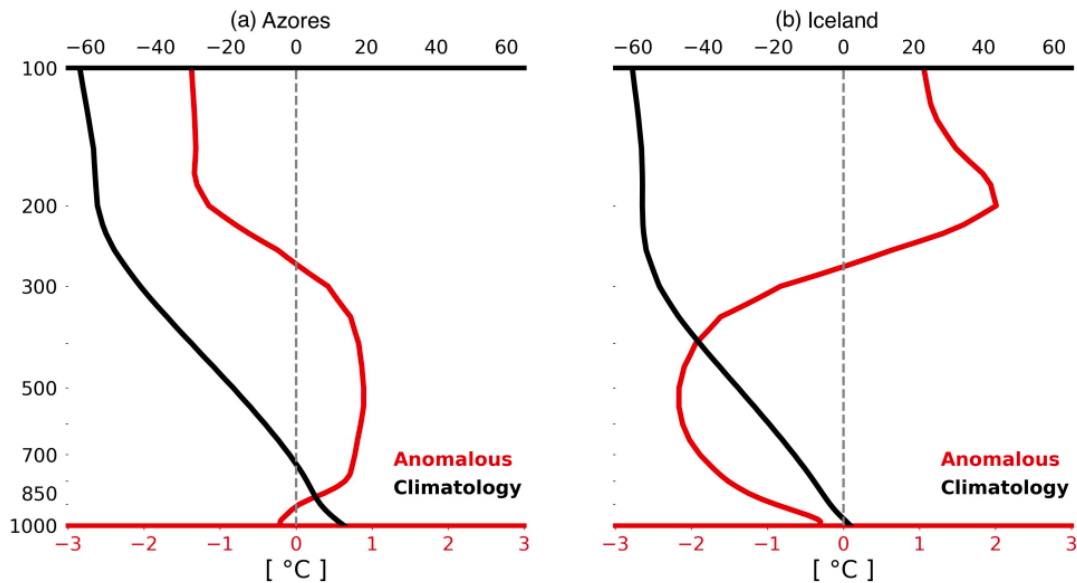


Figure 5.13.: NAO regressions of 5-day mean ERA-Interim atmospheric temperature during DJF 2006-2011 averaged over the (a) Azores and (b) the Iceland domains. Black lines show the climatology. Figure from Papavasileiou et al. (2020), ©2020 The Authors. Quarterly Journal of the Royal Meteorological Society published by John Wiley and Sons Ltd on behalf of the Royal Meteorological Society.

lies. In this perspective, the vertically-integrated negative ACRE anomalies over the Azores during a positive NAO strengthen the high and so act as a positive cloud-radiative feedback. We believe that this framework is better suited to infer the cloud-radiative feedback, as it circumvents potential problems from the vertical mismatch of temperature and CRE anomalies. However, model simulations would be needed to test this observationally based result.

5.5. Conclusions

The North Atlantic Oscillation is a dominant mode of synoptic-scale variability over the North Atlantic region. In this chapter, we have studied i) how NAO variability on synoptic time-scales affects clouds and cloud-radiative effects (CRE), and ii) the potential of these NAO-generated changes in CRE to in turn affect the NAO. Our work was motivated by the hypothesis of Li et al. (2014a) that top-of-atmosphere CRE act as a negative feedback on the NAO and damp NAO variability. Our work is the first to study the NAO-CRE coupling on synoptic time-scales, and to quantify its importance relative to large-scale dynamics and diabatic processes as a whole. Since we are interested in synoptic time-scales we are specifically considering the role of CRE within the atmosphere (ACRE).

The NAO has robust impacts on clouds and ACRE in a range of satellite observations and ERA-Interim short-term forecasts. A positive phase of the NAO is associated with more high-level clouds along the storm track (45°N) and the subpolar Atlantic, and less high-level clouds

poleward and equatorward of it. The high-level cloud changes are consistent with stronger upward motion and a lowered tropopause. For low-level clouds the NAO impact is opposite to that of high-level clouds, with more low-level clouds around the Azores, consistent with stronger descending motion, and less low-level clouds around and south of Iceland. The NAO-associated cloud changes lead to a dipole of anomalous vertically-integrated ACRE cooling over the Azores and heating over Iceland that is robust in sign (but not in magnitude) across satellite datasets and the ERA-Interim short-term forecasts.

To study to what extent the ACRE anomalies in turn affect the NAO and its persistence, we have applied the surface pressure tendency equation (PTE) to ERA-Interim short-term forecast data. This has allowed us to quantify the relative role of ACRE compared to the large-scale circulation and the sum of all diabatic processes. The regression analysis indicates that the NAO-generated ACRE anomalies over the Azores feed back positively on the NAO and so should increase its persistence. This result is in contrast to Li et al. (2014a), who suggested that top-of-atmosphere CRE should decrease the NAO persistence. As discussed in Section 5, we believe the difference between our study and theirs lies in the interpretative framework. While we have considered the surface pressure tendency, Li et al. (2014a) reasoned based on a CRE dampening of NAO-generated temperature anomalies. Irrespective of this difference in the concluded direction of the cloud-radiative impact, our analysis has also shown that the cloud-radiative impact is minor compared to the impact of diabatic processes as a whole. This suggests that cloud-radiative effects are not crucial to the NAO dynamics on synoptic time-scales.

Diabatic processes as a whole, which besides CRE include latent heating, exhibit NAO-generated changes that strongly project onto the NAO surface pressure anomalies. The changes in diabatic processes appear to be dominated by latent heating, consistent with previous work (Greatbatch and Jung, 2007; Woollings et al., 2016). Our PTE analysis indicates that diabatic processes as a whole constitute a substantial positive feedback on the NAO. This is consistent with Woollings et al. (2016) who showed that latent heating shifts with the jet stream and balances the adiabatic destruction of baroclinicity by the circulation. However, our result is in contradiction to the modelling work of Greatbatch and Jung (2007) and Xia and Chang (2014), who argued that latent heating acts as a negative feedback and damps the persistence of the NAO and the annular modes, respectively. As for CRE, we believe the difference results from the chosen interpretative framework. Greatbatch and Jung (2007) and Xia and Chang (2014) argued with a dampening of NAO-generated temperature anomalies, whereas we have reasoned based on the surface pressure tendency.

In summary, we have documented robust impacts of the NAO on clouds and cloud-radiative effects over the North Atlantic and the neighbouring regions. Our analysis suggests that cloud-radiative effects represent a positive but small feedback on the NAO persistence on synoptic

time-scales. In the next chapter we will test our PTE-based hypothesis by means of atmospheric model simulations. This will also allow us to clarify the differences between interpretative frameworks, and to investigate in more detail the role of diabatic processes.

6. The role of cloud-radiative effects and diabatic processes for the NAO short-term dynamics in ICON

The examination of the role of atmospheric cloud-radiative effects and total diabatic heating for the NAO short-term dynamics in satellite observations and reanalysis data in chapter 5 has provided new insights of the interactions and feedback mechanisms that help determine the NAO persistence. However, observations and reanalysis data are constrained by spatiotemporal data availability. Here, we therefore test the robustness of our observational findings in numerical simulations using ICON. The ICON simulations have two advantages. First, using numerical simulations we can explicitly study individual diabatic processes and quantify their role compared to the large-scale dynamics and the sum of all diabatic processes. Second, using ICON in perfect-model hindcast sense, we can quantify the impact of diabatic processes on the NAO persistence through sensitivity simulations that we perturb with NAO-related diabatic heating. In this chapter we provide a modeling analysis that focuses on four aspects: i) the impact of the NAO on clouds and their radiative effects and the total diabatic heating, ii) the role of atmospheric cloud-radiative effects and other diabatic processes for the NAO dynamics, iii) the consistency between ICON and observations, and iv) a quantification of the NAO response to NAO-related cloud-radiative and total diabatic heating.

6.1. The North Atlantic Oscillation in ICON

Before we analyse the linkages between the NAO and cloud fields, it is important to characterize the NAO in the ICON control simulations. This includes a study of the NAO spatial pattern and timescale. We define the NAO as the leading EOF of mean sea-level pressure (MSLP) over the North Atlantic domain (90°W–40°E, 20°N–80°N) during 25 extended winter seasons from December to March. An analysis of 5-day mean MSLP regressions onto the NAO (Fig. 6.1) reveals a pattern similar to the observed NAO pattern. A positive phase of the NAO is characterized by negative anomalies of MSLP over the high latitudes with center of action around Iceland, and positive anomalies of MSLP over the low latitudes with center of action around the western Mediterranean (Fig. 6.1). The changes in MSLP northeast of Iceland are slightly stronger and extend over a larger area that covers most of the subpolar Atlantic in ICON compared to ERA-Interim. On the other hand, in the low latitudes of the North Atlantic, the MSLP anomalies are weaker in magnitude compared to ERA-Interim.

6. The role of cloud-radiative effects and diabatic processes for the NAO short-term dynamics in ICON

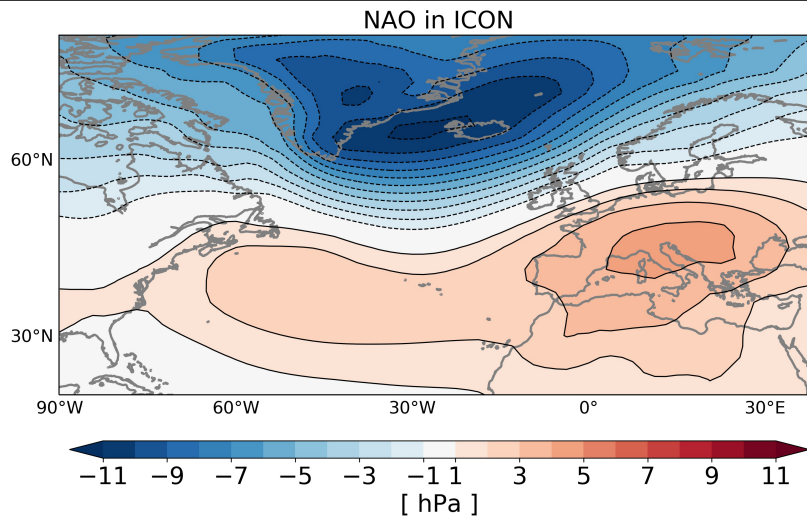


Figure 6.1.: Regressions of 5-day-mean mean sea-level pressure anomalies onto the NAO timeseries for ICON. The results are based on 25 extended winter seasons from December to March. The zero contour is excluded.

Compared to ERA-Interim (Fig. 5.8), the centers of action are shifted eastward in ICON. This is particularly evident for the southern center of action, where a shift from the Azores to southern Europe is found in ICON. This can also be seen by comparing the climatological DJFM geopotential height at 500 hPa, which shows that the stationary trough over eastern North America is shifted to the east in ICON compared to ERA-Interim (Fig. 6.2a). The differences between ICON and ERA-Interim could be linked to the stationary Rossby wave over North America and interactions with synoptic-scale eddies. A potential reason might be a weaker large-scale topographic forcing induced by the Rocky Mountains (Luo et al., 2011), which might lead to an eastward shift of the stationary Rossby wave over North America in ICON. Figure 6.2c illustrates that the Rocky Mountains in ICON are shorter by a few hundred meters compared to ERA-Interim and the topography is smoother in ICON compared to ERA-Interim. However, Fig. 6.2b shows that the mean position of the DJFM jet stream in ICON compares well with ERA-Interim, especially regarding the tilt of the jet which many models struggle to simulate properly (Zappa et al., 2013). Nevertheless, in the jet exit area over the UK the jet stream is stronger in ICON compared to ERA-Interim. This suggests that the mean cyclonic and anticyclonic activity is also shifted eastwards in ICON compared to ERA-Interim, which might explain the eastward shift of the NAO pattern in ICON.

Besides the spatial pattern of the NAO, it is important to characterize the NAO persistence. For that purpose we analyse the NAO timescale based on the autocorrelation of the daily NAO index for the 25 extended winter seasons. Note that the MSLP anomalies that we use to compute the daily NAO index are calculated based on the 25 year DJFM climatology and thus the interannual variability is included here. Figure 6.3a shows that the daily NAO index in ICON

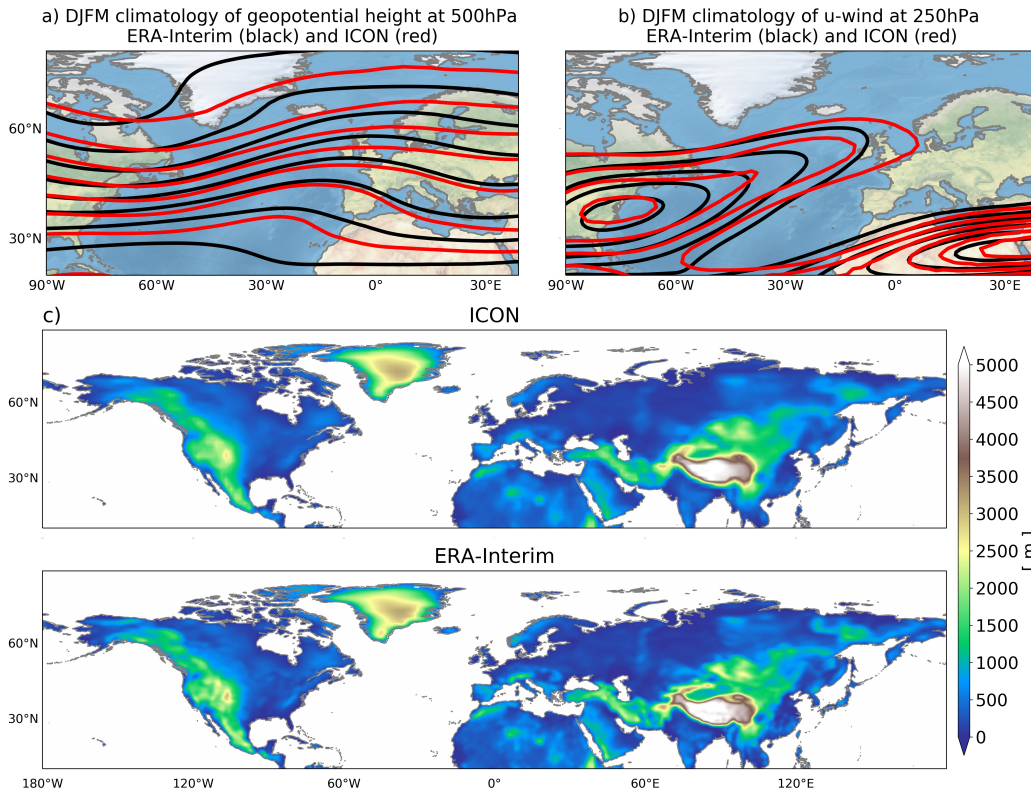


Figure 6.2.: DJFM climatology of (a) geopotential height at 500 hPa and (b) zonal wind at 250 hPa in ERA-Interim (black) and ICON (red). Results are based on ERA-Interim data during 1979-2019, and 25 winter-season model integrations in ICON.

follows a normal distribution. An analysis of the NAO autocorrelation (Fig. 6.3b) shows that the NAO e-folding timescale in ICON, defined as the timescale at which the autocorrelation becomes less than e^{-1} , exhibits considerable interannual variability and varies between 2 to 12 days, with an average of 4.5 days. This suggests that the NAO timescale is strongly influenced by interannual variability (Keeley et al., 2009). It also illustrates the highly variable NAO persistence on synoptic timescales that arises from various internal and external feedback mechanisms.

6.2. NAO impact on clouds and cloud-radiative effects in ICON

Because we are interested in the coupling between cloud-radiative effects and the NAO, we further investigate the link between the NAO and clouds in ICON. We illustrate the linkages between the NAO and clouds as well as their radiative effects from different perspectives to better understand their coupling in ICON.

On average during the winter DJFM more high-level clouds occur along the axis of the North Atlantic jet stream from the southeastern USA to the Norwegian Sea compared to the rest of the domain, which are maximised west of the Azores (Fig. 6.4a). In the mid-troposphere,

6. The role of cloud-radiative effects and diabatic processes for the NAO short-term dynamics in ICON

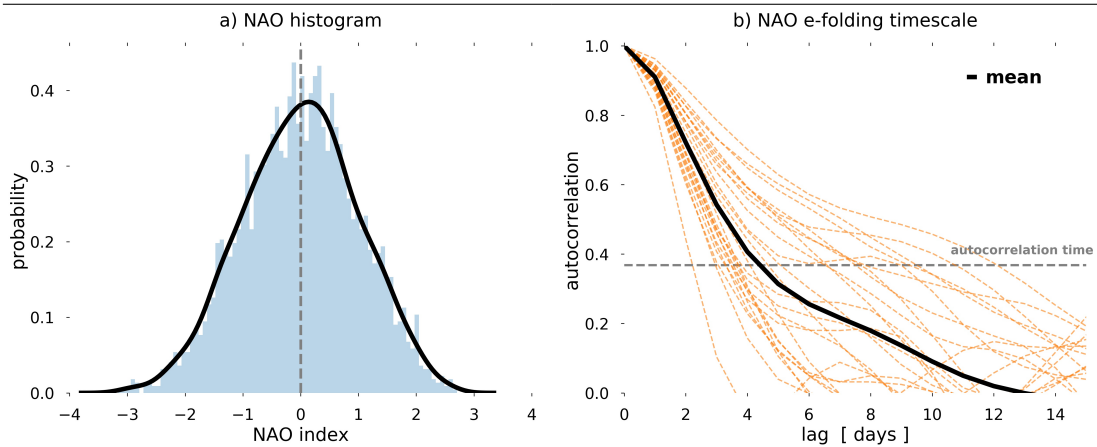


Figure 6.3.: NAO (a) histogram and (b) e-folding timescale in ICON. The results are based on daily NAO index during 25 extended winter seasons from December to March. The black line in (a) illustrates a Gaussian kernel density estimate of the distribution. The orange lines in (b) illustrate the e-folding timescale for each winter and the black line shows the mean over all winters. In (b) the grey dashed line illustrates the e^{-1} value.

more clouds are found over the ocean areas and north of the Azores (Fig. 6.4b), while in the lower troposphere more clouds are evident over the ocean and continental areas in the higher latitudes (Fig. 6.4c). These upper- and mid-tropospheric clouds are associated with midlatitude cyclones that develop and move along the jet axis and areas of large-scale ascent associated with their warm conveyor belts. This is also suggested from the precipitation climatology (Fig. 6.14a; see also Browning, 1986). On the other hand low-level clouds are mostly found over areas of enhanced downward motions and low-level static stability (Li et al., 2014b; Grise and Medeiros, 2016). Although the pressure level chosen to separate high- and mid-level cloud cover is different in ICON (400 hPa) compared to ERA-Interim (450 hPa) and although in ICON we use DJFM instead of DJF, overall we find a qualitatively consistent climatology of cloud cover with ERA-Interim (Fig. 2.3; left panels) over the North Atlantic domain.

To test the impact of the NAO on clouds, we analyse 5-day mean regressions of high-, mid- and low-level cloud cover anomalies from ICON onto the NAO (Fig. 6.4; right panels). Regressions of 5-day mean cloud cover from ICON reveal that a positive phase of the NAO is associated with increased high-level cloud cover in an area that extends from the east coast of the USA to Scandinavia and the subpolar Atlantic, and decreased high-level cloud cover over the Labrador Sea and the lower latitudes over Europe and south of the Azores. In the mid-troposphere, a positive phase of the NAO is associated with increased cloud cover in the higher latitudes of the North Atlantic north of the Azores, and decreased cloud cover over the Labrador Sea and the lower latitudes over Europe and south of the Azores. In the lower-troposphere, a positive NAO is linked with increased cloud cover west of the Azores, the Mediterranean and north of Iceland, and decreased cloud cover south of Iceland and over Europe.

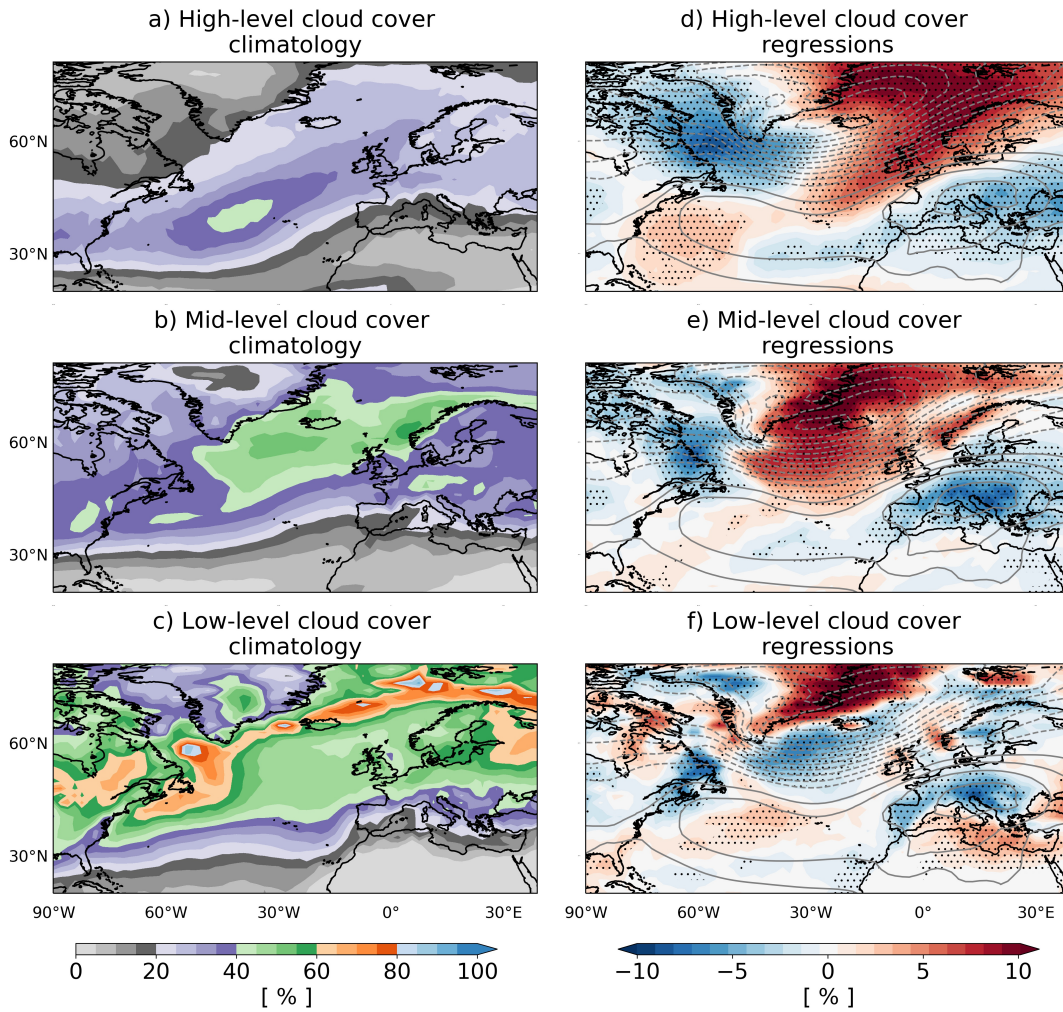


Figure 6.4.: DJFM (a,b,c) climatology and (d,e,f) NAO regressions of (a,d) high-level, (b,e) mid-level, and (c,f) low-level cloud cover from ICON. The boundary between the high- and mid-level clouds is at 400 hPa and the boundary between mid- and low-level clouds is at 800 hPa. The results are based on 25 extended winter from December to March. The grey contours in (d,e,f) denote NAO regressions of 5-day mean surface pressure (contour interval 1 hPa; dash lines indicate negative anomalies; the zero contour is excluded). Stippling indicates statistical significance at the 5% level according to a two-sided Wald test.

These changes in cloud cover are in line with changes in large-scale static stability and vertical motion linked to the NAO phase (Li et al., 2014a; Grise and Medeiros, 2016; Li and Thompson, 2016). For instance, the increase in high- and mid-level cloud cover is associated with large-scale ascending motions linked to the development and eastward propagation of extratropical cyclones along the storm track. On the other hand, the decrease in high- and mid-level cloud cover and increase in low-level cloud cover south of the Azores and over the Mediterranean is in line with large-scale descent and a strengthening of the high-pressure system.

6. The role of cloud-radiative effects and diabatic processes for the NAO short-term dynamics in ICON

Except for some regions, the impact of the NAO on clouds is qualitatively consistent with ERA-Interim reanalysis data (Fig. 5.5) and satellite observations (Fig. 5.2; left panels). The discrepancies between ICON and observations in the lower-troposphere of the North Atlantic lower latitudes are potentially linked to a weaker impact of the NAO and an eastward shift of the southern center of action in ICON. However, this is not problematic since our analysis mainly focuses on ocean areas despite the fact that the impact of the NAO in the lower latitudes of the North Atlantic is not as strong as in observations.

The cloud changes associated with a positive phase of the NAO lead to substantial changes in the vertically integrated atmospheric cloud-radiative effects (ACRE; Fig. 6.5). 5-day mean regressions of vertically integrated ACRE onto the NAO show that a positive NAO is associated with column-mean heating in a region between Iceland and the Azores along a zonal stretch from Nova Scotia to Scandinavia. On the other hand, column-mean cooling occurs in the lower latitudes in a zonal stretch from the west of the Azores to the Mediterranean, and north of Iceland. In most regions this pattern of ACRE anomalies results from an overlap of opposite cloud cover changes between the high-/mid-levels and low-levels. For example, south of Iceland, the column-mean heating largely results from increased high- and mid-level cloud cover, and decreased low-level cloud cover, while the opposite occurs over the lower latitudes south of the Azores and Mediterranean. It is worth pointing out that despite the differences in low-level clouds between ICON and observations (compare Fig. 6.4f with Fig. 5.2c and Fig. 5.5c), the ACRE anomalies are qualitatively consistent (compare Fig. 6.5 with Fig. 5.2f Fig. 5.6b).

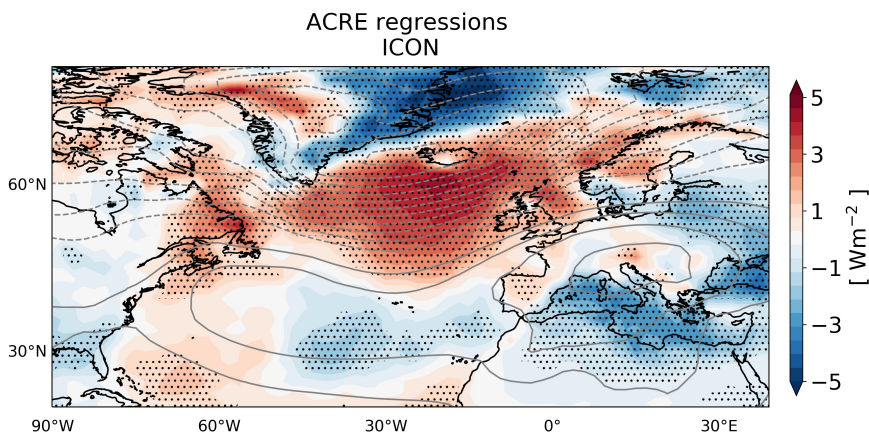


Figure 6.5.: NAO regressions of 5-day mean vertically integrated atmospheric cloud-radiative effects (ACRE) in ICON. The results are based on 25 extended winter from December to March. The grey contours denote NAO regressions of 5-day mean surface pressure (contour interval 1 hPa; dash lines indicate negative anomalies; the zero contour is excluded). Stippling indicates statistical significance at the 5% level according to a two-sided Wald test.

To investigate the vertical distribution of the NAO-related cloud and ACRE changes within the atmosphere over the two centers of action of the NAO we further study regressions of area-averaged 5-day mean vertical profiles of cloud cover and ACRE heating rates over the Iceland

and Azores domain. We define the two domains based on MSLP regressions onto the NAO. Although the maximum impact of the NAO on MSLP over the lower latitudes occurs over Europe, we define the southern center of action only over the North Atlantic ocean to avoid continental areas and areas over the Mediterranean. The threshold that we use for the Azores domain is 2 hPa. On the other hand, for the Iceland domain we use -7 hPa as a threshold and we also exclude land areas over Greenland and Iceland. The averaging domains for ICON are shown in Fig. 6.6. Following our observational work, we exclude the continental areas in order to avoid spurious effects in the lower troposphere induced by topography and to focus our analysis over the North Atlantic ocean.

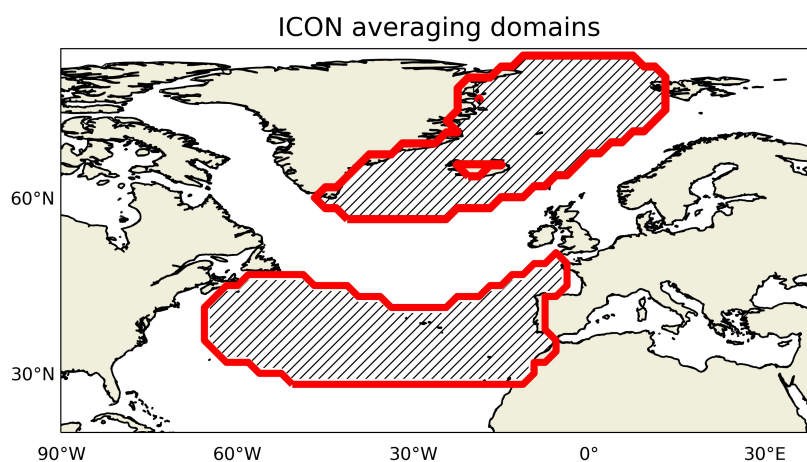


Figure 6.6.: The hatched areas enclosed by the red contour denote the averaging domains over the two centers of action around Iceland in the north and the Azores in the south.

Over the Iceland domain more clouds occur in the mid- and lower-troposphere on average with two distinct maxima at 450 hPa and 850 hPa (black line in Fig. 6.7a). This cloud vertical distribution leads to mean ACRE cooling near the top of these two distinct maxima and mean heating below the lower one near the surface (black line in Fig. 6.7b). On the other hand, over the Azores more high-level clouds occur at roughly 300 hPa and more low-level clouds at roughly 950 hPa (black line in Fig. 6.7c). These clouds lead to mean ACRE cooling near the top of both cloud cover maxima at 900 hPa and 300 hPa and mean ACRE heating below these two layers near the surface and at roughly 500 hPa.

To study the impact of the NAO on the vertical distribution of clouds and ACRE, we analyse 5-day mean regressions for the two domains (Fig. 6.7). Over Iceland, a positive phase of the NAO is associated with statistically significant increased cloud cover for most of the tropospheric depth, with a maximum increase at roughly 500 hPa. These cloud changes are potentially linked to enhanced upward motions and midlatitude cyclones. These cloud changes lead to statistically significant anomalous ACRE heating below 500 hPa that is associated with trapped emitted longwave radiation from the surface, and anomalous ACRE cooling above.

6. *The role of cloud-radiative effects and diabatic processes for the NAO short-term dynamics in ICON*

The anomalous ACRE heating maximizes in the lower troposphere at roughly 950 hPa, while the anomalous ACRE cooling maximizes at roughly 400 hPa.

Over the Azores domain, a positive phase of the NAO is associated with positive anomalies of cloud cover in the lower and upper troposphere that maximize at roughly 850 hPa and 250 hPa, respectively (Fig. 6.7). The cloud changes in the lower troposphere are linked to enhanced downward motions and a strengthening of the high pressure over the Azores. Although the cloud changes are mostly weak and not statistically significant, ACRE changes exhibit weak but statistically significant signals. Anomalous ACRE cooling is evident near the surface and in a layer that extends from roughly 700 hPa up to 300 hPa, while anomalous ACRE heating occurs near the two positive cloud cover anomalies.

A comparison of these findings with satellite observations and ERA-Interim data (chapter 5) reveals qualitatively consistent changes in clouds and ACRE associated with a positive phase of the NAO. However the changes in ICON are weaker, particularly over the Azores domain. Our analysis of vertical profiles of clouds and ACRE suggests that these differences mainly result from differences in the lower tropospheric cloud anomalies. For example, in ICON the NAO has a weaker impact on low-level clouds over the Azores compared to satellite observations and ERA-Interim data. This in turn leads to a weaker ACRE cooling in the lower troposphere in ICON and to a weaker column-mean cooling over the Azores. These discrepancies are not surprising, and in fact the simulation of low-level clouds over the eastern subtropical oceans is a well known issue in climate models (Myers and Norris, 2015). This is also evident when comparing regressions of area-averaged TOA CRE, BOA CRE and vertically integrated ACRE over the two domains (Table 6.1). Our analysis shows that a positive phase of the NAO is linked to an anomalous ACRE dipole with statistically significant column-mean heating over the Iceland domain and column-mean cooling over the Azores domain. These findings are qualitatively consistent with observations and ERA-Interim, but the magnitude is smaller in ICON.

Table 6.1.: NAO impact on vertically-integrated ACRE as well as TOA and BOA CRE during DJFM over the Iceland (left) and Azores (right) domain in ICON. Results are based on 5-day mean data during 25 winter seasons. Bold numbers indicate statistical significance at the 5% level according to a two-sided Wald test, with the confidence interval given in parentheses.

		ICON				ICON	
Iceland	TOA	+4.3	(±0.6)	Azores	TOA	+1.2	(±0.8)
	ACRE	+0.7	(±0.3)		ACRE	-0.4	(±0.3)
	BOA	+3.6	(±0.6)		BOA	+1.6	(±0.7)

After having characterized the NAO in ICON and having analysed its link to clouds and their ACRE on synoptic timescales, we study the dynamical connection between the NAO

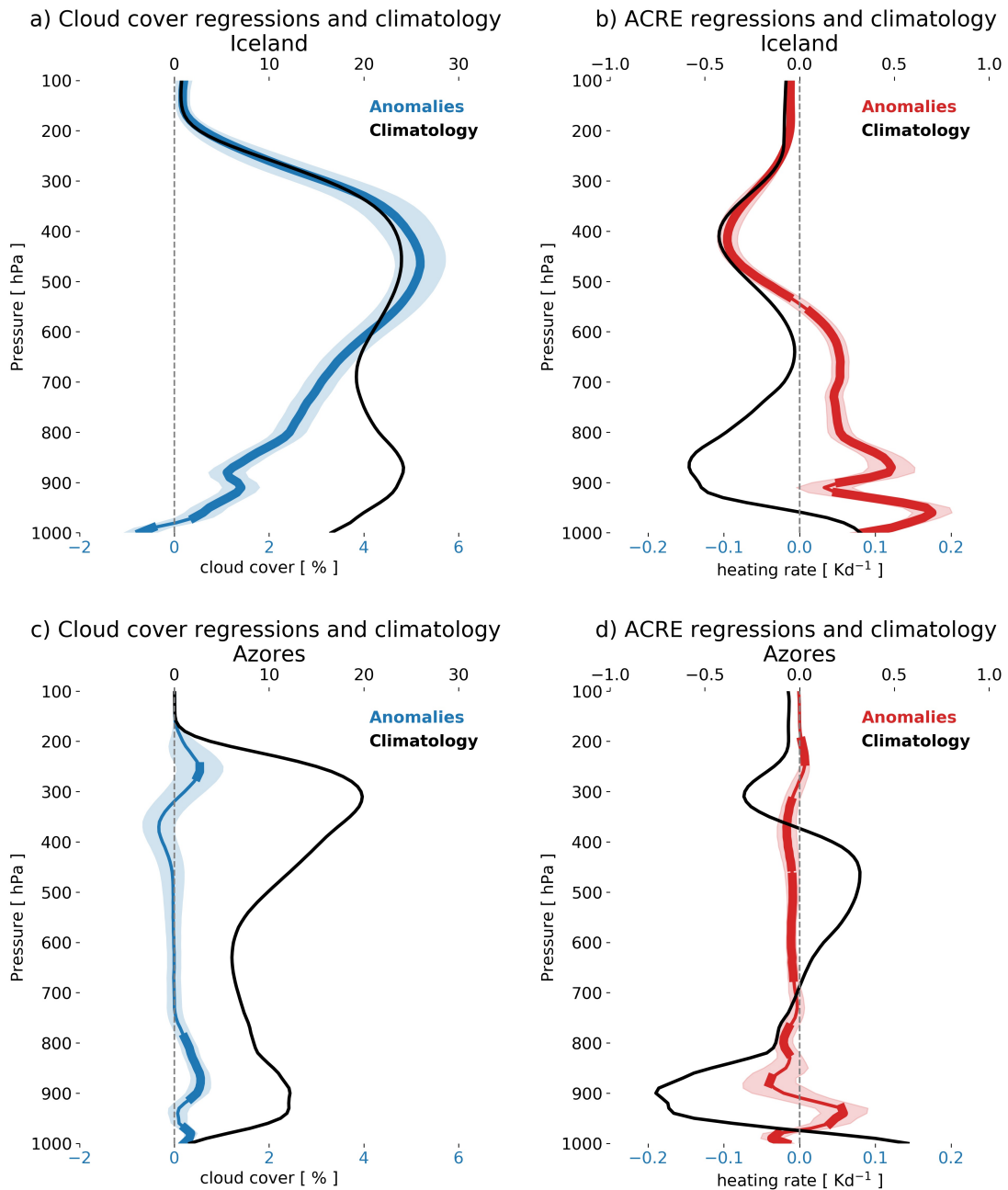


Figure 6.7.: Vertical profiles of cloud cover (a,c) and ACRE (b,d) regressions (blue and red lines) and climatology (black lines) over the Iceland (a,b) and Azores (c,d) domains. Thick blue and red lines denote statistical significance at the 5% level according to a two-sided Wald test, while shading shows the confidence intervals. The averaging domains are shown in Fig. 6.6.

and ACRE and their relative role compared to the sum of all diabatic processes. Here, by means of 5-day mean regressions of ACRE and total diabatic heating onto the NAO index we illustrate their relationship with the NAO dynamics in ICON. We start with an analysis of the zonal-mean perspective over the North Atlantic sector (90°W–40°E) and then proceed with a latitude-longitude view.

6.2.1. Zonal-mean perspective

From a climatological perspective, during DJFM diabatic heating mainly occurs in the lower troposphere across all latitudes (Fig. 6.8a; grey lines). The diabatic heating maximizes in the boundary layer and is associated with surface latent and sensible heat fluxes (Fig. 6.10d; grey lines). In the midlatitudes between 35°N and 65°N the diabatic heating extends in the middle troposphere linked to latent heating associated with midlatitude cyclones and their accompanying precipitation (Fig. 6.10c; grey line). Much weaker diabatic cooling occurs above these levels in the free troposphere, where it is primarily linked to radiative cooling from high-level clouds (Fig. 6.8b, 6.9a). The component of the total diabatic heating that we are interested in here is ACRE. During DJFM, there is ACRE heating near the surface, the middle and upper troposphere primarily linked to trapped longwave radiation emitted from the surface by upper- and lower-tropospheric clouds, while ACRE cooling occurs in the upper troposphere and near the top of the boundary layer, which is associated with emitted longwave radiation from the respective cloud tops (Fig. 6.8b, 6.9a). The arc of middle and upper tropospheric climatological ACRE heating dipole in ICON is linked to ice clouds (Fig. 6.9b), which are known to heat the atmosphere around cloud base and to cool it around cloud top (Atlas et al., 1995; Oreopoulos et al., 2017). On the other hand, the climatological ACRE dipole in the lower troposphere with cooling above 900 hPa and heating below is linked to water clouds (Fig. 6.9c), which are known to cool the boundary layer (Oreopoulos et al., 2017).

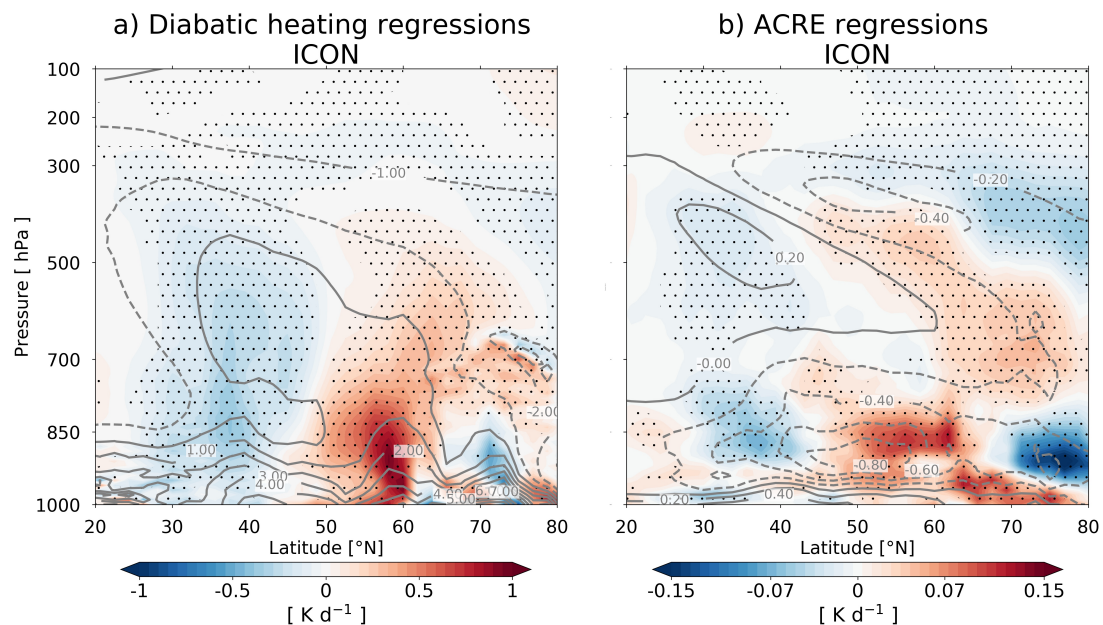


Figure 6.8.: NAO regression of DJFM 5-day-mean zonal-mean (a) total diabatic and (b) ACRE heating rates over the North Atlantic sector (90°W–40°E) in ICON. The grey lines denote the climatology. The results are based on 25 extended winter seasons from December to March. Stippling indicates statistical significance at the 5% level according to a two-sided Wald test.

After having characterizing the climatology of ACRE and the total diabatic heating in ICON, we investigate the link with the NAO by means of 5-day mean regressions of diabatic temperature tendencies onto the NAO index over the North Atlantic sector (Fig. 6.8). Regressions of zonal-mean temperature tendencies due to ACRE (Fig. 6.8b) show that a positive phase of the NAO is associated with a dipole of anomalous ACRE in the lower troposphere at roughly 850 hPa with heating north of the storm track (45°N) and cooling to the south. These ACRE changes are linked to changes in low-level water clouds (Fig. 6.9d,f), where increased (decreased) cloud cover in the lower (higher) latitudes is associated with anomalous ACRE cooling (heating) near the cloud tops. Moreover, a positive phase of the NAO is associated with a vertically tilted dipole of ACRE anomalies with heating roughly below 400 hPa and cooling above. This ACRE dipole is likely linked to anomalies in high- and mid-level ice clouds (Fig. 6.9d,e).

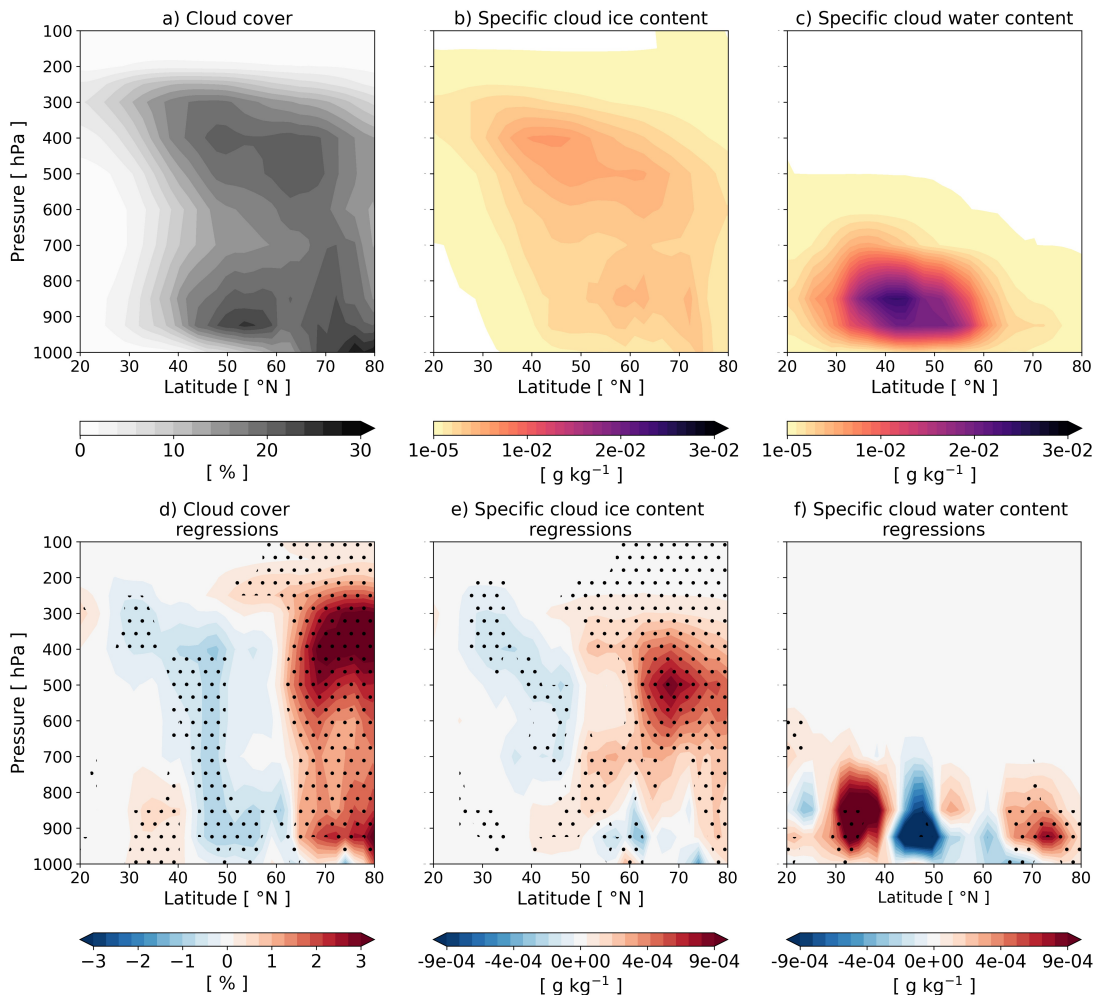


Figure 6.9.: DJFM zonal-mean (a-c) climatology and (d-f) regressions of (a,d) cloud cover, (b,e) specific cloud ice content, and (c,f) specific cloud water content over the North Atlantic sector (90°W–40°E) for ICON. The results are based on 25 extended winter seasons from December to March. Stippling indicates statistical significance at the 5% level according to a two-sided Wald test.

A regression analysis of the total diabatic heating in ICON (Fig. 6.8a) reveals that a positive phase of the NAO is associated with a robust temperature tendency dipole with heating north of the storm track (45°N) and cooling to the south of it. The dipole extends from the surface up to roughly 400 hPa, maximizes between 950 and 700 hPa and reaches a magnitude of up to 60% compared to the climatology. This anomalous total diabatic heating dipole is linked to a poleward shift of the jet stream (Fig. 6.10a) and vertical motions (Fig. 6.10b) and a dipole of anomalous latent heating as well as surface latent- and sensible-heat fluxes, consistent with analogous precipitation (Fig. 6.10c) and surface fluxes (Fig. 6.10d) regressions, respectively.

Overall, the zonal-mean perspective reveals robust ACRE and total diabatic heating changes associated with a positive phase of the NAO. Our analysis in ICON shows that the ACRE changes are linked to changes in the vertical distribution of clouds, while the total diabatic heating changes are primarily associated with changes in precipitation over the North Atlantic.

6.2.2. Latitude-longitude perspective

Given the tilt of the North Atlantic jet stream (Fig. 6.2b) we may expect that the NAO leads to zonally-asymmetric temperature tendency anomalies due to ACRE and total diabatic heating over the North Atlantic sector. This is also suggested from the spatial distribution of cloud anomalies linked to the NAO (Fig. 6.4). A latitude-longitude perspective may therefore be necessary for understanding the spatial distribution of this anomalous heating and its importance for the NAO dynamics.

The regression analysis reveals a rich pattern of the NAO impact on diabatic temperature tendencies at different levels over the North Atlantic sector (Fig. 6.11). Temperature tendency regressions in ICON due to total diabatic heating at 300 hPa exhibit a percentage sign structure with heating over the Labrador and the Mediterranean Sea, and cooling in a stretch from the southeastern US to Scandinavia and the subpolar northeastern Atlantic (Fig. 6.11a). ACRE regressions at 300 hPa reveal the dominating effect of ACRE in the upper troposphere (Fig. 6.11b). The ACRE changes are in line with high-level cloud changes (Fig. 6.4), where anomalous ACRE cooling is evident in areas of positive high-level cloud anomalies and anomalous ACRE heating in areas of negative high-level cloud anomalies.

At 500 hPa the total diabatic heating regressions exhibit heating in a stretch from south of Iceland to the Norwegian Sea and cooling from the Labrador Sea to the Irminger Sea and in a zonal stretch from west of the Azores to the Mediterranean Sea (Fig. 6.11c). In most areas these changes result to some extent from ACRE, which have a magnitude of roughly 10–15% of the total diabatic heating (Fig. 6.11d). The ACRE regressions show cooling over the eastern parts of Greenland along a band that extends from the southern parts of the Labrador Sea to the subpolar Atlantic and in a zonal stretch from southwest of the Azores to the Mediterranean Sea,

6.2. NAO impact on clouds and cloud-radiative effects in ICON

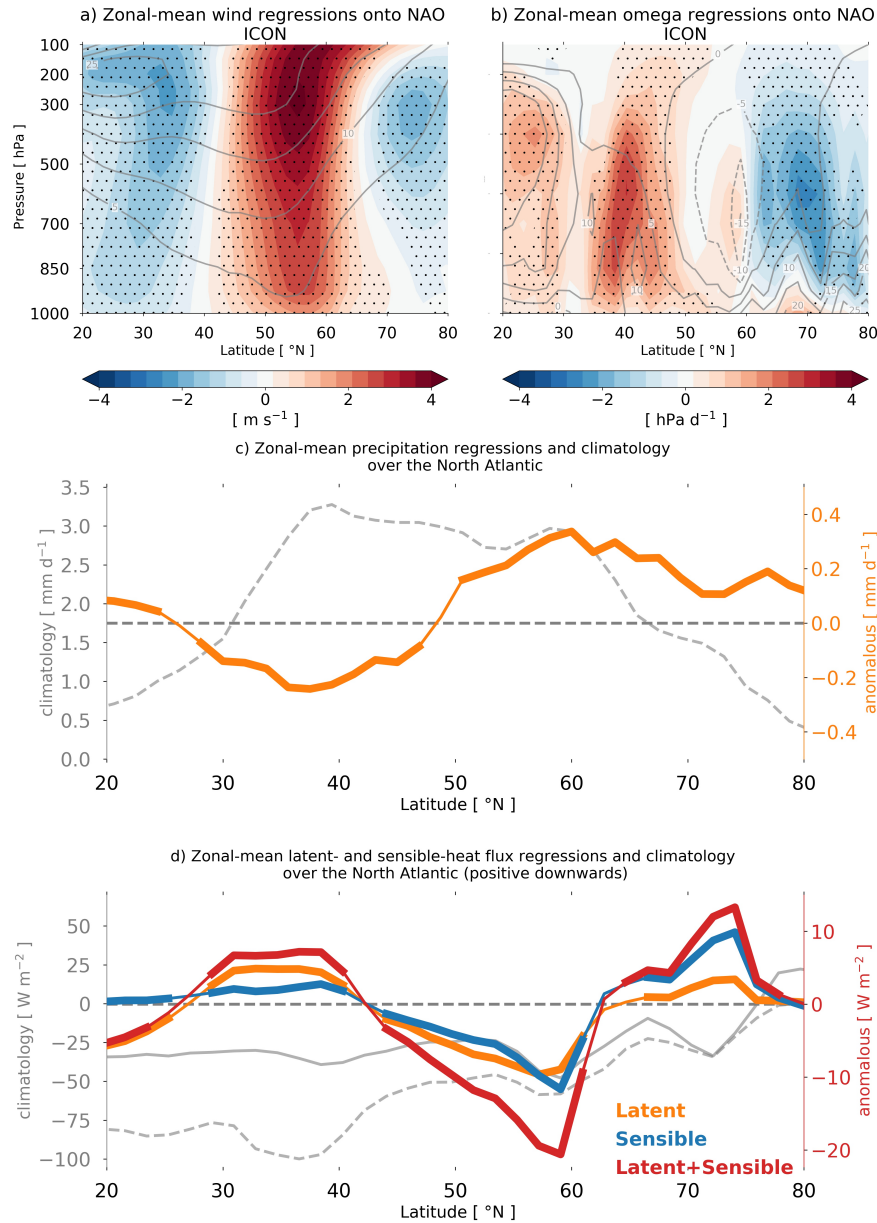


Figure 6.10.: (a, b) DJFM zonal-mean climatology (contours) and regressions (shading) of (a) zonal wind and (b) pressure velocity over the North Atlantic sector (90°W – 40°E) for ICON. (c, d) DJFM zonal-mean climatology (grey lines) and regressions (color lines) of (c) precipitation and (d) sensible- and latent-heat surface fluxes over the North Atlantic sector (90°W – 40°E) for ICON. The results are based on 25 extended winter seasons from December to March. Note that in (b) negative values of pressure velocity denote upward motions. In (d) the dashed grey line denotes latent-heat surface fluxes climatology and the solid grey line denotes sensible-heat surface fluxes climatology. Stippling in (a) and (b) and thick lines in (c) and (d) indicate statistical significance at the 5% level according to a two-sided Wald test.

while heating occurs off the east coast of the US and in a stretch from north of the Azores to the Norwegian Sea and Scandinavia. These ACRE changes are in line with high- and mid-level cloud changes (Fig. 6.4). ACRE heating occurs below the high-level positive cloud anomalies

6. The role of cloud-radiative effects and diabatic processes for the NAO short-term dynamics in ICON

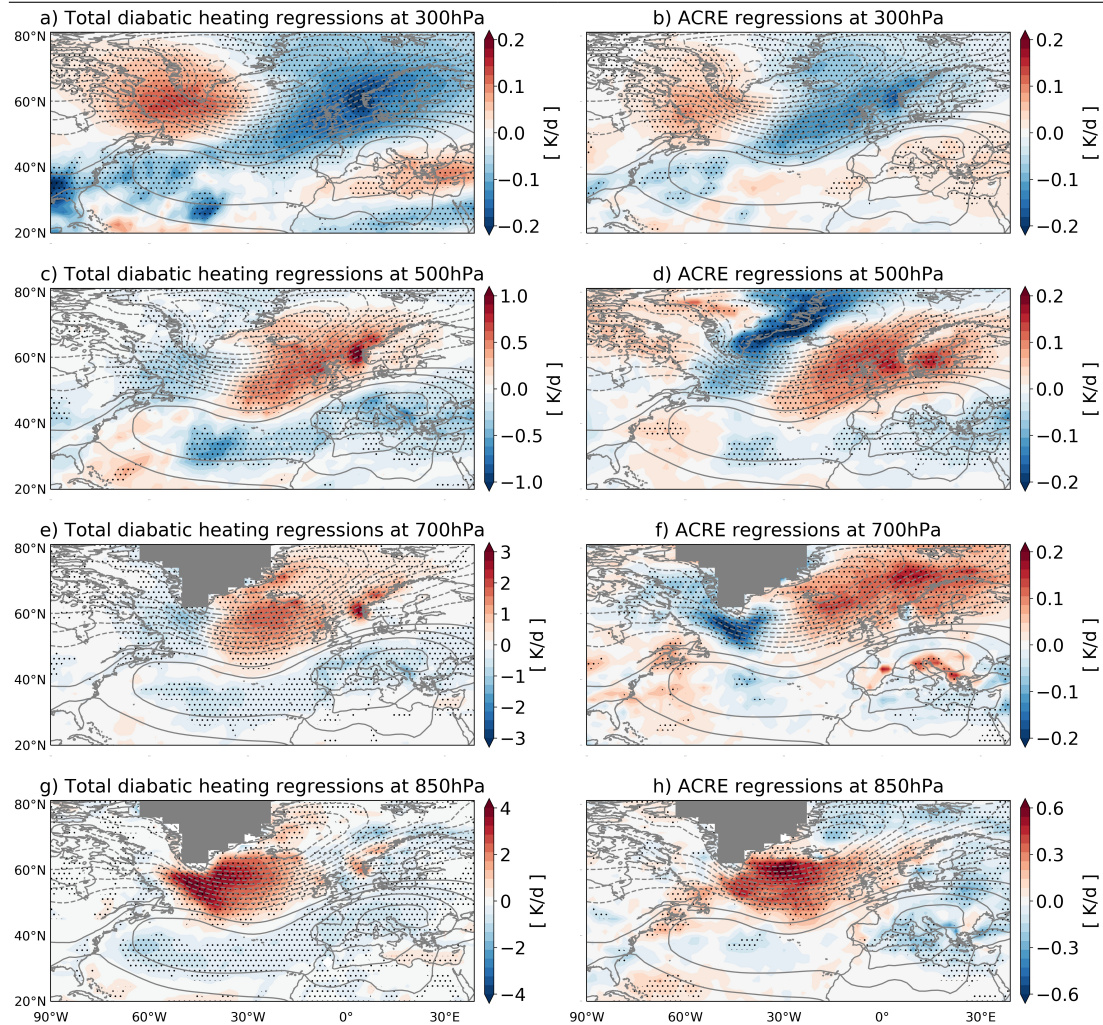


Figure 6.11.: NAO regression of DJFM 5-day-mean (a,c,e,g) total diabatic temperature tendency and (b,d,f,h) ACRE temperature tendency at (a,b) 300 hPa, (c,d) 500 hPa, (e,f) 700 hPa and (g,h) 850 hPa over the North Atlantic region. The black contours denote NAO regressions of 5-day mean surface pressure (contour interval 1 hPa; dash lines indicate negative anomalies; the zero contour is neglected). The results are based on 25 extended winter seasons from December to March in ICON. Stippling indicates statistical significance at the 5% level according to a two-sided Wald test.

and ACRE cooling in either areas of negative high-level cloud anomalies or in areas where positive mid-level clouds dominate.

At 700 and 850 hPa (Fig. 6.11e-h), the regression analysis shows a broad meridional dipole of ACRE and total diabatic heating anomalies. The total diabatic heating temperature tendency regressions for both pressure levels reveal anomalous heating in a zonal stretch from the Irminger Sea to the Norwegian Sea and the subpolar Atlantic, and cooling from the east coast of the US to the Mediterranean Sea. These changes in total diabatic heating are in line with anomalous latent heating associated with precipitation anomalies during a positive phase of the NAO (Fig. 6.14b). The ACRE regressions at 700 hPa show anomalous heating from south of Iceland to the subpolar Atlantic and off the east coast of the US, and cooling west of the

Azores, over the Labrador, the Irminger and the Mediterranean Sea. At 850 hPa, the ACRE regressions show anomalous heating in a stretch from the Labrador Sea to the Norwegian Sea and cooling over the subpolar Atlantic and along a zonal stretch from the east coast of the US to the Mediterranean Sea. The ACRE changes are in line with cloud changes at both pressure levels, where anomalous ACRE heating occurs in areas with decreased low-level clouds, while anomalous ACRE cooling occurs in areas of increased low-level clouds (Fig. 6.4).

Overall, a spatial analysis of the linkages between the NAO and ACRE as well as the total diabatic heating at various atmospheric levels reveals a coherent anomalous heating dipole between the higher and lower latitudes within the middle and lower troposphere. Our analysis shows that the meridional dipole in ACRE heating is linked to increased cloud cover in the higher latitudes and decreased cloud cover in the lower latitudes (Fig. 6.4, 6.9d), which is in line with a poleward shift of the North Atlantic jet stream and anomalous vertical motions (Fig. 6.10a,b). Moreover, regressions of the total diabatic heating temperature tendency and precipitation reveal a meridional anomalous heating dipole mainly in the mid- and low-troposphere that is primarily linked to anomalous precipitation and latent heating during a positive phase of the NAO. The findings in Figure 6.11 also illustrate that ACRE and total diabatic heating changes during a positive NAO vary substantially between the upper and lower troposphere.

These findings motivate us to further study the relative role of ACRE compared to the large-scale dynamics as well as the total diabatic heating for the NAO dynamics using the PTE analysis.

6.3. Role of ACRE and total diabatic heating for the dynamics of the NAO in ICON

In this section we investigate the role of the NAO-related ACRE heating anomalies for the NAO short-term dynamics by means of the PTE analysis. Based on our previous findings in chapter 5 we also aim to test the reproducibility of the observed feedback mechanisms in ICON. As we have previously discussed the PTE allows us to quantify the impact of heating and moisture anomalies on the surface pressure evolution. We use the PTE to assess the relative importance of the NAO-related ACRE, latent heating and total diabatic heating changes with respect to changes in temperature advection by the circulation. A detailed description of the PTE analysis was given in chapter 4.

6.3.1. PTE analysis

We calculate the PTE and its decomposition at hourly intervals in ICON over the North Atlantic domain, and then construct 5-day-means. As previously, we assess the NAO impact on the PTE terms by regressing 5-day-means of the PTE terms onto the NAO index.

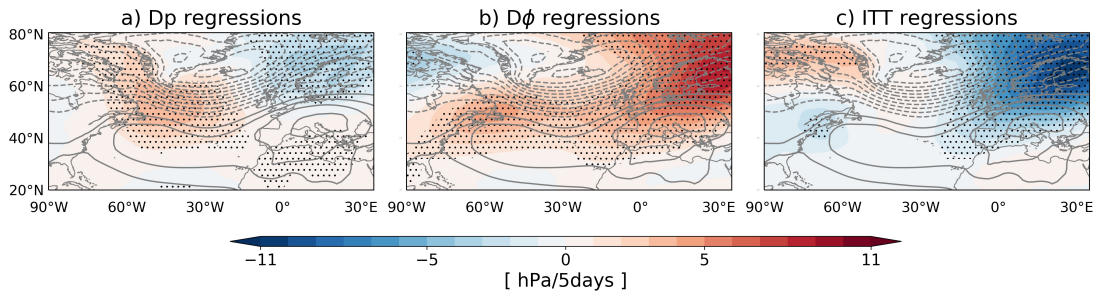


Figure 6.12.: NAO regressions of 5-day-mean (a) surface pressure tendency and contributions from tendencies of (b) the 90 hPa geopotential height and (c) the virtual temperature. The contribution of E-P is near zero and thus neglected here. Grey lines show the NAO-related surface pressure anomaly (contour interval 2 hPa; dash lines indicate negative anomalies). The results are based on 25 extended winter seasons from December to March in ICON model. Stippling indicates statistical significance at the 5% level according to a two-sided Wald test.

We first analyse maps of the NAO regressions of the PTE terms in ICON (Fig. 6.12). A positive NAO is associated with a positive surface pressure tendency over the western parts of the North Atlantic in a region that extends from the Labrador Sea to the north of the Azores, over the Irminger Sea and across the lower latitudes from the west of the Azores to the Mediterranean Sea. A negative surface pressure tendency is found over the Norwegian Sea, Scandinavia and the subpolar Atlantic (Fig. 6.12a). Assuming that during a positive NAO there is an anomalous low-pressure system over Iceland, the surface pressure tendency anomalies are spatially coherent but weaker in magnitude with the warm and cold sector of the low pressure system, where negative surface pressure tendency occurs in the warm sector and positive surface pressure tendency occurs in the cold sector. This surface pressure tendency pattern in most areas results from the compensation between opposite tendencies of the $D\phi$ and ITT terms. The $D\phi$ term dominates over the southern Labrador Sea, the western parts of the North Atlantic and lower latitudes (Fig. 6.12b). On the other hand, the ITT term dominates over the subpolar Atlantic, the Norwegian Sea and Scandinavia (Fig. 6.12c). The $D\phi$ changes have a similar magnitude as the ITT term, and in some cases they are substantially larger, such as in the southern parts of the Labrador Sea and the Irminger Sea. A positive NAO is associated with a slightly weakening or near neutral Iceland low due to a combination of changes in virtual temperature between 90 hPa and the surface (i.e., the ITT term) and the geopotential height at 90 hPa. This is consistent with a beginning decay of the positive phase of the NAO. A comparison with the PTE analysis in ERA-Interim (Fig. 5.8) reveals discrepancies in the sur-

face pressure tendency particularly in higher latitudes, which mainly result from the differences between ICON and ERA-Interim in the compensation between the $D\phi$ and ITT terms. For example over Iceland, the $D\phi$ term in ICON exhibits much weaker and opposite sign of surface pressure tendency anomalies compared to ERA-Interim. This suggests a stronger contribution of the stratosphere on the NAO in ERA-Interim compared to ICON, which in turn is linked with a stronger contribution of the ITT term over Iceland.

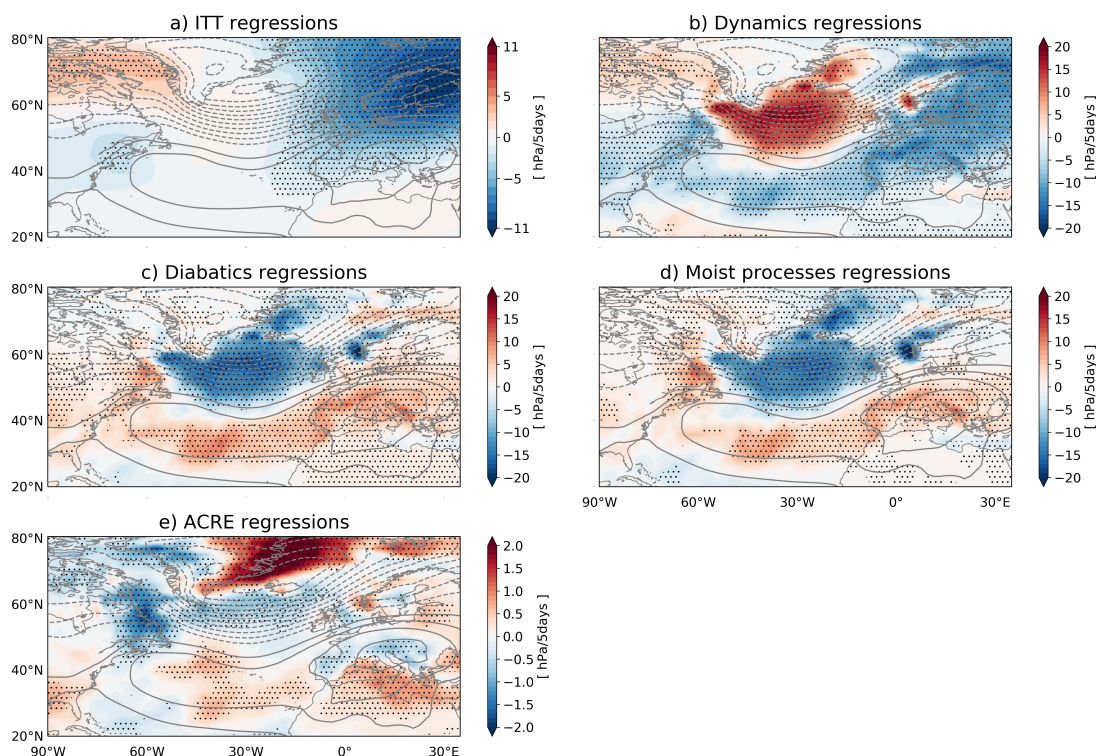


Figure 6.13.: NAO regressions of 5-day-mean surface pressure tendency from (a) changes in virtual temperature (ITT), (b) large-scale dynamics (DYN), (c) diabatic processes (DIAB), (d) latent heating (moist processes) and (e) atmospheric cloud-radiative effects (ACRE). The results are based on 25 extended winter seasons from December to March in ICON. Note the different color scales. The grey contours denote NAO regressions of 5-day mean surface pressure (contour interval 1 hPa; dash lines indicate negative anomalies; the zero contour is excluded). Note the different color scales. Stippling indicates statistical significance at the 5% level according to a two-sided Wald test.

In order to assess the relative importance of different diabatic processes for the NAO dynamics, we further decompose the ITT anomalies associated with a positive NAO into the contributions of Eq. (4.5). As previously, the horizontal advection term TADV and the vertical motions term VMT are shown as the sum and referred to as dynamics ($DYN=TADV+VMT$; Fig. 6.13). Figure 6.13 shows that the ITT anomalies result from spatially coherent and opposite anomalies of surface pressure tendency due to DYN and the total diabatic heating (DIAB). The anomalous surface pressure tendency due to DYN acts to damp the surface pressure anomalies associated with a positive phase of the NAO (Fig. 6.13b), while the surface pressure tendency anomalies due to DIAB work in favour of reinforcing them (Fig. 6.13c). The DIAB anomalies

6. The role of cloud-radiative effects and diabatic processes for the NAO short-term dynamics in ICON

exhibit a magnitude similar to those of DYN, and in some cases are even larger, such as the west coast of Norway, north of Iceland and in an area between Iceland and the British Isles. Latent heating is the dominant diabatic process and acts in favour of positive NAO surface pressure anomalies (Fig. 6.13d). This view is supported by the spatial correspondence with the precipitation regressions (Fig. 6.14b) and is in line with previous work of Greatbatch and Jung (2007) and Woollings et al. (2016). Surface pressure tendency anomalies due to ACRE exhibit a magnitude of up to 10% of DIAB and act in favour of positive NAO surface pressure anomalies mainly in the lower latitudes of the Atlantic. Around Iceland the ACRE pattern is less spatially coherent, with negative surface pressure tendency anomalies due to ACRE south of Iceland and positive anomalies north of Iceland. The surface pressure tendency anomalies due to ACRE are in line with the anomalous vertically integrated ACRE (Fig. 6.5), where areas of column-mean heating due to ACRE are linked to negative surface pressure tendency anomalies and areas of column-mean cooling due to ACRE are linked to positive surface pressure tendency anomalies. Around Iceland, the north-south dipole of surface pressure tendency anomalies due to ACRE is linked to a dipole of low-level cloud cover anomalies associated with a positive NAO. Although positive mid-level cloud cover anomalies occur within the entire Iceland domain, increased low-level water and mixed-phase clouds north of Iceland (Fig. 6.4f,6.9f) induce strong low-level ACRE cooling (Fig. 6.8b) that dominates the vertically integrated ACRE.

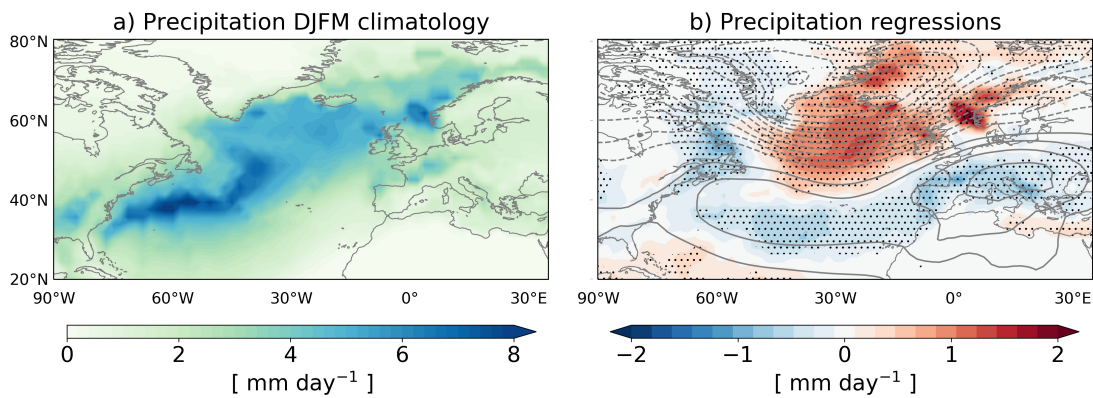


Figure 6.14.: (a) Climatology and (b) 5-day mean NAO regressions of precipitation in ICON during DJFM. The results are based on 25 extended winter seasons from December to March in ICON. The grey contours denote NAO regressions of 5-day mean surface pressure (contour interval 1 hPa; dash lines indicate negative anomalies; the zero contour is excluded). Stippling indicates statistical significance at the 5% level according to a two-sided Wald test.

Overall, the PTE analysis in ICON shows that the NAO-related surface pressure tendency anomalies due to ACRE act to reinforce the NAO-related surface anomalies mainly around the Azores, and therefore constitute a positive feedback to the NAO. However, ACRE have a minor impact compared to the total diabatic heating, which itself has a similar magnitude as the large-scale dynamics and is a substantial positive feedback to the NAO. These findings are

qualitatively in line with our previous observational findings in chapter 5 and suggest that the ACRE and total diabatic heating feedback mechanisms are robust. A comparison of the PTE analysis in ICON (Fig. 6.13) with ERA-Interim (Fig. 5.8) yields spatially coherent and qualitatively consistent surface pressure changes due to ACRE of similar magnitude, despite notable differences in magnitude north of Iceland along the east coast of Greenland. In this area, both ICON and ERA-Interim yield the strongest positive surface pressure tendency anomalies due to ACRE. This results from anomalous ACRE column-mean cooling over this area (Fig. 5.6a,b, 6.5) and is associated with increased cloud cover throughout the entire depth of the troposphere, which in ICON maximises in the mid- and low-levels (Fig. 6.4). On the hand, in ERA-Interim the increased cloud cover maximises in the mid-levels (Fig. 5.5). This suggests that the differences in mid- and low-level clouds and their properties (e.g. ice and water cloud content) might explain the magnitude differences of the ACRE and ACRE-induced surface pressure tendency anomalies between ICON and ERA-Interim.

6.4. Short-term NAO response to imposed diabatic heating

To better understand the impact of the anomalous NAO-related ACRE and total diabatic heating we perform sensitivity simulations with ICON. The simulations use ICON in a hindcast sense and are perturbed by the time-constant NAO-related heating patterns from ACRE and the total diabatic heating processes described in the previous sections. The imposed heating patterns are shown in Fig. 6.11 for four specific atmospheric pressure levels. For a detailed description of these simulations, the reader is referred to chapter 4. Our main aim here is to test to what extent the NAO evolution is indeed affected by the NAO-related diabatic heating, and to what extent this impact depends on the NAO state. To this end we first present maps of the mean short-term response to the imposed heating and then illustrate the time evolution of the NAO response for different initial NAO states.

6.4.1. Latitude-longitude perspective of the response to the NAO-related ACRE heating pattern

We study the model response to the imposed additional heating by means of changes in the mean sea-level pressure (MSLP) between all pairs of control simulations (CTRL) and hindcast simulations forced with the additional NAO-related ACRE and total diabating heating (FORC). The comparison consists of 600 pairs of 15-day long simulations.

The ACRE-induced MSLP response for three selected lead-times (day 2, 5 and 10) shows a consistent and increasing impact of anomalous ACRE on MSLP with time: MSLP decreases along a zonal band from the Labrador Sea to the Norwegian Sea and the northeastern subpolar Atlantic, and increases across the rest of the domain (Fig. 6.15b,d,f). The ACRE-induced

6. *The role of cloud-radiative effects and diabatic processes for the NAO short-term dynamics in ICON*

MSLP anomalies illustrate that ACRE anomalies associated with a positive NAO tend to lower the MSLP to the south and to the east of Iceland and increase it anywhere else. This impact is independent of the initial NAO state. The MSLP changes show some spatial coherence with the NAO-related MSLP anomalies and suggest that the imposed ACRE heating associated with a positive NAO acts in favour of a positive NAO. For most ocean areas except north of Iceland, the MSLP changes on day-5 are qualitatively in line with the diagnosed surface pressure tendency from the PTE analysis (Fig. 6.13e). However, over the continental areas and north of Iceland the MSLP changes are not in line with the PTE analysis. This is potentially due to either a cancelling effect from another process, such as ACRE-induced static stability changes, or non-linear responses to the imposed ACRE heating. For example north of Iceland, the induced ACRE heating pattern may lead to decreased low-level static stability, which may in turn lead to enhanced upward motions and changes in cloud formation in the low- and mid-levels which acts against the ACRE imposed cooling. Furthermore, the spatial distribution of MSLP changes suggests that the mid- and lower-tropospheric anomalous ACRE heating dominate the MSLP response. Another interesting feature is the independence of these experiments to the initial NAO state, which highlights the robustness of ACRE feedback on the NAO. Moreover, the increasing impact of ACRE with time suggests that even though the ACRE impact might be negligible for short lead-times (Fig. 6.15b), its contribution becomes more substantial beyond day 5 (Fig. 6.15f). Overall, the sensitivity simulations illustrate that the ACRE constitute a weak positive feedback to the NAO. This confirms our hypothesis based on the PTE analysis.

6.4.2. **Latitude-longitude perspective of the response to the NAO-related total diabatic heating pattern**

We now analyse the mean difference in MSLP between the CTRL and the FORC simulations that we use the diabatic heating due to all diabatic processes. As for ACRE, this comparison consists of 600 pairs of 15-day long simulations. The MSLP response to the induced total diabatic heating for three selected lead-times (day 2, day 5 and day 10) illustrates a decrease in MSLP in the higher latitudes and an increase in MSLP over the lower latitudes (Fig. 6.15a,c,e). The MSLP changes due to the imposed total diabatic heating are overall spatially coherent with the NAO-related MSLP anomalies. This suggests that the imposed positive NAO-related total diabatic heating acts to make the Iceland low deeper and the Azores high stronger, and therefore acts in favour of a positive NAO phase. The spatial distribution of the MSLP changes suggest that most of the response is caused by the imposed total diabatic heating between the surface and 500 hPa (Fig. 6.11). For most of the areas, the MSLP changes on day 5 are qualitatively in line with the diagnosed surface pressure tendency from the PTE analysis (Fig. 6.13c). Overall, these sensitivity tests in ICON illustrate that the NAO-related total diabatic heating constitutes a positive feedback to the NAO. Again, this is in line with our PTE-based hypothesis.

6.4. Short-term NAO response to imposed diabatic heating

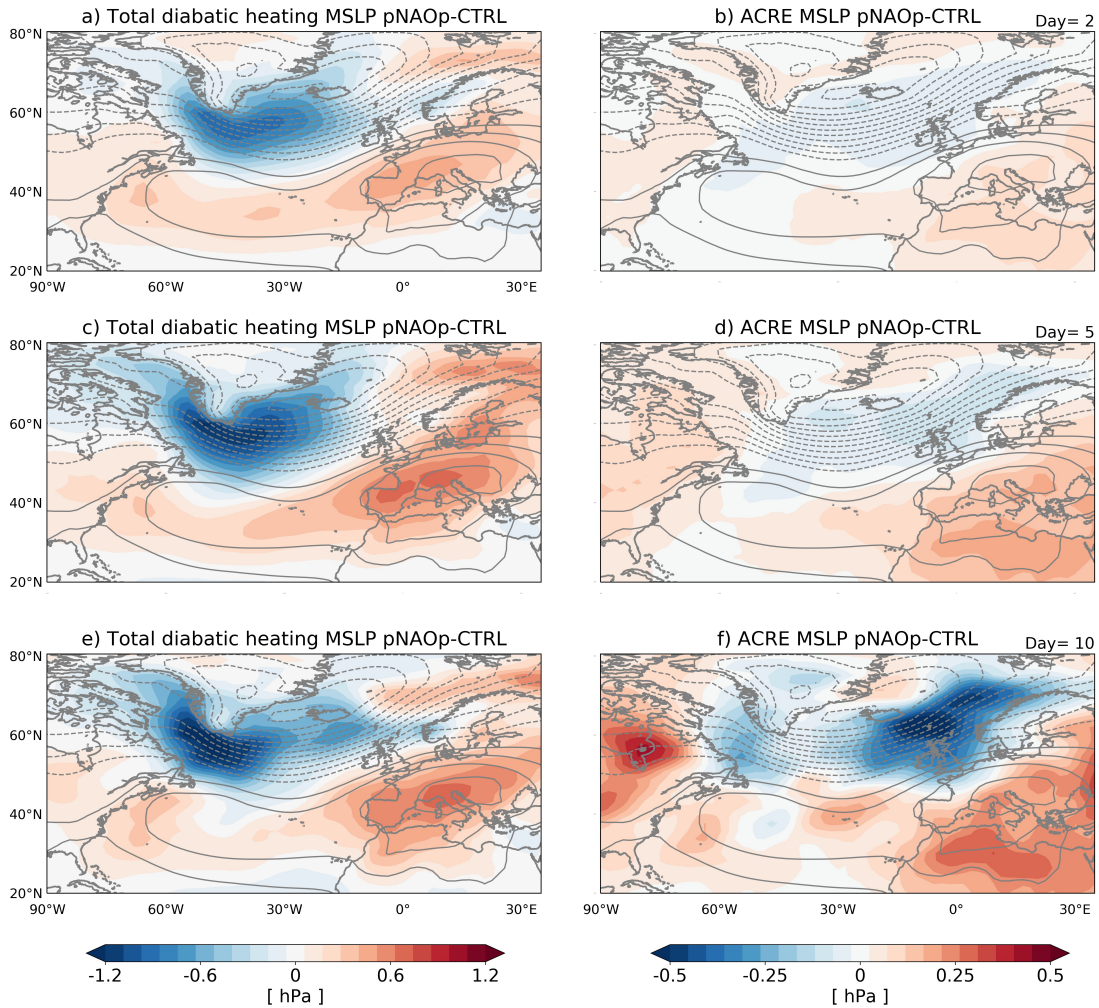


Figure 6.15.: Mean sea-level pressure (MSLP) difference between the forced (pNAOp) and the control (CTRL) simulations, where we impose a positive NAO-related (a,c,e) total diabatic heating and (b,d,f) ACRE heating pattern on (a, b) day 2, (c, d) day 5 and (e, f) day 10 of the simulations. The contours denote NAO regressions of 5-day mean MSLP (contour interval 1 hPa; dash lines indicate negative anomalies; the zero contour is excluded). The results are based on 600 pairs of 15-day CTRL and pNAOp simulations in ICON.

Despite the fact that both ACRE and total diabatic heating constitute positive feedbacks to the NAO short-term dynamics, a comparison of the MSLP responses (Fig. 6.15) between the two heating patterns shows that for short lead-times (up to day 5) the ACRE have a minor impact on MSLP and therefore the NAO, with a magnitude of at most 10% of the total diabatic heating. However, beyond day 5 our analysis suggests that ACRE may have a larger impact on MSLP and the NAO, because on these time scales the ACRE-induced changes have a magnitude of up to 40–50% of the changes induced by the total diabatic heating on day 10 (Fig. 6.15f). A potential reason for that could be the differences in the vertical structure of the imposed heating patterns particularly in the upper troposphere (Fig. 6.8). Moreover, the strong physical relationship between the total diabatic heating and large-scaled dynamics, as it is also

suggested from the PTE analysis, suggests that the total diabatic heating to a larger extent is compensated by the large-scaled dynamics, which is not the case everywhere for ACRE. Thus, a lack of a compensating process in the upper troposphere is potentially linked to a stronger influence of ACRE with longer lead times.

6.4.3. Time dependence of the response to the NAO-related ACRE heating pattern

We now assess the relative role of ACRE heating for the NAO time evolution in the ICON simulations. An analysis of the time evolution of the NAO changes (ΔNAO) for the first 7 days of all the 600 pairs of simulations independent of the NAO initial state illustrates that the additional ACRE heating forces the NAO towards a more positive NAO in the FORC simulations compared to the CTRL simulations. The NAO change mainly occurs after day 2 (Fig. 6.16a). For lead-times of up to 3 days, more than 95% of the FORC simulations show a more positive NAO, while for lead times of up to 5 days more than 50% of the FORC simulations show a more positive NAO. This shows that the ACRE impact is rather weak with a magnitude of up to 1–2% of 1σ NAO. However, as previously discussed our analysis illustrates that the ACRE impact grows in time.

In addition we study the sensitivity of these results to the NAO initial state. To test the impact of the initial state in the time evolution of ΔNAO , we study the FORC simulations that are initialised from a NAO with a standardized deviation larger than $\pm 0.5 \sigma$ or $\pm 1 \sigma$ (Fig. 6.16b,c). The stratification with respect to the NAO initial states shows that up to day 3 more than 95% of the FORC experiments tend to have a more positive NAO compared to the CTRL ones. Thus, the time evolution of ΔNAO is the same as for all NAO cases (Fig. 6.16a) and ΔNAO exhibits no sensitivity to the initial state.

6.4.4. Time dependence of the response to the NAO-related total diabatic heating pattern

We here assess the role of the total diabatic heating for the NAO time evolution in ICON. An analysis of the difference in the NAO (ΔNAO) time evolution for the first 7 days of all the 600 pairs of simulations independent of the NAO initial state illustrates that the additional NAO-related total diabatic heating forces the NAO in the FORC simulations towards a more positive NAO compared to the CTRL simulations (Fig. 6.17a). In lead-times of up to day 4 more than 95% of the FORC experiments exhibit a more positive NAO, while up to day 6 more than 50% of the FORC simulations show a more positive NAO. Moreover, our analysis illustrates that the total diabatic heating impact in the FORC simulations in ICON has a magnitude of up to

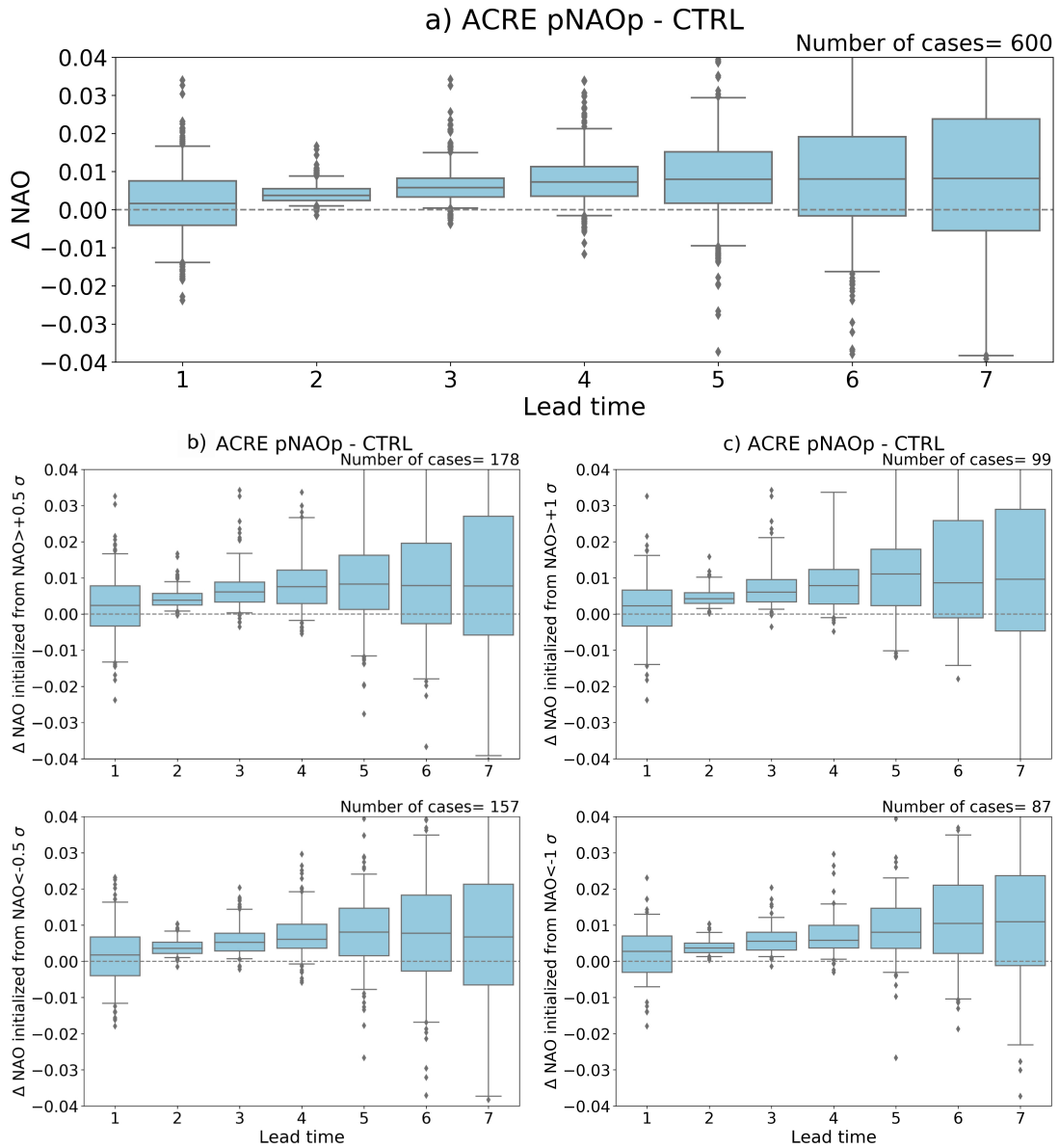


Figure 6.16.: Boxplot of the NAO difference time evolution between the forced and the control simulations initialised from (a) any NAO state, and a state of larger than (b) $+0.5 \sigma$ or (c) $+1 \sigma$ NAO (top panels) or smaller than (b) -0.5σ or (c) -1σ NAO (bottom panels). In the forced simulation a positive NAO-related ACRE heating pattern is imposed. The whiskers represent the 2.5th and 97.5th percentiles. The results are based on 600 pairs of FORC and CTRL simulations in ICON during 25 extended winter DJFM seasons. In the right top corner of each panel the number of pairs that we compare for each NAO initialisation category is provided.

5–10% of 1σ NAO. This conforms that the total diabatic heating has a much more substantial impact on the NAO evolution than ACRE.

We further test the sensitivity of these results to the NAO initial state. A sensitivity test of the time evolution of ΔNAO to the initial NAO state shows that the impact is robust and independent of the initial NAO state (Fig. 6.17b,c). Up to day 4 more than 95% of the FORC

6. The role of cloud-radiative effects and diabatic processes for the NAO short-term dynamics in ICON

simulations tend to have a more positive NAO compared to the CTRL simulations. This shows that the impact of the total diabatic heating on the NAO evolution is independent of the NAO state (Fig. 6.17a).

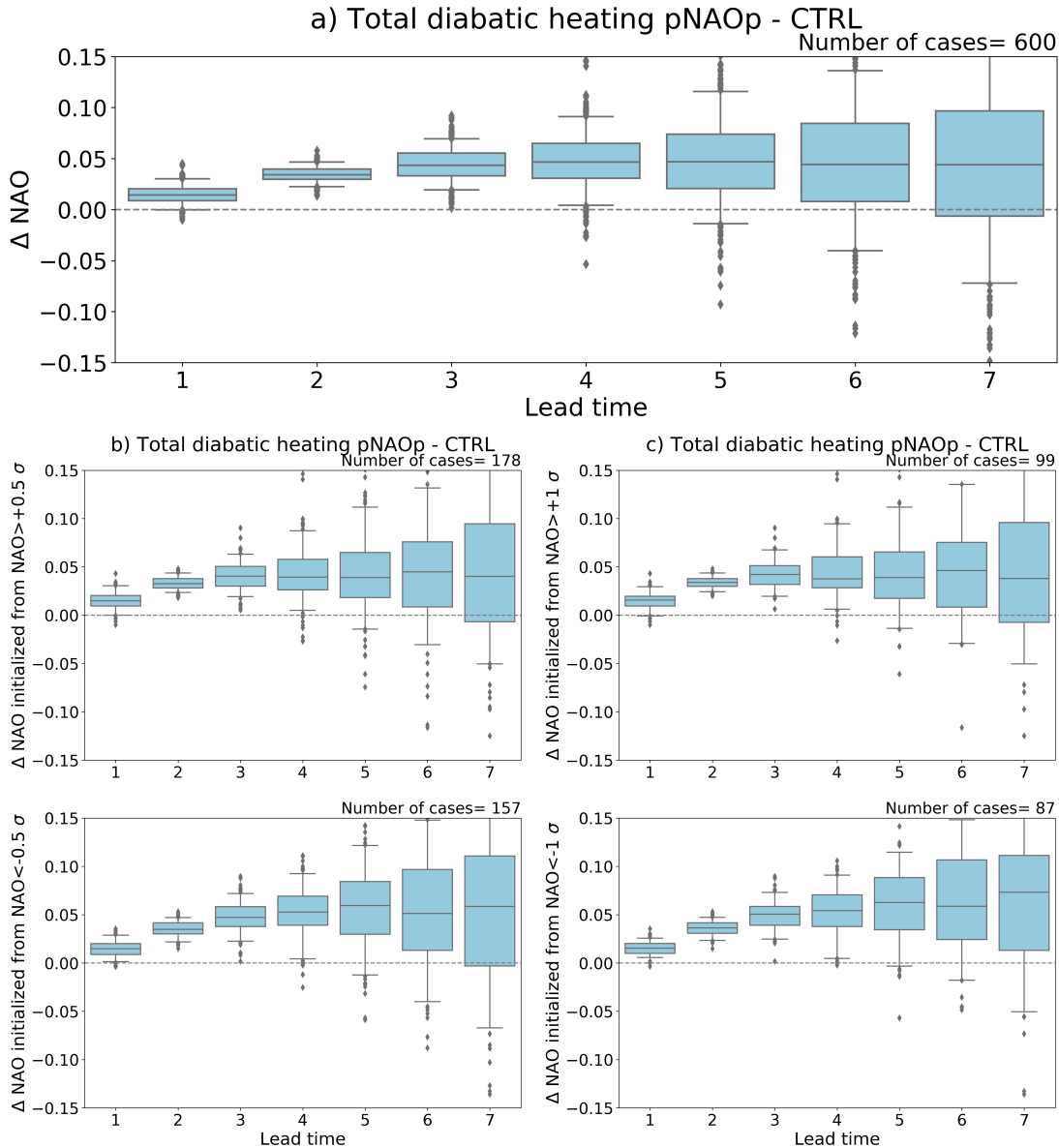


Figure 6.17.: Boxplot of the NAO difference time evolution between the forced and the control simulations initialised from (a) any NAO state, and a state of larger than (b) $+0.5$ or (c) $+1$ σ NAO (top panels) or smaller than (b) -0.5 or (c) -1 σ NAO (bottom panels). In the forced simulation a positive NAO-related total diabatic heating pattern is imposed. The whiskers represent the 2.5th and 97.5th percentiles. The results are based on 600 pairs of FORC and CTRL simulations in ICON during 25 extended winter DJFM seasons. In the right top corner of each panel the number of pairs that we compare for each NAO initialisation category is provided.

Overall, the sensitivity simulations confirm our PTE-based hypothesis of a weak positive feedback of ACRE and a substantial positive feedback of the total diabatic heating.

6.5. Conclusions

Motivated by previous work of Li et al. (2014a), Greatbatch and Jung (2007) and Papavasileiou et al. (2020) in this chapter we studied the coupling between the NAO and ACRE as well as the total diabatic heating on synoptic-scales in ICON simulations. We documented the NAO in ICON and studied i) the NAO impact on clouds, ACRE and the total diabatic heating, and ii) the impact of ACRE and total diabatic heating on synoptical-scale dynamics of the NAO. Our modeling work was in particular motivated by the hypothesis of Papavasileiou et al. (2020) that ACRE and the total diabatic heating are a positive feedback to the NAO and enhance the NAO persistence.

Analysing 5-day means of clouds and ACRE we found that a positive phase of the NAO is associated with robust changes in clouds that lead to anomalous column-mean heating and cooling around Iceland and the Azores, respectively. Using the PTE analysis we assessed the relative role of ACRE and total diabatic heating compared to the large-scale dynamics. Our analysis shows that ACRE constitute a weak but positive feedback to the NAO, and that the total diabatic heating is a substantial positive feedback with a magnitude comparable to the impact of large-scale dynamics. A decomposition of the total diabatic heating in ICON showed that latent heating dominates the total diabatic heating, with a magnitude of more than 90% of the total diabatic heating. The surface pressure tendency anomalies induced by ACRE do not strongly project onto the NAO-related surface pressure anomalies, while the surface pressure tendency anomalies due to the total diabatic heating are more spatially coherent with the NAO pattern. These results are in line with our previous observational findings (chapter 5), suggesting that the ACRE and total diabatic heating constitute a positive feedback to the NAO, with latent heating dominating and ACRE having a minor impact.

We further assessed these impacts in a set of sensitivity tests for which we perturbed the temperature equation with an additional NAO-related diabatic heating due to either ACRE or the total diabatic heating. Our simulations showed that independent of the initial state ACRE feed back positively and their impact is rather negligible with a magnitude of less than 2% of 1σ NAO. This result is in line with previous findings of Grise et al. (2019). On the other hand, the total diabatic heating, which is dominated by latent heating, constitutes a stronger positive feedback with a magnitude of up to 10% of 1σ NAO. This result is in contrast to the modeling work of Greatbatch and Jung (2007) and Xia and Chang (2014), who argued that latent heating acts as a negative feedback and damps the persistence of the NAO and the annular modes, respectively. However, we believe that the differences between our study and theirs are due to the selected time-scale. Greatbatch and Jung (2007) and Xia and Chang (2014) investigated the impact of the total diabatic heating on a climatological perspective while we study this coupling on synoptic time-scales.

6. The role of cloud-radiative effects and diabatic processes for the NAO short-term dynamics in ICON

7. Summary and outlook

7.1. Summary

The weather and climate of the northern hemisphere midlatitudes exhibits substantial variability on a wide range of spatiotemporal scales ranging from days to decades. During winter, a large portion of this variability is explained by a phenomenon that takes place over the North Atlantic ocean and that is called the North Atlantic Oscillation (NAO). Being a large-scale surface pressure seesaw with centers of action around Iceland and the Azores, the NAO modulates the weather and climate over the North Atlantic sector and the surrounding continental areas of North America and Europe. For instance, it modulates the latitudinal position of the jet stream and shapes the large-scale environment for the formation and movement of extratropical cyclones. Extreme and persistent phases of the NAO are associated with high-impact weather events that can have large socio-economic impacts due to floods and temperature extremes, particularly over Europe. Our understanding of the persistence of the NAO and its interaction with diabatic processes of clouds and convection remains limited, which hampers our ability to predict the NAO. Previous studies highlighted the importance of cloud-radiative effects for the mean extratropical circulation response under climate change. However, limited work has been done for the role of clouds and their radiative feedback for the extratropical circulation variability on synoptic time scales. This has motivated this thesis.

The persistence of the NAO depends on many internal and external forcing factors. Previous observational work of Li et al. (2014a) hypothesized that top-of-atmosphere (TOA) cloud-radiative effects (CRE) may act to reduce the NAO persistence and that CRE might be an important but so far overlooked feedback process for NAO dynamics. The main goals of this thesis were to test the hypothesis of Li et al. (2014a) by investigating the coupling between the NAO and atmospheric CRE (ACRE), and to quantify the ACRE impact on the NAO dynamics on synoptic time scales. For this purpose, a systematic analysis in both observations and model simulations was carried out. In chapter 5 by using observations and reanalysis data we have studied i) how NAO variability on synoptic time-scales affects clouds and ACRE, and ii) the potential of these NAO-generated changes in ACRE to in turn affect the NAO. Then motivated by the work of Li et al. (2014a), Greatbatch and Jung (2007) and Papavasileiou et al. (2020) in chapter 6 we have further studied the coupling between the NAO and ACRE as well as the total diabatic heating on synoptic-scales in ICON simulations. In this part of this thesis using ICON

simulations we have investigated i) the NAO impact on clouds, ACRE and the total diabatic heating, and ii) the impact of ACRE and total diabatic heating on synoptic-scale dynamics of the NAO. The work within this thesis was the first to explore the NAO-ACRE coupling and to quantify the role of ACRE as well as total diabatic heating for the short-term dynamics of the NAO. Here we summarize the main research findings presented in chapters 5 and 6 by answering the three research questions posed in chapter 3.

The first research question (RQ 1) has dealt with the investigation of the linkages between the NAO and ACRE in satellite observations, ERA-Interim reanalysis data and numerical simulations in the ICON global atmosphere model. By means of linear regressions we have studied how clouds and ACRE change as a result of synoptic 5-day-mean NAO variability. The main findings of this part of the study are summarized in the following.

RQ 1) How does the NAO impact clouds and their radiative effects?

The analysis of 5-day mean data of cloud satellite retrievals from CloudSat/CALIPSO revealed robust changes of high- and low-level clouds linked to the NAO. A positive phase of the NAO is associated with increased high-level cloud incidence along the storm track and the subpolar Atlantic, and decreased high-level cloud incidence equatorward and poleward of it. Anomalies of opposite sign occur in the lower troposphere. These changes of high-level clouds are consistent with changes in vertical motions, where areas of positive high-level cloud anomalies are linked to enhanced upward motions and areas of negative high-level cloud anomalies are linked to enhanced downward motions. On the other hand the changes of low-level clouds are in line with enhanced downward motions and increased low-level static stability. Moreover, using ERA-Interim short-term forecasts and numerical simulations in ICON we have shown that the cloud changes linked to the NAO are qualitatively consistent with the satellite observations. Our analysis revealed that these robust cloud changes associated with the NAO lead to a dipole of anomalous vertically-integrated ACRE with column-mean heating over the Iceland low and column-mean cooling over the Azores high. Analysing the vertical distribution of these ACRE changes in ICON simulations we have shown that ACRE dominate the total diabatic heating anomalies in the upper troposphere with a magnitude of up to 80%, while in the lower troposphere ACRE constitute only up to 10–15% of the total diabatic heating.

The second research question (RQ 2) dealt with the study of the robustness of the NAO impact on ACRE. Here, a comparison between the observational and model data was conducted

with a particular focus on the two centers of action for the NAO dynamics, one around the Iceland low and one around the Azores high. The main findings of this part of the study are summarized in the following.

RQ 2) To what extent are the NAO-related changes in ACRE robust in observations, reanalysis and model simulations?

The analysis of vertically-integrated ACRE changes over the two centers of action based on satellite retrievals from CloudSat/CALIPSO, CERES-SYN1deg, CERES-EBAF and GERB/SEVIRI, ERA-Interim short-term forecasts and numerical simulations in ICON revealed that the NAO-induced dipole of ACRE anomalies is robust in sign but not in magnitude across datasets. This confirms a qualitatively consistent link between the NAO centers of action and ACRE. However, the comparison among the datasets illustrated the uncertainty in the magnitude of the NAO impact on ACRE. Our analysis showed that these discrepancies in magnitude of the ACRE changes may arise due to differences in the vertical distribution of cloud changes within the troposphere. A study of vertical profiles of cloud and ACRE in observations and ICON simulations illustrated that over the Iceland low NAO-related cloud changes lead to mid- and low-level anomalous ACRE heating and upper-level anomalous ACRE cooling, which varies in magnitude among the datasets due to differences in the vertical distribution of cloud changes. This was particularly evident in the lower troposphere, highlighting the need to better represent low-level clouds in models, which is a well known issue.

Finally, in the third research question (RQ 3) our focus was shifted to investigate the role of these ACRE changes for the short-term dynamics of the NAO. Here, by means of a diagnostic approach and sensitivity simulations we have quantified the relevance of ACRE for the short-term dynamics of the NAO compared to large-scale dynamics as well as other diabatic processes. The main findings of this part of the study are summarized in the following.

RQ 3) What is the role of the NAO-related ACRE anomalies for the dynamics of the NAO on synoptic time-scales, and how does the ACRE impact compare to the impact of total diabatic heating?

The PTE analysis in ERA-Interim data showed that the surface pressure tendency anomalies due to ACRE act to maintain the surface pressure anomalies over the Azores and have no area-averaged impact over Iceland.

Additionally, the PTE analysis in ICON revealed qualitatively consistent with ERA-Interim surface pressure tendency anomalies due to ACRE over the Azores, while over Iceland a mixture of positive and negative surface pressure tendency anomalies was found. The main differences in magnitude over the lower latitudes of the North Atlantic can be attributed to the differences in the NAO impact on surface pressure, clouds and ACRE. In ICON, the southern center of action is shifted eastward over southern Europe and Mediterranean, while in ERA-Interim it is located around the Azores. Because we have focused our analysis over the North Atlantic ocean, the spatial displacement leads to discrepancies in the NAO-related changes magnitude between ICON and ERA-Interim. The PTE analysis showed that ACRE constitute a positive feedback on the NAO and should act to increase the NAO persistence. This result is in contrast to the hypothesis of Li et al. (2014a), who argued that TOA CRE damp the NAO-related temperature anomalies and should decrease the NAO persistence. However, their framework ignored the mismatch between the vertical profiles of CRE and temperature anomalies, and we have argued that the PTE framework is better suited as it regards the entire vertical column. Our analysis further showed that the ACRE impact is minor compared to the total diabatic heating, which is dominated by latent heating and strongly amplifies the NAO-related surface pressure anomalies. The surface pressure tendency anomalies due to the total diabatic heating have a magnitude similar to the large-scale dynamics, which suggests that total diabatic heating is a substantial positive feedback to the NAO and should act to make the NAO more persistent. This indicates that ACRE are not crucial to the NAO dynamics on synoptic time-scales. Overall, the comparison of ICON with ERA-Interim revealed qualitatively consistent ACRE and total diabatic heating feedback mechanisms.

Sensitivity simulations with ICON, for which an additional NAO-related anomalous ACRE or total diabatic heating pattern was imposed, showed that both ACRE and total diabatic heating are a positive feedback to the NAO and increase the persistence of the NAO. The NAO response to the added NAO-related diabatic heating showed that this positive feedback is mostly evident during the first 4–6 days. Our modeling work showed that ACRE feed back positively by up to 1–2% of 1σ NAO, while the total diabatic heating feed back positively by up to 10% of 1σ NAO.

These findings are in qualitative agreement with our PTE-based diagnosed positive feedback and suggested that ACRE play a minor role to the NAO short-term dynamics compared to the total diabatic heating.

7.2. Outlook

The results within this thesis have demonstrated the minor role of ACRE for the NAO variability on synoptic time-scales. However, our modeling work in chapter 6 has illustrated that the atmospheric cloud-radiative effects may have an increasing impact on the surface pressure fields beyond lead times of 10 days. In fact, previous work demonstrated the importance of ACRE for the present-day mean circulation (Li et al., 2015; Watt-Meyer and Frierson, 2017) as well as for the mean circulation response to global warming (Voigt and Shaw, 2015, 2016). The contrast of a small ACRE impact on short time-scales raises the question at which time-scale ACRE starts to become a major factor for the extratropical circulation and its variability. Addressing this question includes numerical simulations in a subseasonal-to-seasonal framework where clouds are scrambled and decorrelated from the circulation by means of cloud-locking (Voigt and Shaw, 2015). Similarly, one could also imagine to gain further process-based insight by investigating the role of different cloud types, such as high-level clouds, over specific regions. This study could also include an investigation of the relative role of different cloud types and their associated radiative effects for extratropical cyclones in present-day climate (Grise et al., 2019) as well as under a warmer climate (Catto et al., 2019).

Our modeling work has demonstrated one particular way to assess the impact of the NAO-related diabatic processes on the NAO evolution. Nonetheless, the imposed diabatic heating in these sensitivity tests represents the average impact of many different NAO events and in fact is much weaker compared to a single NAO event because of the large variability between NAO events. This suggests the need for refined methods to study the NAO impact of different diabatic heating processes. For example, by forcing the model with additional ACRE or total diabatic heating from a snapshot of a particular day when an exceptional cyclonic or anticyclonic event is taking place could allow us to assess to what extent particular clouds, cloud types and their associated ACRE may impact the NAO evolution. In a similar way, by imposing an anomalous heating due to ACRE in different parts of the troposphere we may also be able to assess the relative role of upper-, mid- or lower-tropospheric ACRE or total diabatic heating anomalies for the NAO short-term dynamics. Moreover, in a similar framework as in our modeling work here, one could also test the NAO response to different magnitudes of an additional NAO-related diabatic heating, such as two times larger than 1σ NAO latent heating pattern.

Furthermore, our work focused on the North Atlantic region and the NAO. Motivated by our observational and modeling work it would be of great interest to apply the combination

of observational and reanalysis diagnostics with sensitivity simulations to other oceans and modes of internal variability. One example would be to investigate the synoptic-scale linkages between the Southern Annular Mode (SAM) and ACRE. Additionally, motivated by previous studies that illustrated various pathways of connections between tropical convection (e.g., MJO) and the Pacific-North America (PNA) pattern or the NAO (Barnes et al., 2019), it would be interesting to investigate the relative role of individual diabatic processes such as ACRE over the tropics for the extratropical circulation on synoptic to subseasonal timescales. This could be addressed by means of numerical simulations where additional anomalous ACRE related to MJO will be imposed to test their impact on modes of extratropical circulation variability.

Overall, this thesis demonstrated the advantage of combining state-of-the-art satellite observations, reanalysis data and sensitivity simulations to investigate the interplay between the large-scale circulation and diabatic processes. However, diabatic processes are not directly observed and thus their assessment is always constrained by retrieval uncertainties. This work illustrated the role of ACRE and total diabatic heating for the NAO dynamics and stressed out the need for future modeling work to expand our understanding of such interactions, to test the robustness of our modeling results across different models as well as to constrain the model uncertainties based on observations.

A. Bibliography

- Albern, N., Voigt, A., Buehler, S. A., and Grützun, V. (2018). Robust and nonrobust impacts of atmospheric cloud-radiative interactions on the tropical circulation and its response to surface warming. *Geophysical Research Letters*, 45(16):8577–8585.
- Albern, N., Voigt, A., and Pinto, J. G. (2019). Cloud-radiative impact on the regional responses of the midlatitude jet streams and storm tracks to global warming. *Journal of Advances in Modeling Earth Systems*, 11(7):1940–1958.
- Ambaum, M. H. P. and Hoskins, B. J. (2002). The NAO troposphere–stratosphere connection. *Journal of Climate*, 15(14):1969–1978.
- Ambaum, M. H. P., Hoskins, B. J., and Stephenson, D. B. (2001). Arctic oscillation or North Atlantic Oscillation? *Journal of Climate*, 14(16):3495–3507.
- Athanasiadis, P. J., Wallace, J. M., and Wettstein, J. J. (2010). Patterns of wintertime jet stream variability and their relation to the storm tracks. *Journal of the Atmospheric Sciences*, 67(5):1361–1381.
- Atlas, D., Matrosov, S. Y., Heymsfield, A. J., Chou, M.-D., and Wolff, D. B. (1995). Radar and radiation properties of ice clouds. *Journal of Applied Meteorology*, 34(11):2329–2345.
- Baldwin, M. P., Cheng, X., and Dunkerton, T. J. (1994). Observed correlations between winter-mean tropospheric and stratospheric circulation anomalies. *Geophysical Research Letters*, 21(12):1141–1144.
- Baldwin, M. P. and Dunkerton, T. J. (1999). Propagation of the arctic oscillation from the stratosphere to the troposphere. *Journal of Geophysical Research: Atmospheres*, 104(D24):30937–30946.
- Barnes, E. A. and Hartmann, D. L. (2010). Dynamical feedbacks and the persistence of the NAO. *Journal of the Atmospheric Sciences*, 67(3):851–865.
- Barnes, E. A. and Polvani, L. (2013). Response of the midlatitude jets, and of their variability, to increased greenhouse gases in the cmip5 models. *Journal of Climate*, 26(18):7117–7135.

- Barnes, E. A., Samarasinghe, S. M., Ebert-Uphoff, I., and Furtado, J. C. (2019). Tropospheric and stratospheric causal pathways between the MJO and NAO. *Journal of Geophysical Research: Atmospheres*, 124(16):9356–9371.
- Barnston, A. G. and Livezey, R. E. (1987). Classification, seasonality and persistence of low-frequency atmospheric circulation patterns. *Monthly Weather Review*, 115(6):1083–1126.
- Benedict, J. J., Lee, S., and Feldstein, S. B. (2004). Synoptic view of the North Atlantic Oscillation. *Journal of the Atmospheric Sciences*, 61(2):121–144.
- Bjerknes, J. (1969). Atmospheric teleconnections from the equatorial pacific. *Monthly Weather Review*, 97(3):163–172.
- Blackmon, M. L. (1976). A climatological spectral study of the 500 mb geopotential height of the northern hemisphere. *Journal of the Atmospheric Sciences*, 33(8):1607–1623.
- Bodas-Salcedo, A., Williams, K. D., Field, P. R., and Lock, A. P. (2012). The surface downwelling solar radiation surplus over the southern ocean in the met office model: The role of midlatitude cyclone clouds. *Journal of Climate*, 25(21):7467–7486.
- Bony, S., Colman, R., Kattsov, V. M., Allan, R. P., Bretherton, C. S., Dufresne, J.-L., Hall, A., Hallegatte, S., Holland, M. M., Ingram, W., Randall, D. A., Soden, B. J., Tselioudis, G., and Webb, M. J. (2006). How well do we understand and evaluate climate change feedback processes? *Journal of Climate*, 19(15):3445–3482.
- Bony, S., Stevens, B., Frierson, D. M. W., Jakob, C., Kageyama, M., Pincus, R., Shepherd, T. G., Sherwood, S. C., Siebesma, A. P., Sobel, A. H., Watanabe, M., and Webb, M. J. (2015). Clouds, circulation and climate sensitivity. *Nature Geoscience*, 8(4):261–268.
- Browning, K. A. (1986). Conceptual models of precipitation systems. *Weather and Forecasting*, 1(1):23–41.
- Butler, A. H., Arribas, A., Athanassiadou, M., Baehr, J., Calvo, N., Charlton-Perez, A., Déqué, M., Domeisen, D. I. V., Fröhlich, K., Hendon, H., Imada, Y., Ishii, M., Iza, M., Karpechko, A. Y., Kumar, A., MacLachlan, C., Merryfield, W. J., Müller, W. A., O’Neill, A., Scaife, A. A., Scinocca, J., Sigmond, M., Stockdale, T. N., and Yasuda, T. (2016). The climate-system historical forecast project: do stratosphere-resolving models make better seasonal climate predictions in boreal winter? *Quarterly Journal of the Royal Meteorological Society*, 142(696):1413–1427.
- Cassou, C. (2008). Intraseasonal interaction between the madden–julian oscillation and the north atlantic oscillation. *Nature*, 455:523–527.

- Catto, J. L., Ackerley, D., Booth, J. F., Champion, A. J., Colle, B. A., Pfahl, S., Pinto, J. G., Quinting, J. F., and Seiler, C. (2019). The future of midlatitude cyclones. *Current Climate Change Reports*, 5(2):407–420.
- Ceppi, P. and Hartmann, D. L. (2015). Connections between clouds, radiation, and midlatitude dynamics: a review. *Current Climate Change Reports*, 1:94–102.
- Ceppi, P. and Hartmann, D. L. (2016). Clouds and the atmospheric circulation response to warming. *Journal of Climate*, 29(2):783–799.
- Ceppi, P., Hwang, Y.-T., Frierson, D. M. W., and Hartmann, D. L. (2012). Southern hemisphere jet latitude biases in cmip5 models linked to shortwave cloud forcing. *Geophysical Research Letters*, 39(19).
- Ceppi, P. and Shepherd, T. G. (2017). Contributions of climate feedbacks to changes in atmospheric circulation. *Journal of Climate*, 30(22):9097–9118.
- Ceppi, P., Zelinka, M. D., and Hartmann, D. L. (2014). The response of the southern hemispheric eddy-driven jet to future changes in shortwave radiation in cmip5. *Geophysical Research Letters*, 41(9):3244–3250.
- Chang, E. K. M., Guo, Y., and Xia, X. (2012). Cmp5 multimodel ensemble projection of storm track change under global warming. *Journal of Geophysical Research: Atmospheres*, 117(D23).
- Chang, E. K. M., Lee, S., and Swanson, K. L. (2002). Storm track dynamics. *Journal of Climate*, 15(16):2163–2183.
- CIRA (2007). Cloudsat ecmwf-aux auxiliary data process description and interface control document, available from http://www.cloudsat.cira.colostate.edu/sites/default/files/products/files/ECMWF-AUX_PDICD.P_R04.20070718.pdf. *Cloudsat tech. note*.
- Clark, R. T., Bett, P. E., Thornton, H. E., and Scaife, A. A. (2017). Skilful seasonal predictions for the european energy industry. *Environmental Research Letters*, 12(2):024002.
- Cohen, J. and Barlow, M. (2005). The NAO, the AO, and global warming: How closely related? *Journal of Climate*, 18(21):4498–4513.
- Cook, E. R., D’Arrigo, R. D., and Mann, M. E. (2002). A well-verified, multiproxy reconstruction of the winter north atlantic oscillation index since a.d. 1400. *Journal of Climate*, 15(13):1754–1764.

- Cornes, R. C., Jones, P. D., Briffa, K. R., and Osborn, T. J. (2013). Estimates of the North Atlantic Oscillation back to 1692 using a Paris–London westerly index. *International Journal of Climatology*, 33(1):228–248.
- Cropper, T., Hanna, E., Valente, M. A., and Jónsson, T. (2015). A daily azores–iceland north atlantic oscillation index back to 1850. *Geoscience Data Journal*, 2(1):12–24.
- Dee, D. P., Uppala, S. M., Simmons, A. J., Berrisford, P., Poli, P., Kobayashi, S., Andrae, U., Balmaseda, M. A., Balsamo, G., Bauer, P., Bechtold, P., Beljaars, A. C. M., van de Berg, L., Bidlot, J., Bormann, N., Delsol, C., Dragani, R., Fuentes, M., Geer, A. J., Haimberger, L., Healy, S. B., Hersbach, H., Hólm, E. V., Isaksen, L., Kållberg, P., Köhler, M., Matri-cardi, M., McNally, A. P., Monge-Sanz, B. M., Morcrette, J.-J., Park, B.-K., Peubey, C., de Rosnay, P., Tavolato, C., Thépaut, J.-N., and Vitart, F. (2011). The era-interim reanalysis: configuration and performance of the data assimilation system. *Quarterly Journal of the Royal Meteorological Society*, 137(656):553–597.
- Deser, C. (2000). On the teleconnectivity of the “arctic oscillation”. *Geophysical Research Letters*, 27(6):779–782.
- Dobrynin, M., Domeisen, D. I. V., Müller, W. A., Bell, L., Brune, S., Bunzel, F., Düsterhus, A., Fröhlich, K., Pohlmann, H., and Baehr, J. (2018). Improved teleconnection-based dynamical seasonal predictions of boreal winter. *Geophysical Research Letters*, 45(8):3605–3614.
- Domeisen, D. I. V., Butler, A. H., Fröhlich, K., Bittner, M., Müller, W. A., and Baehr, J. (2014). Seasonal Predictability over Europe Arising from El Niño and Stratospheric Variability in the MPI-ESM Seasonal Prediction System. *Journal of Climate*, 28(1):256–271.
- Eckhardt, S., Stohl, A., Wernli, H., James, P., Forster, C., and Spichtinger, N. (2004). A 15-year climatology of warm conveyor belts. *Journal of Climate*, 17(1):218–237.
- ECMWF (2010). IFS documentation cy36r1, part iv: Physical processes, IFS documentation (4), available from <https://www.ecmwf.int/node/9233>. *ECMWF tech. note*.
- F. Panagiotopoulos, M. Shahgedanova, and D.B. Stephenson (2002). A review of northern hemisphere winter-time teleconnection patterns. *J. Phys. IV France*, 12(10):27–47.
- Fasullo, J. T. and Trenberth, K. E. (2008). The annual cycle of the energy budget. part i: Global mean and land–ocean exchanges. *Journal of Climate*, 21(10):2297–2312.
- Feldstein, S. B. (2003). The dynamics of NAO teleconnection pattern growth and decay. *Quarterly Journal of the Royal Meteorological Society*, 129(589):901–924.

- Feldstein, S. B. and Franzke, C. (2006). Are the north atlantic oscillation and the northern annular mode distinguishable? *Journal of the Atmospheric Sciences*, 63(11):2915–2930.
- Ferranti, L., Magnusson, L., Vitart, F., and Richardson, D. S. (2018). How far in advance can we predict changes in large-scale flow leading to severe cold conditions over europe? *Quarterly Journal of the Royal Meteorological Society*, 144(715):1788–1802.
- Field, P. R., Bodas-Salcedo, A., and Brooks, M. E. (2011). Using model analysis and satellite data to assess cloud and precipitation in midlatitude cyclones. *Quarterly Journal of the Royal Meteorological Society*, 137(659):1501–1515.
- Field, P. R., Gettelman, A., Neale, R. B., Wood, R., Rasch, P. J., and Morrison, H. (2008). Midlatitude cyclone compositing to constrain climate model behavior using satellite observations. *Journal of Climate*, 21(22):5887–5903.
- Field, P. R. and Wood, R. (2007). Precipitation and cloud structure in midlatitude cyclones. *Journal of Climate*, 20(2):233–254.
- Fink, A. H., Pohle, S., Pinto, J. G., and Knippertz, P. (2012). Diagnosing the influence of diabatic processes on the explosive deepening of extratropical cyclones. *Geophysical Research Letters*, 39(7).
- Franzke, C., Fraedrich, K., and Lunkeit, F. (2001). Teleconnections and low-frequency variability in idealized experiments with two storm tracks. *Quarterly Journal of the Royal Meteorological Society*, 127(574):1321–1339.
- Franzke, C., Lee, S., and Feldstein, S. B. (2004). Is the north atlantic oscillation a breaking wave? *Journal of the Atmospheric Sciences*, 61(2):145–160.
- Gassmann, A. and Herzog, H.-J. (2008). Towards a consistent numerical compressible non-hydrostatic model using generalized hamiltonian tools. *Quarterly Journal of the Royal Meteorological Society*, 134(635):1597–1613.
- Gates, W. L. (1992). An ams continuing series: Global change–amip: The atmospheric model intercomparison project. *Bulletin of the American Meteorological Society*, 73(12):1962–1970.
- Gerber, E. P. and Vallis, G. K. (2009). On the zonal structure of the north atlantic oscillation and annular modes. *Journal of the Atmospheric Sciences*, 66(2):332–352.
- Glueck, M. F. and Stockton, C. W. (2001). Reconstruction of the North Atlantic Oscillation, 1429–1983. *International Journal of Climatology*, 21(12):1453–1465.

- Govekar, P. D., Jakob, C., and Catto, J. (2014). The relationship between clouds and dynamics in southern hemisphere extratropical cyclones in the real world and a climate model. *Journal of Geophysical Research: Atmospheres*, 119(11):6609–6628.
- Greatbatch, R. J. and Jung, T. (2007). Local versus tropical diabatic heating and the winter north atlantic oscillation. *Journal of Climate*, 20(10):2058–2075.
- Grise, K. M. and Medeiros, B. (2016). Understanding the varied influence of midlatitude jet position on clouds and cloud radiative effects in observations and global climate models. *Journal of Climate*, 29(24):9005–9025.
- Grise, K. M., Medeiros, B., Benedict, J. J., and Olson, J. G. (2019). Investigating the influence of cloud radiative effects on the extratropical storm tracks. *Geophysical Research Letters*, 46(13):7700–7707.
- Grise, K. M. and Polvani, L. M. (2014). Southern hemisphere cloud–dynamics biases in cmip5 models and their implications for climate projections. *Journal of Climate*, 27(15):6074–6092.
- Grise, K. M., Polvani, L. M., Tselioudis, G., Wu, Y., and Zelinka, M. D. (2013). The ozone hole indirect effect: Cloud-radiative anomalies accompanying the poleward shift of the eddy-driven jet in the southern hemisphere. *Geophysical Research Letters*, 40(14):3688–3692.
- Hall, R., Erdélyi, R., Hanna, E., Jones, J. M., and Scaife, A. A. (2015). Drivers of north atlantic polar front jet stream variability. *International Journal of Climatology*, 35(8):1697–1720.
- Hall, R. J., Scaife, A. A., Hanna, E., Jones, J. M., and Erdélyi, R. (2017). Simple statistical probabilistic forecasts of the winter NAO. *Weather and Forecasting*, 32(4):1585–1601.
- Hansen, F., Greatbatch, R. J., Gollan, G., Jung, T., and Weisheimer, A. (2017). Remote control of north atlantic oscillation predictability via the stratosphere. *Quarterly Journal of the Royal Meteorological Society*, 143(703):706–719.
- Harries, J. E., Russell, J. E., Hanafin, J. A., Brindley, H., Futyán, J., Rufus, J., Kellock, S., Matthews, G., Wrigley, R., Last, A., Mueller, J., Mossavati, R., Ashmall, J., Sawyer, E., Parker, D., Caldwell, M., Allan, P. M., Smith, A., Bates, M. J., Coan, B., Stewart, B. C., Lepine, D. R., Cornwall, L. A., Corney, D. R., Ricketts, M. J., Drummond, D., Smart, D., Cutler, R., Dewitte, S., Clerbaux, N., Gonzalez, L., Ipe, A., Bertrand, C., Joukoff, A., Crommelynck, D., Nelms, N., Llewellyn-Jones, D. T., Butcher, G., Smith, G. L., Szwedczyk, Z. P., Mlynczak, P. E., Slingo, A., Allan, R. P., and Ringer, M. A. (2005). The Geostationary Earth Radiation Budget Project. *Bulletin of the American Meteorological Society*, 86(7):945–960.

- Harrop, B. E. and Hartmann, D. L. (2016). The role of cloud radiative heating in determining the location of the itcz in aquaplanet simulations. *Journal of Climate*, 29(8):2741–2763.
- Hartmann, D. L. (2007). The atmospheric general circulation and its variability. *Journal of the Meteorological Society of Japan. Ser. II*, 85B:123–143.
- Hartmann, D. L., Ockert-Bell, M. E., and Michelsen, M. L. (1992). The effect of cloud type on earth's energy balance: Global analysis. *Journal of Climate*, 5(11):1281–1304.
- Hawcroft, M., Dacre, H., Forbes, R., Hodges, K., Shaffrey, L., and Stein, T. (2017). Using satellite and reanalysis data to evaluate the representation of latent heating in extratropical cyclones in a climate model. *Climate Dynamics*, 48:2255–2278.
- Haynes, J. M., Vonder Haar, T. H., L'Ecuyer, T., and Henderson, D. (2013). Radiative heating characteristics of earth's cloudy atmosphere from vertically resolved active sensors. *Geophysical Research Letters*, 40(3):624–630.
- Henderson, D. S., L'Ecuyer, T., Stephens, G., Partain, P., and Sekiguchi, M. (2013). A multisensor perspective on the radiative impacts of clouds and aerosols. *Journal of Applied Meteorology and Climatology*, 52(4):853–871.
- Holton, J. R. (2004). *An introduction to dynamic meteorology*. International Geophysics Series. Elsevier Academic Press., Burlington, MA, 4 edition.
- Hoskins, B. J. and Valdes, P. J. (1990). On the existence of storm-tracks. *Journal of the Atmospheric Sciences*, 47(15):1854–1864.
- Hurrell, J. W. (1995). Decadal trends in the north atlantic oscillation: Regional temperatures and precipitation. *Science*, 269(5224):676–679.
- Hurrell, J. W. and Deser, C. (2010). North Atlantic climate variability: The role of the North Atlantic Oscillation. *Journal of Marine Systems*, 79(3):231–244.
- Hurrell, J. W., Kushnir, Y., Ottensen, G., and Visbeck, M. (2003). *An Overview of the North Atlantic Oscillation*, pages 1–35. American Geophysical Union (AGU).
- Jones, P. D., Jonsson, T., and Wheeler, D. (1997). Extension to the north atlantic oscillation using early instrumental pressure observations from gibraltar and south-west iceland. *International Journal of Climatology*, 17(13):1433–1450.
- Jung, T., Vitart, F., Ferranti, L., and Morcrette, J.-J. (2011). Origin and predictability of the extreme negative NAO winter of 2009/10. *Geophysical Research Letters*, 38(7).

- Kato, S., Miller, W. F., Sun-Mack, S., Rose, F. G., Chen, Y., and Mlynchak, P. E. (2010). Variable descriptions of the a-train integrated calipso, cloudsat, ceres, and modis merged product (cccm or c3m). *NASA*.
- Keeley, S. P. E., Sutton, R. T., and Shaffrey, L. C. (2009). Does the north atlantic oscillation show unusual persistence on intraseasonal timescales? *Geophysical Research Letters*, 36(22).
- Kidston, J., Scaife, A. A., Hardiman, S. C., Mitchell, D. M., Butchart, N., Baldwin, M. P., and Gray, L. J. (2015). Stratospheric influence on tropospheric jet streams, storm tracks and surface weather. *Nature Geoscience*, 8(6):433–440.
- Knight, J. R., Allan, R. J., Folland, C. K., Vellinga, M., and Mann, M. E. (2005). A signature of persistent natural thermohaline circulation cycles in observed climate. *Geophysical Research Letters*, 32(20).
- Knippertz, P. and Fink, A. H. (2008). Dry-season precipitation in tropical west africa and its relation to forcing from the extratropics. *Monthly Weather Review*, 136(9):3579–3596.
- Knippertz, P., Fink, A. H., and Pohle, S. (2009). Reply. *Monthly Weather Review*, 137(9):3151–3157.
- Krahmann, G. and Visbeck, M. (2003). Variability of the northern annular mode’s signature in winter sea ice concentration. *Polar Research*, 22(1):51–57.
- Kutzbach, J. E. (1970). Large-scale features of monthly mean northern hemisphere anomaly maps of sea-level pressure. *Monthly Weather Review*, 98(9):708–716.
- Lau, N.-C. and Crane, M. W. (1995). A satellite view of the synoptic-scale organization of cloud properties in midlatitude and tropical circulation systems. *Monthly Weather Review*, 123(7):1984–2006.
- Leckebusch, G. C., Koffi, B., Ulbrich, U., Pinto, J. G., Spanghel, T., and Zacharias, S. (2006). Analysis of frequency and intensity of european winter storm events from a multi-model perspective, at synoptic and regional scales. *Climate Research*, 31:59–74.
- L’Ecuyer, T. S., Wood, N. B., Haladay, T., Stephens, G. L., and Stackhouse Jr., P. W. (2008). Impact of clouds on atmospheric heating based on the R04 cloudsat fluxes and heating rates data set. *Journal of Geophysical Research: Atmospheres*, 113(D8).
- Lehner, F., Raible, C. C., and Stocker, T. F. (2012). Testing the robustness of a precipitation proxy-based North Atlantic Oscillation reconstruction. *Quaternary Science Reviews*, 45:85–94.

- Li, C. and Wettstein, J. J. (2012). Thermally Driven and Eddy-Driven Jet Variability in Reanalysis*. *Journal of Climate*, 25(5):1587–1596.
- Li, Y. and Lau, N.-C. (2012a). Contributions of downstream eddy development to the teleconnection between enso and the atmospheric circulation over the north atlantic. *Journal of Climate*, 25(14):4993–5010.
- Li, Y. and Lau, N.-C. (2012b). Impact of enso on the atmospheric variability over the north atlantic in late winter—role of transient eddies. *Journal of Climate*, 25(1):320–342.
- Li, Y. and Thompson, D. W. J. (2016). Observed signatures of the barotropic and baroclinic annular modes in cloud vertical structure and cloud radiative effects. *Journal of Climate*, 29(13):4723–4740.
- Li, Y., Thompson, D. W. J., and Bony, S. (2015). The influence of atmospheric cloud radiative effects on the large-scale atmospheric circulation. *Journal of Climate*, 28(18):7263–7278.
- Li, Y., Thompson, D. W. J., Bony, S., and Merlis, T. M. (2019). Thermodynamic control on the poleward shift of the extratropical jet in climate change simulations: The role of rising high clouds and their radiative effects. *Journal of Climate*, 32(3):917–934.
- Li, Y., Thompson, D. W. J., Huang, Y., and Zhang, M. (2014a). Observed linkages between the northern annular mode/North Atlantic Oscillation, cloud incidence, and cloud radiative forcing. *Geophysical Research Letters*, 41(5):1681–1688.
- Li, Y., Thompson, D. W. J., Stephens, G. L., and Bony, S. (2014b). A global survey of the instantaneous linkages between cloud vertical structure and large-scale climate. *Journal of Geophysical Research: Atmospheres*, 119(7):3770–3792.
- Ling, J. and Zhang, C. (2013). Diabatic heating profiles in recent global reanalyses. *Journal of Climate*, 26(10):3307–3325.
- Liu, Z. and Alexander, M. (2007). Atmospheric bridge, oceanic tunnel, and global climatic teleconnections. *Reviews of Geophysics*, 45(2).
- Loeb, N. G., Doelling, D. R., Wang, H., Su, W., Nguyen, C., Corbett, J. G., Liang, L., Mitrescu, C., Rose, F. G., and Kato, S. (2018). Clouds and the earth’s radiant energy system (ceres) energy balanced and filled (ebaf) top-of-atmosphere (toa) edition-4.0 data product. *Journal of Climate*, 31(2):895–918.
- Loeb, N. G., Wielicki, B. A., Doelling, D. R., Smith, G. L., Keyes, D. F., Kato, S., Manalo-Smith, N., and Wong, T. (2009). Toward optimal closure of the earth’s top-of-atmosphere radiation budget. *Journal of Climate*, 22(3):748–766.

- Lorenz, D. J. and Hartmann, D. L. (2001). Eddy–zonal flow feedback in the southern hemisphere. *Journal of the Atmospheric Sciences*, 58(21):3312–3327.
- Lorenz, E. (1956). Empirical orthogonal functions and statistical weather prediction. *Technical report, Statistical Forecast Project Report 1, Dept. of Meteor, MIT*, page 49.
- Lorenz, E. N. (1951). Seasonal and irregular variations of the northern hemisphere sea-level pressure profile. *Journal of Meteorology*, 8(1):52–59.
- Luo, D., Diao, Y., and Feldstein, S. B. (2011). The variability of the atlantic storm track and the north atlantic oscillation: A link between intraseasonal and interannual variability. *Journal of the Atmospheric Sciences*, 68(3):577–601.
- Luterbacher, J., Schmutz, C., Gyalistras, D., Xoplaki, E., and Wanner, H. (1999). Reconstruction of monthly NAO and EU indices back to AD 1675. *Geophysical Research Letters*, 26(17):2745–2748.
- Mace, G. G., Zhang, Q., Vaughan, M., Marchand, R., Stephens, G., Trepte, C., and Winker, D. (2009). A description of hydrometeor layer occurrence statistics derived from the first year of merged cloudsat and calipso data. *Journal of Geophysical Research: Atmospheres*, 114(D8).
- Madenach, N., Carbajal Henken, C., Preusker, R., Sourdeval, O., and Fischer, J. (2019). Analysis and quantification of enso-linked changes in the tropical atlantic cloud vertical distribution using 14 years of modis observations. *Atmospheric Chemistry and Physics*, 19(21):13535–13546.
- Madonna, E., Li, C., and Wettstein, J. J. (2019). Suppressed eddy driving during southward excursions of the north atlantic jet on synoptic to seasonal time scales. *Atmospheric Science Letters*, 20(9):e937.
- Maranan, M., Fink, A. H., Knippertz, P., Francis, S. D., Akpo, A. B., Jegede, G., and Yorke, C. (2019). Interactions between convection and a moist vortex associated with an extreme rainfall event over southern west africa. *Monthly Weather Review*, 147(7):2309–2328.
- Marchand, R., Mace, G. G., Ackerman, T., and Stephens, G. (2008). Hydrometeor detection using cloudsat—an earth-orbiting 94-ghz cloud radar. *Journal of Atmospheric and Oceanic Technology*, 25:519–533.
- Marshall, J., Kushnir, Y., Battisti, D., Chang, P., Czaja, A., Dickson, R., Hurrell, J., McCartney, M., Saravanan, R., and Visbeck, M. (2001). North Atlantic climate variability: phenomena, impacts and mechanisms. *International Journal of Climatology*, 21(15):1863–1898.

- McIntyre, M. E. and Palmer, T. N. (1985). A note on the general concept of wave breaking for Rossby and gravity waves. *Pure and applied geophysics*, 123:964–975.
- Mo, K. C. and Livezey, R. E. (1986). Tropical-extratropical geopotential height teleconnections during the northern hemisphere winter. *Monthly Weather Review*, 114(12):2488–2515.
- Müller, W. A., Appenzeller, C., and Schär, C. (2005). Probabilistic seasonal prediction of the winter North Atlantic Oscillation and its impact on near surface temperature. *Climate Dynamics*, 24(24):213–226.
- Myers, T. A. and Norris, J. R. (2015). On the Relationships between Subtropical Clouds and Meteorology in Observations and CMIP3 and CMIP5 Models*. *Journal of Climate*, 28(8):2945–2967.
- Namias, J. (1950). The index cycle and its role in the general circulation. *Journal of Meteorology*, 7(2):130–139.
- Naud, C. M., Booth, J. F., Jeyaratnam, J., Donner, L. J., Seman, C. J., Zhao, M., Guo, H., and Ming, Y. (2019). Extratropical cyclone clouds in the gfdl climate model: Diagnosing biases and the associated causes. *Journal of Climate*, 32(20):6685–6701.
- Naud, C. M., Del Genio, A. D., Bauer, M., and Kovari, W. (2010). Cloud vertical distribution across warm and cold fronts in cloudsat–calipso data and a general circulation model. *Journal of Climate*, 23(12):3397–3415.
- Neale, R. B., Gettelman, A., Park, S., and Coauthors (2011). Description of the near community atmosphere model (cam5). *NCAR Tech. Note*.
- Nobre, G. G., Jongman, B., Aerts, J., and Ward, P. J. (2017). The role of climate variability in extreme floods in europe. *Environmental Research Letters*, 12(8):084012.
- Obukhov, A. (1947). Statistically homogeneous fields on a sphere. *Uspehi Matematicheskikh Nauk*, 2:196–198.
- O’Reilly, C. H., Heatley, J., MacLeod, D., Weisheimer, A., Palmer, T. N., Schaller, N., and Woollings, T. (2017). Variability in seasonal forecast skill of northern hemisphere winters over the twentieth century. *Geophysical Research Letters*, 44(11):5729–5738.
- Oreopoulos, L., Cho, N., and Lee, D. (2017). New insights about cloud vertical structure from cloudsat and calipso observations. *Journal of Geophysical Research: Atmospheres*, 122(17):9280–9300.

- Oreopoulos, L. and Rossow, W. B. (2011). The cloud radiative effects of international satellite cloud climatology project weather states. *Journal of Geophysical Research: Atmospheres*, 116(D12).
- Ortega, P., Lehner, F., Swingedouw, D., Masson-Delmotte, V., Raible, C. C., Casado, M., and Yiou, P. (2015). A model-tested north atlantic oscillation reconstruction for the past millennium. *Nature*, 523:71–74.
- Osborn, T. J. (2006). Recent variations in the winter north atlantic oscillation. *Weather*, 61(12):353–355.
- Osborn, T. J. (2011). Winter 2009/2010 temperatures and a record-breaking north atlantic oscillation index. *Weather*, 66(1):19–21.
- Papavasileiou, G., Voigt, A., and Knippertz, P. (2020). The role of observed cloud-radiative anomalies for the dynamics of the north atlantic oscillation on synoptic time-scales. *Quarterly Journal of the Royal Meteorological Society*, 146(729):1822–1841.
- Papritz, L. and Grams, C. M. (2018). Linking low-frequency large-scale circulation patterns to cold air outbreak formation in the northeastern north atlantic. *Geophysical Research Letters*, 45(5):2542–2553.
- Pasquier, J. T., Pfahl, S., and Grams, C. M. (2019). Modulation of atmospheric river occurrence and associated precipitation extremes in the north atlantic region by european weather regimes. *Geophysical Research Letters*, 46(2):1014–1023.
- Perlwitz, J. and Graf, H.-F. (1995). The statistical connection between tropospheric and stratospheric circulation of the northern hemisphere in winter. *Journal of Climate*, 8(10):2281–2295.
- Perlwitz, J., Knutson, T., Kossin, J. P., and LeGrande, A. N. (2017). *Large-scale circulation and climate variability*, pages 161–184. U.S. Global Change Research Program, Washington, D.C.
- Petoukhov, V. and Semenov, V. A. (2010). A link between reduced barents-kara sea ice and cold winter extremes over northern continents. *Journal of Geophysical Research: Atmospheres*, 115(D21).
- Pinto, J. G., Zacharias, S., Fink, A. H., Leckebusch, G. C., and Ulbrich, U. (2009). Factors contributing to the development of extreme north atlantic cyclones and their relationship with the NAO. *Climate Dynamics*, 32:711–737.

- Ramanatha, V., Cess, R. D., Harrison, E. F., Minnis, P., Barkstrom, B. R., Ahmad, E., and Hartmann, D. (1989). Cloud-radiative forcing and climate: Results from the earth radiation budget experiment. *Science*, 243(4887):57–63.
- Renggli, D., Leckebusch, G. C., Ulbrich, U., Gleixner, S. N., and Faust, E. (2011). The skill of seasonal ensemble prediction systems to forecast wintertime windstorm frequency over the north atlantic and europe. *Monthly Weather Review*, 139(9):3052–3068.
- Robinson, W. A. (2006). On the self-maintenance of midlatitude jets. *Journal of the Atmospheric Sciences*, 63(8):2109–2122.
- Rossby, C. G. and Willett, H. C. (1948). The circulation of the upper troposphere and lower stratosphere. *Science*, 108(2815):643–652.
- Rossow, W. B. and Zhang, Y. (2010). Evaluation of a Statistical Model of Cloud Vertical Structure Using Combined CloudSat and CALIPSO Cloud Layer Profiles. *Journal of Climate*, 23(24):6641–6653.
- Rutan, D. A., Kato, S., Doelling, D. R., Rose, F. G., Nguyen, L. T., Caldwell, T. E., and Loeb, N. G. (2015). Ceres synoptic product: Methodology and validation of surface radiant flux. *Journal of Atmospheric and Oceanic Technology*, 32(6):1121–1143.
- Sanderson, B. M., Piani, C., Ingram, W. J., Stone, D. A., and Allen, M. R. (2008). Towards constraining climate sensitivity by linear analysis of feedback patterns in thousands of perturbed-physics gcm simulations. *Climate Dynamics*, 30:175–190.
- Scaife, A. A., Arribas, A., Blockley, E., Brookshaw, A., Clark, R. T., Dunstone, N., Eade, R., Fereday, D., Folland, C. K., Gordon, M., Hermanson, L., Knight, J. R., Lea, D. J., MacLachlan, C., Maidens, A., Martin, M., Peterson, A. K., Smith, D., Vellinga, M., Wallace, E., Waters, J., and Williams, A. (2014). Skillful long-range prediction of european and north american winters. *Geophysical Research Letters*, 41(7):2514–2519.
- Scaife, A. A., Folland, C. K., Alexander, L. V., Moberg, A., and Knight, J. R. (2008). European climate extremes and the north atlantic oscillation. *Journal of Climate*, 21(1):72–83.
- Scaife, A. A., Knight, J. R., Vallis, G. K., and Folland, C. K. (2005). A stratospheric influence on the winter nao and north atlantic surface climate. *Geophysical Research Letters*, 32(18).
- Schäfer, S. A. K. and Voigt, A. (2018). Radiation weakens idealized midlatitude cyclones. *Geophysical Research Letters*, 45(6):2833–2841.
- Schöne, B. R., Oschmann, W., Roessler, J., Castro, A. D. F., Houk, S. D., Kroencke, I., Dreyer, W., Janssen, R., Rumohr, H., and Dunca, E. (2003). North Atlantic Oscillation dynamics recorded in shells of a long-lived bivalve mollusk. *Geology*, 31(12):1037–1040.

- Semenov, V. A. and Latif, M. (2015). Nonlinear winter atmospheric circulation response to arctic sea ice concentration anomalies for different periods during 1966–2012. *Environmental Research Letters*, 10(5):054020.
- Shaw, T. A., Baldwin, M., Barnes, E. A., Caballero, R., Garfinkel, C. I., Hwang, Y.-T., Li, C., O’Gorman, P. A., Rivière, G., Simpson, I. R., and Voigt, A. (2016). Storm track processes and the opposing influences of climate change. *Nature Geoscience*, 9:656–664.
- Shepherd, T. G. (2014). Atmospheric circulation as a source of uncertainty in climate change projections. *Nature Geoscience*, 7:703–708.
- Simpkins, G. (2017). Progress in climate modelling. *Nature Climate Change*, 7:684–685.
- Simpson, I. R., Shaw, T. A., and Seager, R. (2014). A diagnosis of the seasonally and longitudinally varying midlatitude circulation response to global warming. *Journal of the Atmospheric Sciences*, 71(7):2489–2515.
- Slingo, A. and Slingo, J. M. (1988). The response of a general circulation model to cloud longwave radiative forcing. i: Introduction and initial experiments. *Quarterly Journal of the Royal Meteorological Society*, 114(482):1027–1062.
- Stan, C., Straus, D. M., Frederiksen, J. S., Lin, H., Maloney, E. D., and Schumacher, C. (2017). Review of tropical-extratropical teleconnections on intraseasonal time scales. *Reviews of Geophysics*, 55(4):902–937.
- Stephens, G. L. and Kummerow, C. D. (2007). The remote sensing of clouds and precipitation from space: A review. *Journal of the Atmospheric Sciences*, 64(11):3742–3765.
- Stephens, G. L., Vane, D. G., Tanelli, S., Im, E., Durden, S., Rokey, M., Reinke, D., Partain, P., Mace, G. G., Austin, R., L’Ecuyer, T., Haynes, J., Lebsock, M., Suzuki, K., Waliser, D., Wu, D., Kay, J., Gettelman, A., Wang, Z., and Marchand, R. (2008). Cloudsat mission: Performance and early science after the first year of operation. *Journal of Geophysical Research: Atmospheres*, 113(D8).
- Stevens, B., Bony, S., and Webb, M. (2012). Clouds on-off climate intercomparison experiment (cookie). *Clouds On-Off Climate Intercomparison Experiment (COOKIE) summary*.
- Stockdale, T. N., Molteni, F., and Ferranti, L. (2015). Atmospheric initial conditions and the predictability of the arctic oscillation. *Geophysical Research Letters*, 42(4):1173–1179.
- Stocker, T., Qin, D., Plattner, G.-K., Tignor, M., Allen, S., Boschung, J., Nauels, A., Xia, Y., Bex, V., and (eds.), P. M. (2013). IPCC, 2013: Climate change 2013: The physical science

- basis. contribution of working group i to the fifth assessment report of the intergovernmental panel on climate change. *Cambridge University Press*.
- Strong, C. and Magnusdottir, G. (2008). Tropospheric Rossby wave breaking and the NAO/NAM. *Journal of the Atmospheric Sciences*, 65(9):2861–2876.
- Su, W., Bodas-Salcedo, A., Xu, K.-M., and Charlock, T. P. (2010). Comparison of the tropical radiative flux and cloud radiative effect profiles in a climate model with clouds and the earth’s radiant energy system (ceres) data. *Journal of Geophysical Research: Atmospheres*, 115(D1).
- Tanelli, S., Durden, S. L., Im, E., Pak, K. S., Reinke, D. G., Partain, P., Haynes, J. M., and Marchand, R. T. (2008). Cloudsat’s cloud profiling radar after two years in orbit: Performance, calibration, and processing. *IEEE Transactions on Geoscience and Remote Sensing*, 46(11):3560–3573.
- Thompson, D. W. J., Lee, S., and Baldwin, M. P. (2003). *Atmospheric Processes Governing the Northern Hemisphere Annular Mode/North Atlantic Oscillation*, pages 81–112. American Geophysical Union (AGU).
- Thompson, D. W. J. and Wallace, J. M. (1998). The arctic oscillation signature in the winter-time geopotential height and temperature fields. *Geophysical Research Letters*, 25(9):1297–1300.
- Thompson, D. W. J. and Wallace, J. M. (2000). Annular modes in the extratropical circulation. part i: Month-to-month variability. *Journal of Climate*, 13(5):1000–1016.
- Timmermann, A., An, S.-I., Kug, J.-S., Jin, F.-F., Cai, W., Capotondi, A., Cobb, K. M., Lengaigne, M., McPhaden, M. J., Stuecker, M. F., Stein, K., Wittenberg, A. T., Yun, K.-S., Bayr, T., Chen, H.-C., Chikamoto, Y., Dewitte, B., Dommenges, D., Grothe, P., Guilyardi, E., Ham, Y.-G., Hayashi, M., Ineson, S., Kang, D., Kim, S., Kim, W., Lee, J.-Y., Li, T., Luo, J.-J., McGregor, S., Planton, Y., Power, S., Rashid, H., Ren, H.-L., Santoso, A., Takahashi, K., Todd, A., Wang, G., Wang, G., Xie, R., Yang, W.-H., Yeh, S.-W., Yoon, J., Zeller, E., and Zhang, X. (2018). El niño–southern oscillation complexity. *Nature*, 559:535–549.
- Trenberth, K. E. and Paolino, D. A. (1981). Characteristic patterns of variability of sea level pressure in the northern hemisphere. *Monthly Weather Review*, 109(6):1169–1189.
- Trouet, V., Esper, J., Graham, N. E., Baker, A., Scourse, J. D., and Frank, D. C. (2009). Persistent positive North Atlantic Oscillation mode dominated the medieval climate anomaly. *Science*, 324(5923):78–80.

- Tselioudis, G., Lipat, B. R., Konsta, D., Grise, K. M., and Polvani, L. M. (2016). Midlatitude cloud shifts, their primary link to the hadley cell, and their diverse radiative effects. *Geophysical Research Letters*, 43(9):4594–4601.
- Tselioudis, G., Rossow, W., Zhang, Y., and Konsta, D. (2013). Global weather states and their properties from passive and active satellite cloud retrievals. *Journal of Climate*, 26(19):7734–7746.
- Tyrlis, E. and Hoskins, B. J. (2008). The Morphology of Northern Hemisphere Blocking. *Journal of the Atmospheric Sciences*, 65(5):1653–1665.
- Tyrrell, G. C., Karoly, D. J., and McBride, J. L. (1996). Links between tropical convection and variations of the extratropical circulation during toga coare. *Journal of the Atmospheric Sciences*, 53(18):2735–2748.
- Vallis, G. K., Zurita-Gotor, P., Cairns, C., and Kidston, J. (2015). Response of the large-scale structure of the atmosphere to global warming. *Quarterly Journal of the Royal Meteorological Society*, 141(690):1479–1501.
- Verlinden, K. L., Thompson, D. W. J., and Stephens, G. L. (2011). The three-dimensional distribution of clouds over the southern hemisphere high latitudes. *Journal of Climate*, 24(22):5799–5811.
- Vial, J., Dufresne, J.-L., and Bony, S. (2013). On the interpretation of inter-model spread in cmip5 climate sensitivity estimates. *Climate Dynamics*, 41:3339–3362.
- Visbeck, M. (2002). The ocean’s role in atlantic climate variability. *Science*, 297(5590):2223–2224.
- Visbeck, M. H., Hurrell, J. W., Polvani, L., and Cullen, H. M. (2001). The north atlantic oscillation: Past, present, and future. *Proceedings of the National Academy of Sciences*, 98(23):12876–12877.
- Voigt, A., Albern, N., and Papavasileiou, G. (2019). The atmospheric pathway of the cloud-radiative impact on the circulation response to global warming: Important and uncertain. *Journal of Climate*, 32(10):3051–3067.
- Voigt, A. and Shaw, T. A. (2015). Circulation response to warming shaped by radiative changes of clouds and water vapour. *Nature Geoscience*, 8(2):102–106.
- Voigt, A. and Shaw, T. A. (2016). Impact of regional atmospheric cloud radiative changes on shifts of the extratropical jet stream in response to global warming. *Journal of Climate*, 29(23):8399–8421.

- Walker, G. T. (1925). Correlation in seasonal variations of weather—a further study of world weather. *Monthly Weather Review*, 53(6):252–254.
- Walker, G. T. and Bliss, E. W. (1932). World weather v. *Mem. Roy. Meteorol. Soc.*, page 53–84.
- Wall, C. J., Hartmann, D. L., and Ma, P.-L. (2017). Instantaneous linkages between clouds and large-scale meteorology over the southern ocean in observations and a climate model. *Journal of Climate*, 30(23):9455–9474.
- Wallace, J. M. and Gutzler, D. S. (1981). Teleconnections in the geopotential height field during the northern hemisphere winter. *Monthly Weather Review*, 109(4):784–812.
- Wan, H., Giorgetta, M. A., Zängl, G., Restelli, M., Majewski, D., Bonaventura, L., Fröhlich, K., Reinert, D., Rípodas, P., Kornbluh, L., and Förstner, J. (2013). The icon-1.2 hydrostatic atmospheric dynamical core on triangular grids â“ part 1: Formulation and performance of the baseline version. *Geoscientific Model Development*, 6(3):735–763.
- Wang, W., Anderson, B. T., Kaufmann, R. K., and Myneni, R. B. (2004). The relation between the North Atlantic Oscillation and SSTs in the North Atlantic basin. *Journal of Climate*, 17(24):4752–4759.
- Wanner, H., Brönnimann, S., Casty, C., Gyalistras, D., Luterbacher, J., Schmutz, C., Stephenson, D. B., and Xoplaki, E. (2001). North Atlantic Oscillation - concepts and studies. *Surveys in Geophysics*, 22(4):321–381.
- Watt-Meyer, O. and Frierson, D. M. W. (2017). Local and remote impacts of atmospheric cloud radiative effects onto the eddy-driven jet. *Geophysical Research Letters*, 44(19):10,036–10,044.
- Weisheimer, A., Schaller, N., O'Reilly, C., MacLeod, D. A., and Palmer, T. (2017). Atmospheric seasonal forecasts of the twentieth century: multi-decadal variability in predictive skill of the winter North Atlantic Oscillation (NAO) and their potential value for extreme event attribution. *Quarterly Journal of the Royal Meteorological Society*, 143(703):917–926.
- Wilks, D. S. (2011). *Statistical methods in the atmospheric sciences*. Elsevier Academic Press.
- Willison, J., Robinson, W. A., and Lackmann, G. M. (2013). The importance of resolving mesoscale latent heating in the north atlantic storm track. *Journal of the Atmospheric Sciences*, 70(7):2234–2250.

- Winker, D. M., Pelon, J., Coakley, J. A., Ackerman, S. A., Charlson, R. J., Colarco, P. R., Flamant, P., Fu, Q., Hoff, R. M., Kittaka, C., Kubar, T. L., Le Treut, H., McCormick, M. P., Mégie, G., Poole, L., Powell, K., Trepte, C., Vaughan, M. A., and Wielicki, B. A. (2010). The calipso mission. *Bulletin of the American Meteorological Society*, 91(9):1211–1230.
- Woollings, T. (2010). Dynamical influences on european climate: an uncertain future. *Philosophical Transactions of the Royal Society A: Mathematical, Physical and Engineering Sciences*, 368(1924):3733–3756.
- Woollings, T., Hannachi, A., and Hoskins, B. (2010). Variability of the North Atlantic eddy-driven jet stream. *Quarterly Journal of the Royal Meteorological Society*, 136(649):856–868.
- Woollings, T., Hoskins, B., Blackburn, M., and Berrisford, P. (2008). A New Rossby Wave–Breaking Interpretation of the North Atlantic Oscillation. *Journal of the Atmospheric Sciences*, 65(2):609–626.
- Woollings, T., Papritz, L., Mbengue, C., and Spengler, T. (2016). Diabatic heating and jet stream shifts: A case study of the 2010 negative north atlantic oscillation winter. *Geophysical Research Letters*, 43(18):9994–10,002.
- Xia, X. and Chang, E. K. M. (2014). Diabatic damping of zonal index variations. *Journal of the Atmospheric Sciences*, 71(8):3090–3105.
- Yadav, P. and Straus, D. M. (2017). Circulation response to fast and slow MJO episodes. *Monthly Weather Review*, 145(5):1577–1596.
- Yao, Y. and Luo, D. (2018). An asymmetric spatiotemporal connection between the euro-atlantic blocking within the NAO life cycle and european climates. *Advances in Atmospheric Sciences*, 35:796–812.
- Zanardo, S., Nicotina, L., Hilberts, A. G. J., and Jewson, S. P. (2019). Modulation of economic losses from european floods by the north atlantic oscillation. *Geophysical Research Letters*, 46(5):2563–2572.
- Zappa, G., Shaffrey, L. C., and Hodges, K. I. (2013). The Ability of CMIP5 Models to Simulate North Atlantic Extratropical Cyclones*. *Journal of Climate*, 26(15):5379–5396.
- Zelinka, M. D., Grise, K. M., Klein, S. A., Zhou, C., DeAngelis, A. M., and Christensen, M. W. (2018). Drivers of the low-cloud response to poleward jet shifts in the north pacific in observations and models. *Journal of Climate*, 31(19):7925–7947.

- Zelinka, M. D., Myers, T. A., McCoy, D. T., Po-Chedley, S., Caldwell, P. M., Ceppi, P., Klein, S. A., and Taylor, K. E. (2020). Causes of higher climate sensitivity in cmip6 models. *Geophysical Research Letters*, 47(1):e2019GL085782. e2019GL085782 10.1029/2019GL085782.
- Zhang, W., Wang, Z., Stuecker, M. F., Turner, A. G., Jin, F.-F., and Geng, X. (2019). Impact of enso longitudinal position on teleconnections to the nao. *Climate Dynamics*, 52:257–274.
- Zängl, G., Reinert, D., Rípodas, P., and Baldauf, M. (2015). The icon (icosahedral non-hydrostatic) modelling framework of dwd and mpi-m: Description of the non-hydrostatic dynamical core. *Quarterly Journal of the Royal Meteorological Society*, 141(687):563–579.

B. List of abbreviations

ACRE	Atmospheric cloud-radiative effects
AO	Arctic Oscillation
AMIP	Atmospheric Model Intercomparison Project
BOA	Bottom-of-atmosphere
CRE	Cloud-radiative effects
CALIPSO	Cloud–Aerosol Lidar and Infrared Pathfinder Satellite Observations
CERES	Clouds and Earth’s Radiant Energy System
CTRL	Control
CPR	CloudSat Cloud Profiling Radar
CVS	Cloud vertical structure
DJF	December to February
DJFM	December to March
EA	East Atlantic pattern
ECMWF	European Centre for Medium-Range Weather Forecasts
ENSO	El Niño–Southern Oscillation
EOF	Empirical Orthogonal Function
FORC	Forced
GERB/SEVIRI	Geostationary Earth Radiation Budget/Spinning Enhanced Visible and InfraRed Imager
ICON	ICOsahedral Non-hydrostatic model
IFS	Integrated Forecast System
MJO	Madden–Julian Oscillation
MSLP	mean sea-level pressure
NASA	National Aeronautics and Space Administration
NAM	Northern Annular Mode
NAO	North Atlantic Oscillation
NOAA-CPC	National Oceanic and Atmospheric Administration Climate Prediction Centre
NWP	Numerical weather prediction
PCA	Principal component analysis

PTE Surface pressure tendency equation

SST Sea surface temperature

TOA Top-of-atmosphere

C. Acknowledgements

First and foremost, I would like to thank my advisors, Dr. Aiko Voigt and Prof. Dr. Peter Knippertz, for their continuous support, constructive feedback and guidance throughout these years. Your enthusiasm and keen passion was an additional inspiration for me from day one. In particular, I would like to sincerely express my gratitude to Dr. Aiko Voigt who gave me the opportunity to start this PhD position and become a member of the CONSTRain family. You have always tried to promote my path as a scientist and your constructive criticism was always boosting my need to become a better researcher. Besides the valuable scientific discussions, I would like to thank you both for organizing the best group dinner and summer BBQ parties that help in creating bonds within the institute.

I would like to thank, of course, all of my colleagues from the working group "CONSTRain" as well as people outside the working group, also those who have now left KIT, for always being there for me. In particular, the guys that we shared the same office throughout these years being supportive to work and personal issues, sharing any kind of thoughts, baking the best cakes, helping with paperwork and German bureaucracy, and illustrated great patience to my endless monologues. Moreover, I thank the guys that we had a great time in many local breweries in Karlsruhe watching football and Formula 1, playing pool or just having fun. Special thanks also to the "Thursday football group" for displaying world-class skills, high quality of football tactics and team spirit! Many thanks also to the HD(CP)² community for bringing together all these bright minds closer and particularly the guys from TROPOS in Leipzig.

Last but not least, I would like to express my profound gratitude and dedicate this work to my wife, Sonia for your loving support and patience from the early beginning of my academic endeavour, my parents, Rita and Ioannis, and my brother Panagiotis for everything you did for me and your unlimited support to pursue my career as a meteorologist since I was a child. To my grandparents Georgios, Maria, Katerina and Panagiotis for being there always for me. This PhD couldn't happen without you.